九州大学学術情報リポジトリ
Kyushu University Institutional Repository

Studies on Production and Conversion of Cellulose-derived Platform Chemicals

黄, 鑫

https://doi.org/10.15017/2534469

出版情報：Kyushu University, 2019, 博士（工学）, 課程博士
バージョン：
権利関係：

Studies on Production and Conversion of Cellulose-derived Platform Chemicals

Xin Huang

Department of Applied Science for Electronics and Materials

Interdisciplinary Graduate School of Engineering Sciences

Kyushu University, Japan

2019

Contents

Thesis Summary

Against a background of depletion of fossil resources and global environmental problems caused by carbon dioxide emission, energy and chemical production industries in our society are requested to shift from the system with fossil fuel-derived feedstocks to sustainable system with renewable feedstocks. Lignocellulosic biomass is an only abundant renewable feedstock for chemicals on the earth. Among the constituents of biomass, cellulose accounts for 40-60% of its portion and considered to be the main feedstock for chemical industry in future because of the structure consisting of glucose. The strategy for producing chemicals from lignocellulosic biomass generally involves extraction of cellulose, saccharification of cellulose to glucose, and then conversion of glucose to a variety of chemicals. Therefore, glucose has been considered as a type of platform chemical. There have been numerous R&D works during these decades on the basis of this strategy; however, the number of technologies, reaching the commercial production, is quite limited. One of drawbacks of the conventional scheme is in the saccharification step. Saccharification of cellulose generally uses costly enzymes, and the reaction rate is slow, which significantly affect the overall process cost and efficiency.

A main focus of the present study is on chemicals, which are produced by pyrolysis of cellulose, and its conversion to valuable chemicals. Pyrolysis is considered as one of the most promising ways for cellulose depolymerization because it is very fast and does not need any chemical reagent. Pyrolysis of cellulose does not produce glucose, but,

instead, produces levoglucosan (LGA; a type of anhydrosugar) as a main product. In this study, a novel process for the cellulose conversion to variable chemicals has been proposed, where cellulose is pyrolyzed to produce anhydrosugars, consisting mainly of LGA, as chemical platform, and the anhydrosugars are converted into glucose or anhydrosugars-derived valuable chemicals. The strategy has a potential for enabling high-throughput chemicals production since it consists only of thermochemical conversion. However, anhydrosugars are still minor chemicals in the research field of biomass refinery. It is, therefore, important to develop chemistries and processes that enable their mass production and conversion to valuable chemicals.

This thesis thus aims to develop a novel and efficient technology that produces and converts cellulose-derived chemicals, anhyrosugars in particular, to valuable chemicals. Thesis contents are as follows:

Chapter 1 introduces the background and outlines of this study.

Chapter 2 develops a two-step continuous process that consists of an updraft fixed bed reactor for fast pyrolysis of cellulose to produce LGA and a catalytic reformer for in-situ conversion of the volatiles, mainly LGA, to levoglucosenone (LGO). The updraft fixed bed pyrolyzer enabled suppression of interaction between volatiles and pyrolyzing cellulose, and produced LGA with the yield of 38.4% on a carbon basis (%-C) at the optimized temperature of 500 °C. The yield was relatively high among the yields reported so far for a large scale reactor with continuous cellulose feeding. LGO, produced from the reformer, was a derivative of anhydrosugars and considered to be a

bio-renewable building block. The yield of LGO significantly depended on the type of catalyst used for the reforming of volatiles. Acidic activated carbons prepared with sulfuric acid or phosphoric acid treatment showed good catalytic activity toward LGO formation when mixed with cellulose in the catalytic pyrolysis in a separated experiment, but were unavailable in the two-step process due to the quick deactivation by coke deposition. Supported ionic liquid (IL: 1-butyl-2,3-dimethylimidazolium triflate) phase catalysts enabled selective production of LGO independent of the support material examined (silica, γ-alumina, and activated carbon). The continuous operation was possible with the maximum LGO yield of 16.6 %-C, but the IL catalysts also suffered from problems such as coke deposition and IL decomposition. The problems were quantitatively assessed in the experiments at different conditions.

Chapter 3 investigates the acid-catalyzed reaction of LGA in liquid phase. In pure organic solvent, the main LGA conversion pathway was dehydration to give LGO as a main product. The best performance of LGO production was achieved by DMSO and Amberlyst 70 as solvent and catalyst, respectively. The highest yield was 39.3% on a carbon basis. This was the first study that demonstrated LGO production from LGA with liquid phase reaction. When water was used as the solvent, LGA was selectively converted into glucose. The yield and selectively were almost 100%. This was also the first study demonstrating the glucose production in a very clean reaction system, consisting of water and solid acid catalyst, from cellulose-derived anhydrosugars.

In chapter 4, aqueous phase conversion of LGO to 5-hydroxymethylfurfural (HMF)

and levulinic acid (LA) over solid acid catalyst is investigated. HMF and LA are promising building blocks in glucose-based bio- chemical industry. This study found that these important chemicals can be produced from LGO with a clean reaction system at high yields. Several types of solid acid catalysts such as zeolites, strongly acidic ion-exchange resin, and sulfonated activated carbon, were investigated for this reaction. Among the tested catalysts, ZSM-5 and Amberlyst 70 showed the best performances for selectively producing the target products, resulting in the highest total yield of HMF and LA at 72.2 % on a molar basis. Factors decreasing the reaction selectivity were identified through the comparison of catalysts and kinetic analysis to the pore morphology, presence of Lewis acid sites, and formation of degradation products directly from LGO or its hydrated product. ZSM-5 and Amberlyst 70, after a single-batch experiment, contained deposits from the degradation products but could be reused with little loss in activity, although calcination was required for ZSM-5. The catalytic system, employing LGO as feedstock and recyclable solid acid catalysts, uses only water as reaction media and thus has the potential to be a clean route for producing the key building blocks HMF and LA.

Chapter 5 develops catalytic reaction systems that convert cellulose-derived γ-valerolactone (GVL) into 2-methyltetrahydrofuran (2-MTHF), which has a potential to be used as solvent. Among prepared catalysts, $RhMo/SiO_2$ showed the best performance for the target 2-MTHF with the selectivity of 86% in heptane at 120 °C. The high catalytic performance of Rh-based catalyst was attributed to an acidity induced

by the presence of additional metals such as Mo or Re. When mixed with solid acid catalysts such as zeolite (ZSM-5), $RhMo/SiO_2$ enabled the conversion of GVL to 2-MTHF even in water with the selectivity over 76%. The reaction at higher temperature (160 °C) caused further hydrodeoxygenation of 2-MTHF, resulting to the formation of pentane.

Chapter 6 summarizes the findings described in the preceding chapters.

Chapter 1

General Introduction

1.1 Background

With the depletion of fossil resources and the global environmental problems caused by the utilization of fossil resources, it is increasingly urgent to promote the development of renewable energy. **Fig. 1-1** shows the total primary energy demand in the sustainable development scenario predicted by International Energy Agency (IEA). Biomass resources, as the only renewable energy that can be directly converted into liquid fuels, have attracted worldwide attention due to its advantages of storage, large reserves, renewability and carbon recycles [1]. Biomass is the first energy source harnessed by mankind, which remains the primary source of energy for more than half the world's population. Biomass is the most abundant renewable natural raw material on the earth. Therefore, the development of renewable energy conversion from lignocellulosic biomass as an alternative for fossil resources for the production of fuels and platform chemicals is ultimately essential for the survival of the human beings.

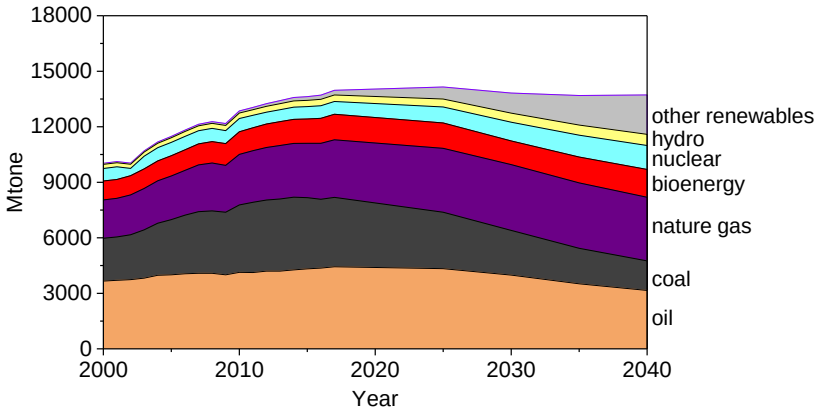

Fig. 1-1 Total primary energy demand in world predicted by IEA.

1.2 Extraction of cellulose from lignocellulosic biomass

Lignocellulosic biomass is mainly composed of three types of polymers: cellulose, hemicelluloses and lignin along with small amounts of ash, pectins, and proteins. Typically, hemicellulose, cellulose and lignin account for 20–40%, 40–60% and 10–25%, respectively, of lignocellulosic biomass [2]. Hemicellulose, a branched C5 polymer with a low degree of polymerization, is normally decomposed at 220–315 °C [3, 4]. Cellulose maintains highly ordered and stable crystalline structures consisting of a linear chain of several hundred to many thousands of glycosidic bonds. As a result, it usually undergoes decomposition at temperature range of 315–400 °C [3]. Lignin is a three-dimensional polymer of hydroxyl phenylpropane monomers, and bound adjacent to the cellulose fibers to form a lignocellulose [4, 5]. The lignin is more refractory than the other two components while having functional groups with widely distributed thermal stability, resulting in a board decomposition temperature range of 160–900 °C [3].

Among the three main components of biomass, cellulose is the most abundant bio-renewable resource in nature. Cellulose contains 44.4% carbon, 6.2% hydrogen, and 49.4% oxygen. The chemical formula of cellulose is $(C_6H_{10}O_5)n$ where n is the degree of polymerization and represents the number of glucose groups. The inherent stiffness and high degree of crystallinity showed great potential in the application of biomaterials. Apart from this, cellulose is also an ideal raw material for the production of biofuels (bioethanol) and bio-based chemical. Prior to utilize cellulose, isolation it from

lignocellulosic biomass is unavoidable. The structure of lignocellulosic biomass is a complex matrix in which cellulose is surrounded by a monolayer of hemicellulose and embedded in a matrix of hemicellulose and lignin [6]. This makes cellulose difficult to be extracted from biomass cell wall. Generally, cellulose extraction methods from lignocellulosic biomass are divided into alkaline treatment, ultrasound procedure, enzyme technology, diluted acid treatment as well as ionic liquid treatment.

1.2.1 Alkaline treatment

The alkaline treatment usually uses aqueous alkaline solutions such as NaOH, Na_2CO_3, KOH, and K_2CO_3. Initially, the dried lignocellulosic biomass is digested at 80–200 °C in an alkaline solution with some specific times. This procedure dissolves most part of lignin and removes a large amount of hemicellulose which is subsequently converted to mainly C5 sugars. Then the reaction is separated by filtration, lignin and hemicellulose are mainly in the filtrate, while cellulose is dominated in the filter cake. The filter cake is subsequently added into the mixture of sodium chlorite/glacial acetic acid to bleach [6], simultaneously the small amount of lignin and hemicellulose left in the filter cake would be further removed. Followed by repeatedly washing the bleached cellulose with firstly aqueous sodium hydroxide and then deionized water until pH neutral. At last, the cellulose was obtained after drying.

1.2.2 Ultrasound procedure

Ultrasonic irradiation application during the separation of hemicellulose, cellulose and lignin from biomass affects positively the yield of extractable materials. In addition,

the ultrasonic procedure is supposed to be simple and more effective compared to conventional techniques in the process of cellulose extraction [7]. The ultrasound procedure for extraction of cellulose is performed in aqueous alkaline peroxide with ultrasonic system in some specific time and desired temperature. Then the insoluble residue is collected by filtration and subsequently washed with deionized water, followed by drying. The mass transfer is significantly enhanced by the sonomechanical effect of ultrasound which improves the penetration of the solvent and heat into cellular structures [8]. Ultrasonication induces localized high pressure and temperature, which results to produce highly reactive free radicals, such as OH^-, H^+, and H_2O_2, leading to enhancement of chemical reactions [8]. The purity of cellulose is therefore rather high.

1.2.3 Enzyme technology

The enzyme technology for the extraction of cellulose from biomass is based on the idea of selective conversion of other parts of biomass component, i.e. hemicellulose and lignin, while retaining the cellulose portion. Usually the residue pretreated by the Kraft pulping is used as the starting material. Kraft pulping, generally operating at about 175 °C for 2–5 h [9], necessitating treatment of biomass with a hot mixture of water, sodium hydroxide (NaOH), and sodium sulfide (Na_2S), known as white liquor, that breaks the biomass matrix, in other words, the cleavage between lignin, hemicellulose, and cellulose. The raw cellulose is firstly soaked in water and autoclave, followed by adding the fungal culture to the suspension with appropriate portion of sucrose and yeast extract to support the growth of fungal. Then the fungus acts on the raw cellulose

at ambient temperature for specific time with slow agitation. The cellulose is then autoclaved, repeatedly washed with deionized water and made into sheets of 10% residue consistency. This raw cellulose is subsequently sheared in a refiner for 125,000 revolutions. Then, the cellulose is cryocrushed in which the cellulose fiber is frozen by liquid nitrogen, and a high shear is applied by using a mortar and a pestle [6]. This step is signficant in liberating the micro-fibrils from the cell wall. The cryocrushed fiber is then dispersed into water suspension using a disintegrator, followed by filtration, and dry [6].

1.2.4 Diluted acid treatment

In nature, the cellulose molecular chains are composed of amorphous and crystalline domains [10]. The former one can be easily broken down by acid attack, owing to random orientation in a spaghetti-like arrangement that results in a lower density in noncrystalline areas [11]. Therefore, the acid hydrolysis pretreatment can obtain the nano-cellulose. The nano-cellulose dimension dependents not only on process parameters, such as acid type, acid concentration, reaction time and temperature, but also on the originality of biomass resources [12]. The procedures for acid pretreatment are as follows [6, 13]: the biomass is first using Wiley milled to decrease the interactions of hemicellulose, cellulose and lignin. Then the biomass sample is presoaked in an aqueous diluted acid solution, for example in 1% sulfuric acid solution, with continuous agitation at room temperature. Then the presoaked slurry is separated by simple filtration and the filter cake is repeatedly washed with deionized water until

pH neutral. The solid filter cake is transferred to a high pressure autoclave in 1% sulfuric acid solution and heated to around 160 °C. After with some prescribed time, the autoclave is immersed into an ice-water bath to stop the reaction. Subsequently, the pretreated slurry is filtered to separate solid residue, and washed with excess of deionized water, followed by drying. The hot diluted acid treatment of lignocellulosic biomass can significantly enhance digestibility owing to hemicellulose dissolution and lignin redistribution.

1.2.5 Ionic liquid treatment

Ionic liquids are salts in the liquid state with molting point generally below 100 °C. Ionic liquids have many attractive properties, such as chemical and thermal stability, zero or minimal vapor pressure, very low flammability, high solvation capacity, and good recyclability [14, 15]. Wang et al. [15] reported a method to extract of cellulose from lignocellulosic biomass using 1-allyl-3-methylimidazolium chloride (AmimCl). Briefly, AmimCl was mixed with the dimethyl sulfoxide (DMSO) solvent to form a homogeneous solution. Then the biomass sample was added to the AmimCl/DMSO solution in a three-neck flask. The mixture was subsequently heated to the desired temperate in an oil-bath or with microwave heating with continuous stirring. After a prescribed time, a dark, amber-colored and viscous biomass suspension was observed. Then the suspension was separated by filtration, after water was added to the filtrate, a cellulose-enriched extract was obtained.

1.3 Thermochemical conversion of cellulose

1.3.1 Combustion

Combustion, or burning in a scientific word, is a high-temperature exothermic redox chemical reaction between the substances and oxygen, which produces oxidized gaseous products, usually accompanied by the generation of heat and light in the form of flame. The combustion rate is extremely high, partly due to the nature of the chemical reaction itself, and partly because generated energy through combustion can escape into the surrounding medium, resulting in raised substance temperature and accelerating the reaction much more. In general, combustion is one of the most important chemical reactions and may be considered a culminating step in the oxidation of certain kinds of substances. The below equation gives the combustion of cellulose:

$$C_6H_{12}O_6 + 6O_2 \rightarrow 6CO_2 + 6H_2O$$

Cellulose molecule reacts with the O_2 resulting in the formation of CO_2 and H_2O. Both the CO_2 and H_2O are released as gaseous product because the combustion temperate is quite high. Usually, the temperature for hot gaseous products over combustion can reach to 800–1000 °C [16].

1.3.2 Gasification

Gasification is a process that converts carbonaceous materials into synthetic gas, i.e. CO CO_2 and H_2O. These gases can be further used to produce electricity and other value-added products, such as fuels, chemicals and fertilizers. Different from combustion, gasification introduces a gasifying media, which can be air, pure oxygen, steam, or carbon dioxide [17], into gasifier to covert carbonaceous materials directly

into syngas. The calorific value of the syngas is totally dependent on the gasifying agent. A heating value of around 4–7 MJ/Nm^3 obtained from air gasification whereas that of from pure oxygen gasification can be as high as 12–18 MJ/Nm^3 [18]. However, tar formation during biomass gasification can cause serious problems. Tar is a stick and thick viscous liquid. It may cause some operation problems through downstream blockage and degrades the quality of the target gases resulting in the significant decrease in the efficiency of the gasifier. Thermal cracking, steaming reforming, dry reforming, and carbon formation and partial oxidation are effective ways to efficiently reduce the tar content [17]. The property and quality of the syngas is significantly affected by the feedstock type and dimensions, gasifying agent, reaction temperature and pressure, the presence of catalyst and sorbent, as well as the gasifier type. The biomass gasifiers generally classified into fixed bed, fluidized bed, and entrained gasifiers. Among them, fluidized bed gasifiers are widely used in gasification industry.

1.3.3 Pyrolysis

Pyrolysis is a thermal decomposition of biomass into heterogeneous gases, bio-oil and bio-char in the absence of oxygen. It is also the first step of combustion and gasification. Different form the total or partial oxidation of the primary products induced by combustion and gasification, respectively, the primary products by pyrolysis will not undergo oxidation reaction owing to the absence of oxygen. The gases can be used as syngas and further processed by means of the Fischer-Tropsch process into methanol, ethanol and other valuable chemicals. The bio-char can be used as a fuel and

soil amendment [19]. More importantly, the bio-oil has a potential to be used as a fuel and contains a variety of value-added chemicals. High reaction temperatures and long residence times generally promote biomass conversion to gas, whereas moderate temperatures and short residence times are optimum for producing bio-oil. Pyrolysis is differentiated between fast pyrolysis, with residences of seconds to optimize for the bio-oil production, and slow pyrolysis, with residence times ranging from minutes to days with the aim to bio-char production [20]. In fast pyrolysis, biomass decomposes very fast to form primary volatiles and some bio-char. After cooling and condensation of the primary volatiles, a light yellow to dark brown bio-oil is observed. In order to obtain high yield of bio-oil, the essential features of a fast pyrolysis process are listed as follows, according to Bridgwater [21]: at first, a finely ground biomass particles less than 3 mm is generally required duo to very high heating and heat-transfer rate at the reaction interface. Secondly, pyrolysis temperature of 500 ℃ and vapor phase temperature of 400–450 ℃ should be carefully controlled. Thirdly, short hot volatile residence is typically less than 2 s. At last, rapid cooling and condensation of the primary volatiles should be operated in order to get high yield of bio-oil product.

In the terms of fast pyrolysis of cellulose, the bio-oil formation pathway takes place in a temperature of approximately 300 ℃. In this case, cellulose pyrolysis produces a large amount of bio-oil, mainly anhydrosugars including levoglucosan that can be decomposed easily into small fragments. Thermal decomposition can also occur through char forming pathway. In this process, cellulose is firstly converted to active

cellulose and then further decomposed to small gaseous products, mainly including CO_2 and H_2O, and the left cellulose contains a lot of carbons.

1.3.4 Hydrothermal liquefaction

Hydrothermal liquefaction, proposed by the Shell Oil Company in the 1980s, is a thermal depolymerization process used to convert wet biomass into target products, i.e., bio-oil, bio-gas or bio-char under moderate temperature and high pressure. The process is generally conducted in aqueous phase at temperature range of 250-374 °C under pressure of 4-22 MPa. In the hydrothermal liquefaction process, thermal degradation of biomass occurs in aqueous phase and affects physicochemical properties of water [22]. The dielectric constant of water is significant reduced at high temperatures, resulting that non-polar substances can be dissolved well in water under supercritical conditions, whereas they are insoluble in water under normal conditions [23]. Hydrothermal liquefaction of cellulose in acidic, neutral and alkaline conditions shows very different chemical composition of bio-oil. The main compound of bio-oil under acidic and neutral conditions is 5-hydroxymethylfurfural, while that of under alkaline conditions are C2-5 carboxylic acids [24].

1.4 Platform chemicals

1.4.1 Levoglucosan

Levoglucosan (LGA, 1,6-anhydro-β-D-glucopyranose), a major anhydro-monosaccharide formed during cellulose primary pyrolysis with a wide range of 5–80% carbon yield, is a prospective intermediate as a carbon and energy source [25].

The formation mechanism of LGA from cellulose can be concluded into glucose intermediate, free-radical mechanism, ionic mechanism, and LGA chain-end mechanism, as shown in **Fig. 1-2**. The free-radical mechanism, firstly proposed by Pakhomov [26] in 1957, supposed that cellulose chain can be decomposed into dehydroglucose diradicals which will further form LGA. Another radical mechanism proposed by Shen and Gu [27], supposed LGA radical with one unpaired electron can be transferred into LGA through reacting with hydroxyl radical. Zhang et al [28, 29] conceded that levuglucosan can be formed by two steps, at first the free radicals undergo a hydrogen donor reaction which transfers a hydrogen atom from one oxygen atom to another oxygen atom, then a bridge structure is formed, i.e. levuglucosan, due to a strong affinity between the active oxygen atom and the active carbon atom. Another mechanism of LGA formation is ionic intermediate. Compared to radical intermediate, ionic intermediate was proved to need quite more energy than radical cleavage under the gas atmosphere for real biomass gasification. The ionic mechanism firstly proposed by Ponder et al. [30] involved a glucosyl cation end group formation by ionic glycosidic bond cleavage, subsequently leading to formation of 1,6-anhydride, and then another glycosidic bond cleavage with a proton shifted to produce LGA [31]. Nevertheless in the glucose intermediate mechanism, cellulose was firstly decomposed into glucose units by hydrolysis, and then these glucose units can be dehydrated to form LGA. Zhang et al. [29] made an analogy of glucose intermediate mechanism by processing into a cellobiosan reaction with one molecule water to produce two molecule glucose unites. Two pathways reveal that one

molecule water can attack either C1–O or C4'–O to form two molecule glucose units, the cleavage of C1–O position to from glucose units is easier to happen by hydrolysis duo to its weaker bond, as the energy barriers for hydrolysis is 264 kJ/mol at C1–O position while that is 346 kJ/mol at C4'–O position [29]. The most widely recognized formation of LGA mechanism is LGA chain-end mechanism duo to its quite low energy barrier, which described two transglycosylation steps. During the first glycosidic cleavage step, a cellulose chain is depolymerized into two polymeric fragments: a cellulose-like polymer with a terminal LGA-like end and a shorter cellulose chain [32]. After that a molecule of LGA is released from the chain end for each subsequent scission of a glycosidic bond by depropagation steps. The depropagation step can be repeated until the cellulose chains are fully decomposed into LGA molecules.

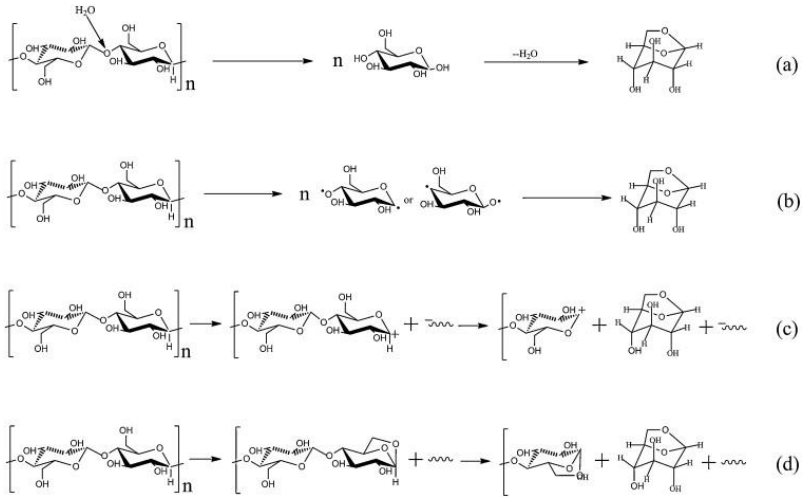

Fig. 1-2 Main LGA formation mechanisms from cellulose pyrolysis [29]. (a) glucose intermediate; (b) free-radical mechanism; (c) ionic mechanism; (d) chain-end mechanism. Copy right: Elsevier.

1.4.2 Levoglucosenone

Levoglucosenone (LGO, 1,6-anhydro-3,4-dideoxy-β-d-glycero-hex-3-enopyranos-

2-ulose) is a promising intermediate as a biorenewable platform for the production of sustainable chemicals [33-37], as shown in, **Fig. 1-3**. LGO has an advantage over other biomass-derived platform chemicals due to its application in synthesis of asymmetric and enantiopure compounds. There are several methodologies to produce LGO. Pretreatment of cellulose with mineral acid before pyrolysis could lead a higher yield of LGO compared to non-pretreatment [38-42]. But this process produces significant amounts of waste chemicals and causes environmental pollution. Solvent-assisted is also an effective methodology to produce LGO. Cao et al. [43] showed that LGO can be obtained from cellulose in 51% carbon yield over sulfuric acid in tetrahydrofuran. Kawamoto et al. [44] obtained 42.2% mol yield of LGO form cellulose in sulfolane with sulfuric acid. Moreover, catalytic pyrolysis is an effective approach to increase LGO yield. Sulfonated or phosphorated metal oxides or activated carbon catalysts could increase the LGO yield up to 18.1 wt% [45-47]. Casoni's group work showed LGO with 53 wt% yield was obtained with catalytic pyrolysis of cellulose over Al-MCM-41 [48]. Kudo et al. revealed 38% carbon yield of LGO by pyrolysis of cellulose mechanically mixed with an equivalent mass of high thermal stability and strong acidity of ionic liquid (IL) [49, 50]. In addition, he reported another two-step process method, where volatiles, consisting mainly of LGA, from cellulose pyrolysis were catalytically reformed to produce LGO [51]. The first step was to obtain the primary volatiles mainly LGA from cellulose pyrolysis, followed by catalytic conversion of LGA in the gas phase. That study revealed that an employment of supported ionic liquid phase catalyst

enables the conversion of LGA to LGO with a substantial yield.

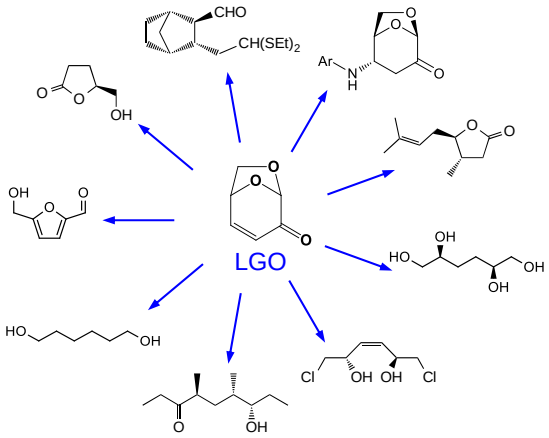

Fig. 1-3 Production of sustainable chemicals from LGO.

1.4.3 5-Hydroxymethylfurfural and levulinic acid

5-Hydroxymethylfurfural (HMF) and levulinic acid (LA) are typical platform chemicals with great industrial potential. HMF can be rehydrated to levulinic acid (LA) and formic acid (FA) under acid conditions. Even though LA is a high value-added chemical, HMF is more valuable in more potential applications, such as fuels, polymers etc. HMF has vast potential to be an important building block in future bio-based chemical industry, and, therefore, often referred to as "sleeping giant" [52]. As evidenced by many studies and depicts in **Fig. 1-4**, HMF can be converted to chemicals used in a wide range of markets/applications such as fuels, solvents, polymers, and pharmaceuticals [53]. The industrial scale production has already been started by some companies. On the other hand, the price is still high as a platform chemicals to be competitive with petroleum derived chemicals. Although there are many factors affecting the price, most importantly, it is necessary to reduce the cost of chemicals

needed to convert the feedstock into HMF. In other words, development of more efficient process is required.

Saccharides are generally employed as feedstock for HMF in researches and industries. Fructose is the best option for achieving higher yields. Glucose is also converted to HMF basically after isomerization to glucose. Polysaccharides including cellulose or lignocellulosic biomass can be used as the feedstock but need depolymerization that causes lower yields in general. As summarized in recent review studies [52-54], much effort has been made for achieving the high HMF yield through development of catalytic and solvent systems. However, even for fructose and using costly catalyst and solvent, it is hard to achieve near-complete conversion of the feedstock to HMF. This is due to the occurrence of side-reactions in the course of multi-step removing of three water molecules from saccharides. The complexity of reaction thus has been a drawback of HMF production from conventional resources.

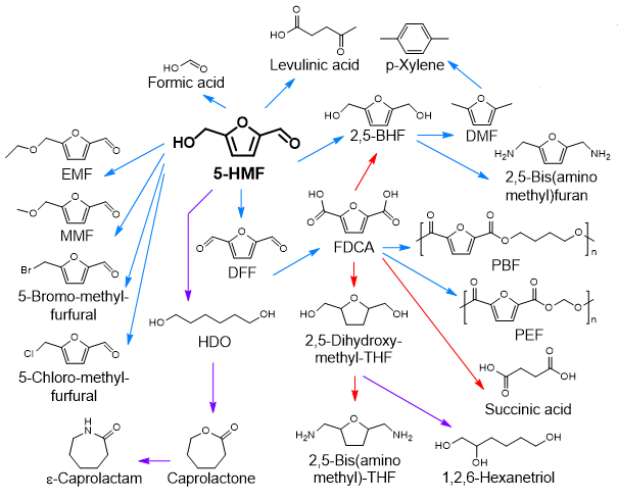

Fig. 1-4 HMF as a platform chemical.

LA, one of the twelve most promising value added chemicals from biomass by the

Biomass Program of the US Department of Energy in 2004 [55], is a member of the gamma-keto acids that itself is a promising chemical intermediate to produce a number of bio-chemicals including succinic acid, resins, polymers, herbicides, pharmaceuticals and flavoring agents, solvents, plasticisers, anti-freeze agents and biofuels/oxygenated fuel additives [56-58], as shown in **Fig. 1-5**.

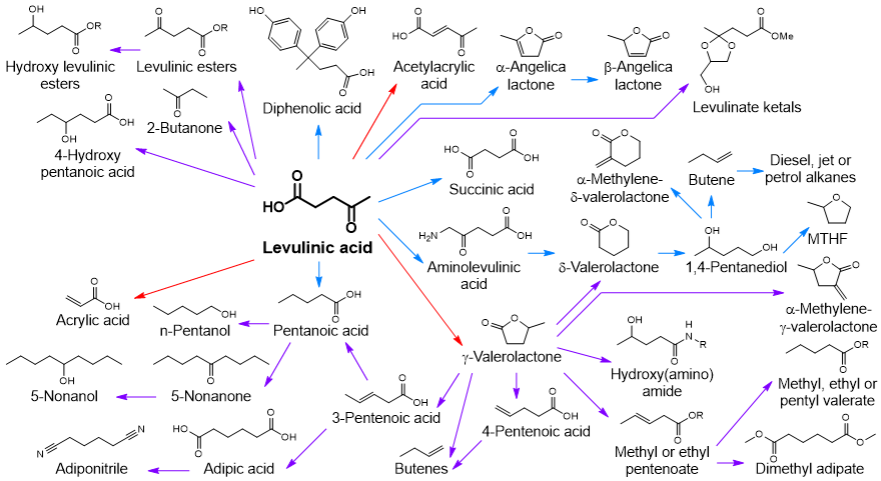

Fig. 1-5 LA as a platform chemical.

1.4.4 2-Methyltetrahydrofuran

2-Methyltetrahydrofuran (2-MTHF) is a promising alternative chemical as a renewable solvent [59] or a fuel additive in a more suitable biofuel compared to ethanol due to its higher hydrophobic property and a higher heating value and density [60]. It is reported that 2-MTHF can be blended up to 70% in gasoline [61]. Although the heating value of 2-MTHF is lower than that of regular petroleum, the higher specific gravity of 2-MTHF would promote mileage from 2-MTHF blended fuel. In addition, 2-MTHF could drastically reduce the vapor pressure of ethanol when co-blended in gasoline [62,

63]. Its chemical and physical characteristics, such as low boiling point, low miscibility with water (13 mg/ml in water), and remarkable stability compared to THF, make it appealing for chemical applications in syntheses involving organocatalysis, organometallics, and biotransformations and biorefineries. The utilization of 2-MTHF is not only rely on academic research, industrial labs also started to assess its use in several synthetic procedures, which will certainly trigger more research in the field of sustainable chemistry.

1.5 Objective of this study

Cellulose has become a wide interest for worldwide scientists and industries. With the aim to contribute to the construction of a feasible chemical industry using cellulose as starting material, a series of studies for production and conversion of cellulose-derived chemicals are conducted, as shown in **Fig. 1-6**. Pyrolysis is considered as one of the most promising ways for depolymerization of cellulose, resulting in producing a large amount of LGA and anhyosugar oligomers, which can be further converted into LGO in the gas phase catalytic reforming over ionic liquid supported phase (**Chapter 2**) or in the liquid phase reaction over sulfonated resins (**Chapter 3**), or into glucose in aqueous phase (**Chapter 3**). LGO is subsequently converted to 5-hydroxylmethylfurfural and levulinic acid in an aqueous phase over solid acid catalyst (**Chapter 4**). At last, the levulinic acid derived γ-valerolactone is hydrogenolyzed to 2-MTHF under mild conditions over silica-supported RhRe and RhMo bimetallic catalysts (**Chapter 5**).

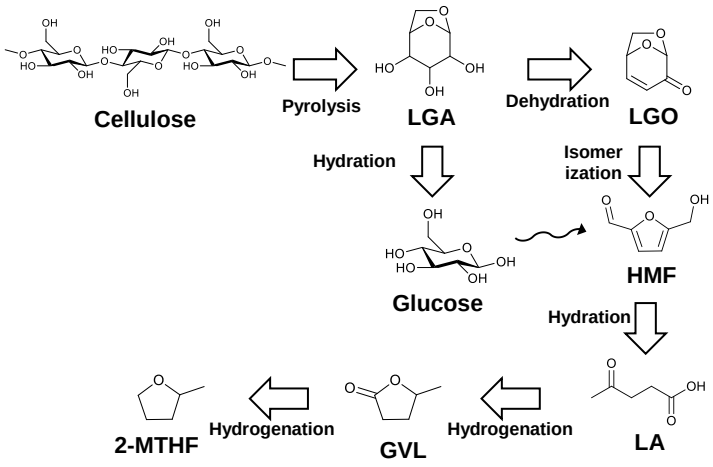

Figure 1-6 Reaction flow chart of this study.

1.6 Outline of this study

In chapter 1, the current technologies, including alkaline treatment, ultrasound procedure, enzyme technology, diluted acid treatment, ionic liquid treatment, for the extraction of cellulose from lignocellulosic biomass are simply introduced. Various approaches, including combustion, gasification, pyrolysis, hydrothermal liquefaction, to effectively convert cellulose into gas, bio-oil, and bio-char are summarized. Specifically, the cellulose-derived platform chemicals, i.e. LGA, LGO, HMF, LA and 2-MTHF are interfered.

In chapter 2, a two-step continuous process that consists of an updraft fixed bed reactor for fast pyrolysis of cellulose and a catalytic reformer for the volatiles conversion was designed. The first steps is to pyrolyze cellulose with the aim to maximize the LGA yield, while the second step is to catalytically reform LGA to LGO, a promising bio-renewable platform for the fine and commodity chemical industries. The process performance is presented, and through investigation of the influence of

operating conditions such as pyrolysis/reforming temperature and the type of catalyst, important issues are identified for developing the system that works effectively and continuously.

In chapter 3, a study employed LGA as the starting material to produce LGO or glucose in liquid phase reaction is carried out for the first time. The influence of parameters varied including solvent, catalyst, reaction temperature, and reaction time on the dehydration of LGA. Specifically, an anhydrosugar mixture from bio-oil, mainly containing LGA by cellulose pyrolysis, is used as the reagent for LGO and glucose production.

In chapter 4, an aqueous phase conversion of LGO to HMF and LA over solid acid catalyst is reported. Several types of solid acid catalysts such as zeolites, strongly acidic ion-exchange resin, and sulfonated activated carbon are investigated for this reaction. Specifically, to clearly describe the difference in reaction selectivity, the experimental results are kinetically analyzed with the reaction pathway by assuming all first-order reactions.

In chapter 5, selective hydrodeoxygenation of cellulose-derived γ-valerolactone to 2-MTHF in heptane solvent under mild conditions over silica-supported RhRe and RhMo bimetallic catalysts is performed. The reaction parameters, such as solvent, reaction temperature, were optimized to construct a feasible chemical industry. Specifically, a cleaner approach to produce 2-MTHF employing the aqueous phase conversion has been investigated.

In chapter 6, general conclusions of this study are described.

1.7 References

[1] T. Bridgwater, Biomass for energy, J. Sci. Food Agric., 86 (2006) 1755-1768.

[2] P. McKendry, Energy production from biomass (part 1): overview of biomass, Bioresour. Technol., 83 (2002) 37-46.

[3] M.A. Islam, M. Asif, B. Hameed, Pyrolysis kinetics of raw and hydrothermally carbonized Karanj (Pongamia pinnata) fruit hulls via thermogravimetric analysis, Bioresour. Technol., 179 (2015) 227-233.

[4] H. Yang, R. Yan, H. Chen, D.H. Lee, C. Zheng, Characteristics of hemicellulose, cellulose and lignin pyrolysis, Fuel, 86 (2007) 1781-1788.

[5] S. Yaman, Pyrolysis of biomass to produce fuels and chemical feedstocks, Energy Convers. Manage., 45 (2004) 651-671.

[6] K. Radotić, M. Mićić, Methods for extraction and purification of lignin and cellulose from plant tissues, in: sample preparation techniques for soil, plant, and animal samples, Springer, 2016, pp. 365-376.

[7] C. Pappas, P. Tarantilis, I. Daliani, T. Mavromoustakos, M. Polissiou, Comparison of classical and ultrasound-assisted isolation procedures of cellulose from kenaf (Hibiscus cannabinus L.) and eucalyptus (Eucalyptus rodustrus Sm.), Ultrason. Sonochem., 9 (2002) 19-23.

[8] N. Dinh Vu, H. Thi Tran, N.D. Bui, C. Duc Vu, H. Viet Nguyen, Lignin and cellulose extraction from Vietnam's rice straw using ultrasound-assisted alkaline treatment method, Int. J. Polym. Sci., 2017 (2017) 1-8.

[9] M. Holtzapple, Lignin, Encyclopedia of Food Sciences and Nutrition (Second Edition), (2003) 3535-3542.

[10] R. Li, J. Fei, Y. Cai, Y. Li, J. Feng, J. Yao, Cellulose whiskers extracted from mulberry: A novel biomass production, Carbohydr. Polym., 76 (2009) 94-99.

[11] M.M. de Souza Lima, R. Borsali, Rodlike cellulose microcrystals: structure, properties, and applications, Macromol. Rapid Commun., 25 (2004) 771-787.

[12] M.A.S. Azizi Samir, F. Alloin, A. Dufresne, Review of recent research into cellulosic whiskers, their properties and their application in nanocomposite field, Biomacromolecules, 6 (2005) 612-626.

[13] S.V. Pingali, V.S. Urban, W.T. Heller, J. McGaughey, H. O'Neill, M. Foston, D.A. Myles, A. Ragauskas, B.R. Evans, Breakdown of cell wall nanostructure in dilute acid pretreated biomass, Biomacromolecules, 11 (2010) 2329-2335.

[14] H. Lateef, S. Grimes, P. Kewcharoenwong, B. Feinberg, Separation and recovery of cellulose and lignin using ionic liquids: a process for recovery from paper-based waste, J. Chem. Technol. Biotechnol., 84 (2009) 1818-1827.

[15] X. Wang, H. Li, Y. Cao, Q. Tang, Cellulose extraction from wood chip in an ionic liquid 1-allyl-3-methylimidazolium chloride (AmimCl), Bioresour. Technol., 102 (2011) 7959-7965.

[16] I. Obernberger, Decentralized biomass combustion: state of the art and future development, Biomass Bioenerg., 14 (1998) 33-56.

[17] V.S. Sikarwar, M. Zhao, P. Clough, J. Yao, X. Zhong, M.Z. Memon, N. Shah, E.J. Anthony, P.S. Fennell, An overview of advances in biomass gasification, Energy Environ. Sci., 9 (2016) 2939-2977.

[18] S. Rapagnà, N. Jand, A. Kiennemann, P.U. Foscolo, Steam-gasification of biomass in a fluidised-bed of olivine particles, Biomass Bioenerg., 19 (2000) 187-197.

[19] J.L. Field, C.M. Keske, G.L. Birch, M.W. DeFoort, M.F. Cotrufo, Distributed biochar and bioenergy coproduction: a regionally specific case study of environmental benefits and economic impacts, Gcb Bioenergy, 5 (2013) 177-191.

[20] B. Babu, Biomass pyrolysis: a state-of-the-art review, Biofuel., Bioprod. Biorefin., 2 (2008) 393-414.

[21] A.V. Bridgwater, Chapter 7 Fast pyrolysis of biomass for energy and fuels, thermochemical conversion of biomass to liquid fuels and chemicals, (2010) pp. 146-191.

[22] G. Brunner, Near critical and supercritical water. Part I. Hydrolytic and hydrothermal processes, J. Supercrit Fluid, 47 (2009) 373-381.

[23] K. Tekin, S. Karagöz, S. Bektaş, A review of hydrothermal biomass processing, Renewable Sustainable Energy Rev., 40 (2014) 673-687.

[24] S. Yin, Z. Tan, Hydrothermal liquefaction of cellulose to bio-oil under acidic, neutral and alkaline conditions, Appl. Energy, 92 (2012) 234-239.

[25] E.M. Prosen, D. Radlein, J. Piskorz, D.S. Scott, R.L. Legge, Microbial utilization of levoglucosan in wood pyrolysate as a carbon and energy source, Biotechnol. Bioeng., 42 (1993) 538-541.

[26] A. Pakhomov, Free-radical mechanism of the thermodegradation of cellulose and formation of levoglucosan, Russ. Chem. Bull., 6 (1957) 1525-1527.

[27] D.K. Shen, S. Gu, The mechanism for thermal decomposition of cellulose and its main products, Bioresour. Technol., 100 (2009) 6496-6504.

[28] X. Zhang, J. Li, W. Yang, W. Blasiak, Formation mechanism of levoglucosan and formaldehyde during cellulose pyrolysis, Energy & Fuels, 25 (2011) 3739-3746.

[29] X. Zhang, W. Yang, C. Dong, Levoglucosan formation mechanisms during cellulose pyrolysis, J. Anal. Appl. Pyrolysis, 104 (2013) 19-27.

[30] G.R. Ponder, G.N. Richards, T.T. Stevenson, Influence of linkage position and orientation in pyrolysis of polysaccharides: A study of several glucans, J. Anal. Appl. Pyrolysis, 22 (1992) 217-229.

[31] R. Vinu, L.J. Broadbelt, A mechanistic model of fast pyrolysis of glucose-based carbohydrates to predict bio-oil composition, Energy Environ. Sci., 5 (2012) 9808-9826.

[32] H.B. Mayes, L.J. Broadbelt, Unraveling the Reactions that Unravel Cellulose, J. Phys. Chem. A, 116 (2012) 7098-7106.

[33] S.H. Krishna, T.W. Walker, J.A. Dumesic, G.W. Huber, Kinetics of levoglucosenone isomerization, ChemSusChem, 10 (2016) 129-138.

[34] A. Flourat, A. Peru, A. Teixeira, F. Brunissen, F. Allais, Chemo-enzymatic synthesis of key intermediates (S)-γ-hydroxymethyl-α, β-butenolide and (S)-γ-hydroxymethyl-γ-butyrolactone via lipase-mediated Baeyer-Villiger oxidation of levoglucosenone, Green Chem., 17 (2015) 404-412.

[35] C. Paris, M. Moliner, A. Corma, Metal-containing zeolites as efficient catalysts for the transformation of highly valuable chiral biomass-derived products, Green Chem., 15 (2013) 2101-2109.

[36] S.H. Krishna, D.J. McClelland, Q.A. Rashke, J.A. Dumesic, G.W. Huber, Hydrogenation of levoglucosenone to renewable chemicals, Green Chem., 19 (2017) 1278-1285.

[37] M.B. Comba, Y.h. Tsai, A.M. Sarotti, M.I. Mangione, A.G. Suárez, R.A. Spanevello, Levoglucosenone and its new applications: valorization of cellulose residues, Eur. J. Org. Chem., 2018 (2018) 590-604.

[38] X.W. Sui, Z. Wang, B. Liao, Y. Zhang, Q.X. Guo, Preparation of levoglucosenone through sulfuric acid promoted pyrolysis of bagasse at low temperature, Bioresour. Technol., 103 (2012) 466-469.

[39] Y. Halpern, R. Riffer, A. Broido, Levoglucosenone (1, 6-anhydro-3,4-dideoxy-. DELTA. 3-.beta.-D-pyranosen-2-one). Major product of the acid-catalyzed pyrolysis of cellulose and related carbohydrates, J. Org. Chem, 38 (1973) 204-209.

[40] G. Dobele, G. Rossinskaja, G. Telysheva, D. Meier, O. Faix, Cellulose dehydration and depolymerization reactions during pyrolysis in the presence of phosphoric acid, J. Anal. Appl. Pyrolysis, 49 (1999) 307-317.

[41] G. Dobele, T. Dizhbite, G. Rossinskaja, G. Telysheva, D. Meier, S. Radtke, O. Faix, Pre-treatment of biomass with phosphoric acid prior to fast pyrolysis: a promising method for obtaining 1, 6-anhydrosaccharides in high yields, J. Anal. Appl. Pyrolysis, 68 (2003) 197-211.

[42] H. Zhang, X. Meng, C. Liu, Y. Wang, R. Xiao, Selective low-temperature pyrolysis of microcrystalline cellulose to produce levoglucosan and levoglucosenone in a fixed bed reactor, Fuel Process. Technol., 167 (2017) 484-490.

[43] F. Cao, T.J. Schwartz, D.J. McClelland, S.H. Krishna, J.A. Dumesic, G.W. Huber, Dehydration of cellulose to levoglucosenone using polar aprotic solvents, Energy Environ. Sci., 8 (2015) 1808-1815.

[44] H. Kawamoto, S. Saito, W. Hatanaka, S. Saka, Catalytic pyrolysis of cellulose in sulfolane with some acidic catalysts, J.Wood Sci., 53 (2007) 127-133.

[45] X.N. Ye, Q. Lu, X. Wang, H.Q. Guo, M.S. Cui, C.Q. Dong, Y.P. Yang, Catalytic fast pyrolysis of cellulose and biomass to selectively produce levoglucosenone using activated carbon catalyst, ACS Sustainable Chem. Eng., 5 (2017) 10815-10825.

[46] D. Fabbri, C. Torri, I. Mancini, Pyrolysis of cellulose catalysed by nanopowder metal oxides: production and characterisation of a chiral hydroxylactone and its role as building block, Green Chem., 9 (2007) 1374-1379.

[47] X. Wei, Z. Wang, Y. Wu, Z. Yu, J. Jin, K. Wu, Fast pyrolysis of cellulose with solid acid catalysts for levoglucosenone, J. Anal. Appl. Pyrolysis, 107 (2014) 150-154.

[48] A.I. Casoni, M.L. Nievas, E.L. Moyano, M. Álvarez, A. Diez, M. Dennehy, M.A. Volpe, Catalytic pyrolysis of cellulose using MCM-41 type catalysts, Appl. Catal., A, 514 (2016) 235-240.

[49] S. Kudo, Z. Zhou, K. Norinaga, J. Hayashi, Efficient levoglucosenone production by catalytic pyrolysis of cellulose mixed with ionic liquid, Green Chem., 13 (2011) 3306-3311.

[50] S. Kudo, Z. Zhou, K. Yamasaki, K. Norinaga, J. Hayashi, Sulfonate ionic liquid as a stable and active catalyst for levoglucosenone production from saccharides via catalytic pyrolysis, Catalysts, 3 (2013) 757-773.

[51] S. Kudo, N. Goto, J. Sperry, K. Norinaga, J. Hayashi, Production of levoglucosenone and dihydrolevoglucosenone by catalytic reforming of volatiles from cellulose pyrolysis using supported ionic liquid phase, ACS Sustainable Chem. Eng., 5 (2016) 1132-1140.

[52] A. Mukherjee, M.J. Dumont, V. Raghavan, Sustainable production of hydroxymethylfurfural and levulinic acid: Challenges and opportunities, Biomass Bioenerg., 72 (2015) 143-183.

[53] R.J. Van Putten, J.C. Van Der Waal, E. De Jong, C.B. Rasrendra, H.J. Heeres, J.G. de Vries, Hydroxymethylfurfural, a versatile platform chemical made from renewable resources, Chem. Rev., 113 (2013) 1499-1597.

[54] L. Qi, Y.F. Mui, S.W. Lo, M.Y. Lui, G.R. Akien, I.n.T. Horváth, Catalytic conversion of fructose, glucose, and sucrose to 5-(hydroxymethyl) furfural and levulinic and formic acids in γ-valerolactone as a green solvent, ACS Catal., 4 (2014) 1470-1477.

[55] T. Werpy, G. Petersen, A. Aden, J. Bozell, J. Holladay, J. White, A. Manheim, D. Eliot, L. Lasure, S. Jones, Top value added chemicals from biomass. Volume 1-Results of screening for potential candidates from sugars and synthesis gas, in, U.S. Department of Energy: Washington, DC, 2004, pp. 45-47.

[56] J.J. Bozell, L. Moens, D. Elliott, Y. Wang, G. Neuenscwander, S. Fitzpatrick, R. Bilski, J. Jarnefeld, Production of levulinic acid and use as a platform chemical for derived products, Resour. Conserv. Recycl., 28 (2000) 227-239.

[57] D.W. Rackemann, W.O. Doherty, The conversion of lignocellulosics to levulinic acid, Biofuels, Bioprod. Biorefin., 5 (2011) 198-214.

[58] B. Kamm, P.R. Gruber, M. Kamm, Biorefineries-industrial processes and products, Biorefineries-industrial processes and products. Wiley-VCH, Weinheim., (2006) pp. 139-163.

[59] V. Pace, P. Hoyos, L. Castoldi, P. Domínguez de María, A.R. Alcántara, 2-Methyltetrahydrofuran (2-MeTHF): A biomass-derived solvent with broad application in organic chemistry, ChemSusChem, 5 (2012) 1369-1379.

[60] I. Obregón, I. Gandarias, N. Miletić, A. Ocio, P.L. Arias, One-pot 2-methyltetrahydrofuran production from levulinic acid in green solvents using Ni-Cu/Al_2O_3 catalysts, ChemSusChem, 8 (2015) 3483-3488.

[61] V. Fábos, G. Koczó, H. Mehdi, L. Boda, I.T. Horváth, Bio-oxygenates and the peroxide number: a safety issue alert, Energy Environ. Sci., 2 (2009) 767-769.

[62] J.C. Serrano-Ruiz, D.J. Braden, R.M. West, J.A. Dumesic, Conversion of cellulose to hydrocarbon fuels by progressive removal of oxygen, Appl. Catal., B, 100 (2010) 184-189.

[63] D.J. Hayes, An examination of biorefining processes, catalysts and challenges, Catal. Today, 145 (2009) 138-151.

Chapter 2

Pyrolysis of Cellulose to Levoglucosan and Levoglucosenone

2.1 Introduction

In recent years, lignocellulosic biomass has attracted extensive interest as a renewable source for the production of biofuels and biochemicals to reduce the dependence on fossil fuels [1, 2]. Several thermochemical conversion routes of biomass, including, for example, combustion, gasification, liquefaction, hydrolysis, and pyrolysis, are currently under development [3-5]. Among these technologies, pyrolysis is considered as one of the most promising ways due to its fast reaction rate, producing bio-oil which has a potential to be used as a fuel and contains a variety of value-added chemicals [6, 7]. Among the three main components of lignocellulosic biomass (lignin, hemicellulose, and cellulose), cellulose, accounting for 35-50 wt%, is the most abundant bio-renewable resource in nature [8-10]. Cellulose is a polysaccharide consisting of a linear chain of glucose connected by β-1,4-glycoside linkage [11]. Recent researches report that cellulose-derived levoglucosenone (LGO, 1,6-anhydro-3,4-dideoxy-β-d-glycero-hex-3-enopyranos-2-ulose) is a promising intermediate as a biorenewable platform for the production of sustainable fuels, commodity/fine chemicals, and polymers [12-17].

There have been proposed several effective methods for the production of LGO, all of which are based on cellulose pyrolysis [18-25]. The first large scale LGO production process, Furacel process, developed by Circa Group in Australia has contributed to

dramatic reduction of the price of this premium chemical and afforded selling hydrogenated levoglucosenone (Cyrene) as a green solvent by the liter [26, 27]. On the other hand, there is leeway for the price to be reduced, and the process uses mineral acid and solvent, which necessitates post-processing of waste stream for avoiding environmental pollution. Addressing this challenge, a two-step LGO production system has been proposed, consisting of cellulose pyrolysis, followed by catalytic reforming of the volatiles [21]. The system consists only of fast reactions and does not essentially require costly chemicals. Supported ionic liquid (IL) phase was used as a packed bed catalyst of the reformer. In the preliminary study, when employed IL having triflate as an anion, LGO could be obtained mainly from levoglucosan (LGA) in the volatiles with the high yield of 31.6% on a carbon basis. However, the reaction was carried out mainly with a type of batch experiment using a small scale reactor.

The most important role of the first step, cellulose pyrolysis, is to convert cellulose into LGA and feed it to the reformer. Since LGA is a main precursor of LGO, the yield should be as high as possible. There have been many reports showing high LGA yield (up to 79.3%) with milligram scale reactors [28, 29]. The mini reactors for analytical purpose can suppress the secondary reactions of volatiles with solid (cellulose or pyrolyzing cellulose) and in the gas phase, enabling the high LGA yield. Information available from literatures on the continuous LGA production from cellulose in a large scale reactor is rather limited. Fluidized bed and a reactor with vacuum system are often employed as a pyrolyzer for improving the yield of volatiles (especially, in bio-oil

production), although the LGA yield is generally low, compared to that from mini reactors [29]. As discussed in a later section, conditions of volatiles such as temperature, flow rate, and contamination of char, are also needed to be considered in the selection of pyrolyzer. Regarding the second step, excepting our previous study [21], several types of solid acid catalysts have been reported for their activity to produce LGO in catalytic rapid or fast pyrolysis of cellulose. Solid acids (metal oxides or activated carbon) prepared by treatment with sulfuric acid and phosphoric acid selectively produced LGO in the yield of up to 18.1 wt% [19, 24, 30, 31]. However, because in this reaction system the catalyst was supplied to the reactor simultaneously with cellulose in one shot or continuously at a relatively high ratio of catalyst to cellulose, the catalytic performance in our two-step conversion system cannot be estimated.

In this context, the present study aims to go further with the two-step LGO production system using a relatively large scale updraft fixed bed as the pyrolyzer. The process performance is presented, and, through investigation of the influence of operating conditions such as pyrolysis/reforming temperature and the type of catalyst, important issues are identified for developing the system that works effectively and continuously.

2.2 Experimental

2.2.1 Catalyst preparation

IL used in this study was 1-butyl-2,3-dimethylimidazolium triflate ([BMMIM]OTf, > 99.0%, Ionic Liquids Technologies). For simplification, [BMMIM]OTf is hereafter

denoted as IL. The supported IL phase catalyst was prepared by impregnating IL over porous materials such as SiO_2 (nanopowder, Sigma-Aldrich), Al_2O_3 (γ-type, nanopowder, Sigma-Aldrich), and activated carbon (from palm shell, Wako Pure Chemical Industries). Before the impregnation, SiO_2 and Al_2O_3 were pressed, crushed, and sieved to sizes in the range of 0.5-1.0 mm. The activated carbon (AC) in a granular form was washed with water for removing fines, crushed, and then sieved to sizes in the range of 0.5-1.0 mm. The support materials were added to methanol containing prescribed amount of IL in a flask. The suspension was mixed well and then dried with a rotary evaporator for obtaining the supported IL phase catalysts, namely, IL/SiO_2, IL/Al_2O_3, and IL/AC. The contents of IL were 33, 33, and 50 wt%, respectively. Sulfonated activated carbon (S/AC) was prepared by a treatment of AC in concentrated sulfuric acid at 150 ℃ for 15 h under N_2, followed by washing with water until no sulfate was detected in the filtrate [32]. Activated carbon with phosphorus-containing group (P/AC) was prepared by mixing phosphoric acid with Japanese cedar and then pyrolysis at 500 ℃ for 2 h, according to a reported method [19]. The S/AC and P/AC were also in the sizes of 0.5-1.0 mm. The pore structures of catalysts, analyzed with the N_2 ad/desorption isotherms (**Fig. 2-1**), are listed in **Table 2-1**.

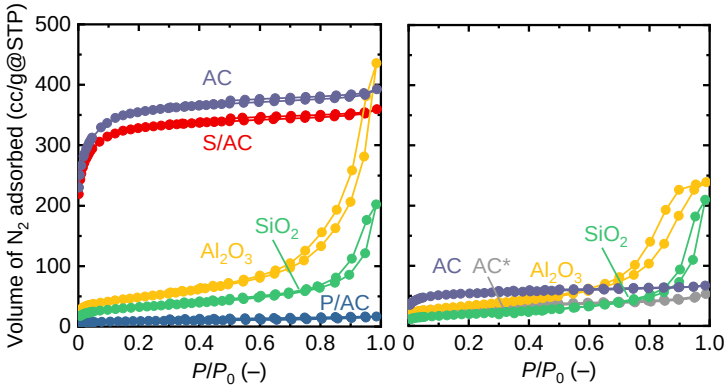

Fig. 2-1 N_2 ad/desorption isotherms of catalyst and support material (left: fresh, right: spent). The supported IL phase catalysts were washed with ethanol for removing IL, filtered and dried to obtain the support material. The spent support material was from the reforming at 350 °C. AC* was from the reforming at 275 °C.

Table 2-1 Structural characteristics of catalyst and support material.

Catalyst or support	S_{BET} (m^2/g)	V_{total} [a] (cm^3/g)	V_{micro} [b] (cm^3/g)
Fresh			
S/AC	1242	0.558	0.496
P/AC	32	0.026	0.009
Al_2O_3	169	0.676	-
SiO_2	111	0.313	0.016
AC	1322	0.608	0.535
Spent [c]			
Al_2O_3	118	0.375	-
SiO_2	82	0.311	-
AC	201	0.104	0.076
AC[d]	108	0.082	0.036

[a] Calculated from maximum N_2 adsorption in isotherm. [b] Calculated with t-plot method. [c] Spent in the reforming at 350 °C. Before the N_2 ad/desorption measurement, supported IL phase catalysts were washed with ethanol for removing IL, filtered and dried to obtain the support material. [d] Reforming at 275 °C.

2.2.2 Catalytic rapid pyrolysis of cellulose by a micro pyrolyzer

Microcryscalline cellulose purchased from Sigma-Aldrich was used as feedstock for the catalytic rapid pyrolysis and catalytic reforming of volatiles from updraft fixed bed pyrolyzer. Catalytic rapid pyrolysis was performed on a Curie point pyrolyzer

(JCI-22, Japan Analytical Industry) using P/AC, S/AC, or IL as the catalyst. Cellulose was physically mixed with the catalyst at a ratio of 3 : 1 on a weight basis. P/AC and S/AC were crushed to fines and then mixed with cellulose in this experiment. About 1 mg of the mixture was wrapped by a pyrofoil with Curie point at 358 °C (F358, Japan Analytical Industry), set into the pyrolyzer, and then pyrolyzed. The pyrolysis was performed at 358 °C for 5 s in helium. Volatiles from the pyrolysis were directly injected into the injection port of a GC/MS (PerkinElmer, Clarus SQ 8). GC/MS was equipped with a capillary column TC-1701 (GL Sciences, 60 m length, 0.25 mm inner diameter, 0.25 μm film thickness) and a quadrupole analyzer. Its operation conditions can be found elsewhere [33, 34].

2.2.3 Catalytic reforming of volatiles by an updraft fixed bed pyrolyzer

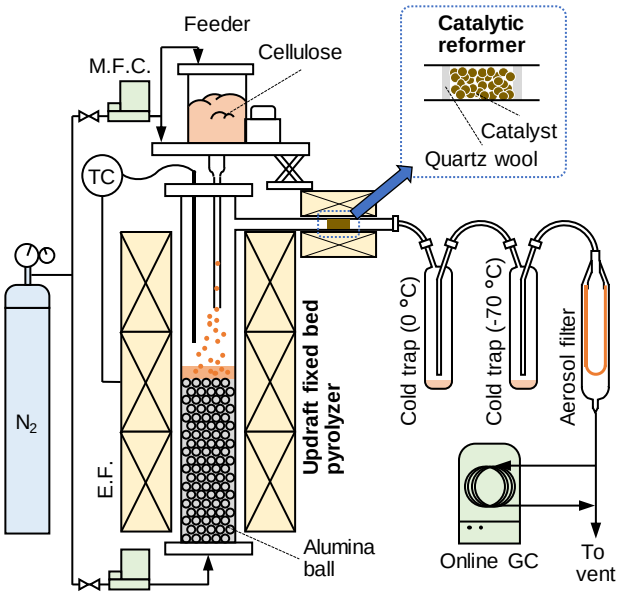

Fig. 2-2 Schematic of the experimental system for two-step cellulose conversion. M.F.C., E.F., and T.C. denote mass flow controller, electric furnace, and temperature controller, respectively.

A schematic diagram of the experimental set up for the two-step conversion of

cellulose to LGO is presented in **Fig. 2-2**. The updraft fixed bed pyrolyzer consisted of stainless tube (i.d. = 3.5 cm), aluminum balls (diameter = 0.6 cm), and cellulose feeding tube. The reactor was heated by an electrical furnace under a flow of nitrogen (100 mL/min from cellulose feeder and 900 mL/min from the reactor bottom). After confirming the temperature inside the reactor, cellulose was continuously fed into the pyrolysis zone with a particle feeder (TF-70-CT, Aishin NanoTechnology) at a rate of 0.15 g/min for 0.5 h. The pyrolysis volatiles generated from cellulose in the course of dropping or after dropping passed through hot void space above the alumina ball (residence time = 1.8 s) and then entered the catalytic reformer. The catalyst particles were loaded in the reformer (i.d. = 0.9 cm) by sandwiching with quartz wools. 1.0 g of P/AC, S/AC or IL (excluding support) were used in each experiment. The condensable vapor from the reformer was collected in two cold traps (0 °C and -70 °C) and an aerosol filter (room temperature) as a bio-oil. The bio-oil was recovered from the condensers with methanol and then subjected to composition analysis with GC/MS operated at conditions above. The recovered bio-oil was also analyzed by liquid chromatography on a Shimadzu LC-20 prominence series equipped with a photo diode array and refractive index detectors for quantification of LGA and LGO. The standard samples of LGA and LGO were purchased from Wako Pure Chemical Industries and Circa Group, respectively. Analytes were separated with a BioRad Aminex 87H column at 35 °C and 5 mM sulfuric acid as a mobile phase at a flow rate of 0.6 mL/min. Non-condensable gas was analyzed by an online gas chromatograph (Micro GC 490,

Agilent).

Fourier transform infrared (FT-IR) spectrum of the bio-oil was recorded on a PerkinElmer FT-IR spectrometer in an attenuated total reflection mode. Thermogravimetric analysis of AC before and after the experiment was conducted in a thermogravimetric analyzer (TGA, model STA7200, Hitachi Hi-Tech Science). The sample was heated to 800 °C with a heating rate of 5 °C/min under a flow of 10% O_2/N_2 (300 mL/min).

2.3 Results and discussion

2.3.1 Catalytic rapid pyrolysis of cellulose with the micro pyrolyzer

The catalysis of prepared catalysts was tested with catalytic rapid pyrolysis using Curie point pyrolyzer. This was to simulate experiments in a previous paper [19], which revealed that LGO was selectively formed from fast pyrolysis of cellulose, when mixed with P/AC, in a drop tube type reactor. The pyrolysis temperature of 358 °C was selected to avoid volatilization and decomposition of IL [23] while was high enough to release volatiles from cellulose with a sufficient reaction time. Since active sites of supported IL phase catalysts are IL, in this experiment, IL itself, without use of support, was mechanically mixed with cellulose and pyrolyzed. **Fig. 2-3** shows GC/MS chromatograms of volatiles from the non-catalytic and catalytic rapid pyrolysis. In the non-catalytic pyrolysis of cellulose, LGA was a primary product together with a small amount of other anhydrosugars such as LGO and 1,6-anhydro-β-D-glucofuranose (AGF). The presence of employed catalysts significantly altered the volatiles

composition, producing LGO as the primary product. The catalytic performance of S/AC and P/AC was thus confirmed. This is in accordance with the reported result [19]. These catalysts promote the dehydration of cellulose, anhydrosugar oligomers and LGA to form LGO by acidic catalysis. On the other hand, despite the absence of acidic function, IL also showed a good catalysis for the LGO formation. Moreover, as quantitatively presented in **Fig. 2-4**, IL showed higher LGO yield than S/AC and P/AC, although this is not necessarily a fair comparison due to the difference in the amount of active sites. The volatiles from catalytic pyrolysis also contained noticeable amount of other compounds, mainly furans, indicating the excess catalysis toward side reactions.

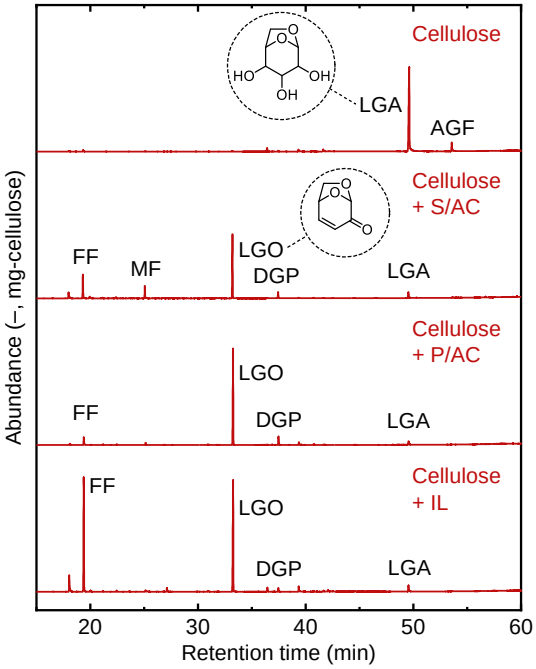

Fig. 2-3 GC/MS chromatograms of volatiles from catalytic rapid pyrolysis of cellulose at 358 °C. The catalyst/cellulose ratio was fixed at 1/3 by weight. (FF) furfural, (MF) 5-methylfurfural, (LGO) levoglucosenone, (DGP) 1,4:3,6-dianhydro-α-D-glucopyranose, (LGA) legoclucosan, (AGF) 1,6-anhydro-β-D-glucofuranose.

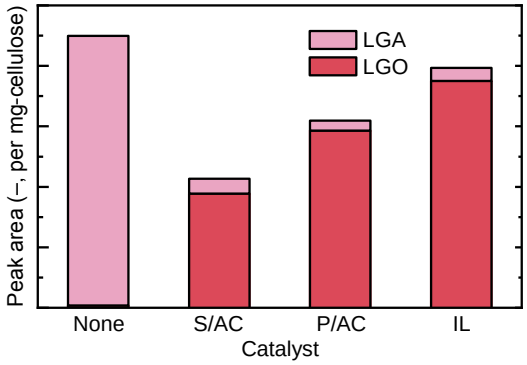

Fig. 2-4 Peak area of LGA and LGO in GC/MS chromatograms of volatiles from catalytic rapid pyrolysis of cellulose at 358 °C.

2.3.2 Cellulose pyrolysis in the updraft fixed bed reactor

Prior to the catalytic reforming test, experimental conditions for cellulose pyrolysis in the updraft fixed bed reactor were optimized. The feeding rate of cellulose and flow rate of carrier gas (N_2) were fixed at 0.15 g/min and 1000 mL/min, respectively, and the influence of pyrolysis temperature on the product distribution was investigated. Under the present experimental conditions, flow out of cellulose and char particles to the catalytic reformer was not observed. The reformer was installed at the outlet of the pyrolyzer and kept at 350 °C, but the catalyst was not loaded in this experiment. The experimental results are summarized in **Fig. 2-5**. The yield of char was determined from the solid residue at the reactor bottom. The yield of coke, including sticky heavy molecules, deposited over the reactor wall was calculated by difference of the total product yield (gas, bio-oil, and char) from 100 wt%. The yields of char and coke decreased with increase in the reaction temperature. Within the employed range of temperature, higher temperature was thus better for suppressing condensation of volatiles and led to higher yield of volatiles (gas + bio-oil). A sharp increase of gas yield

from 500 to 600 °C indicates occurrence of severer cracking of volatiles above this range of temperature. This is also clear from the changes in the gas composition shown in **Fig. 2-5(b)**. Below 400 °C, CO_2 was the dominant gaseous product, which was mainly directly from the primary volatiles [35]. The yield of H_2 and CO sharply increased when ramping the temperature from 400 to 600 °C due to the secondary thermal reactions of the primary volatiles. As a result, the bio-oil yield showed a maximum of 71.3 wt% at 450 °C.

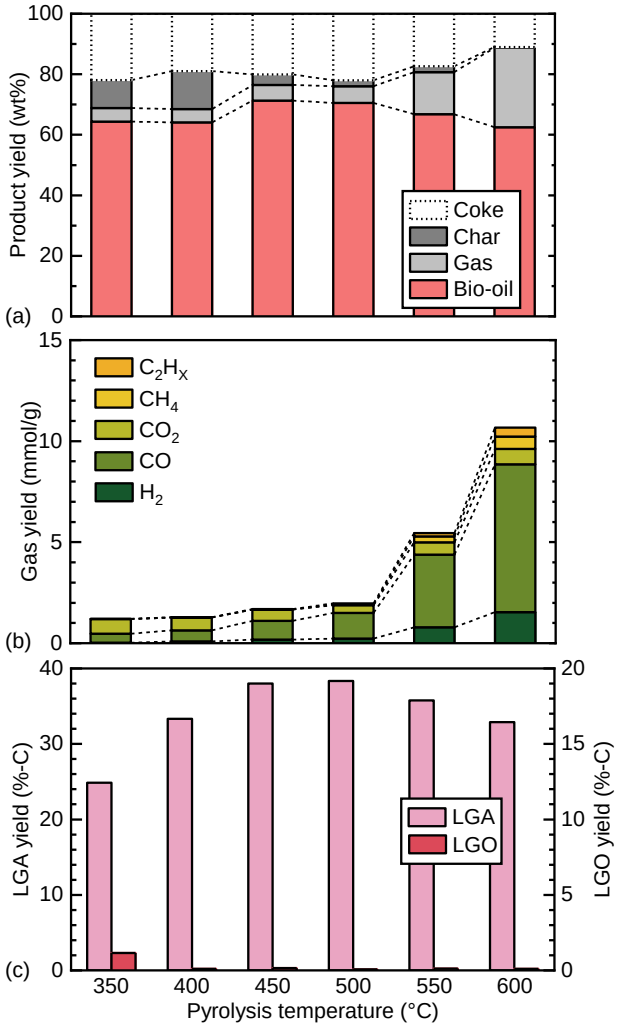

Fig. 2-5 Yields of products from pyrolysis of cellulose in the updraft fixed bed at different temperatures without catalytic reforming.

Table 2-2 Relative peak area (%) of compounds identified in bio-oil by GC/MS analysis.

		Without reforming						With reforming (pyrolysis at 500 ℃)						
		Pyrolysis temperature (℃)						Reforming at 350 ℃				IL/AC (℃)		
Peak	Compound name	350	400	450	500	550	600	P/AC	S/AC	IL/Al_2O_3	Il/SiO_2	350	275	200
1	Methylglyoxal	<0.1	0.1	0.1	0.4	0.7	0.7	0.4	0.6	4.5	4.2	1.0	0.1	1.6
2	Glycolaldehyde	-	0.2	0.3	0.6	1.4	1.8	0.6	0.7	-	-	0.8	0.9	1.9
3	Formic acid	-	-	-	0.1	0.2	0.5	-	0.2	<0.1	<0.1	0.2	0.3	0.8
4	Acetic acid	-	0.1	0.1	0.1	0.3	0.6	0.2	0.5	-	-	0.9	0.6	2.7
5	Acetol	-	-	0.2	0.3	1.1	0.2	0.3	0.9	-	-	<0.1	<0.1	2.6
6	1,3-Dihydroxypropan-2-one	-	-	<0.1	0.1	0.1	0.1	<0.1	0.1	-	-	0.1	<0.1	0.2
7	Acetoin	-	-	-	-	<0.1	0.1	<0.1	<0.1	-	-	<0.1	<0.1	-
8	Propanoic acid	-	-	-	<0.1	0.1	0.2	0.1	0.3	-	-	0.3	0.2	0.5
9	2-Oxobutanol	-	-	<0.1	0.1	0.1	0.1	0.1	0.1	0.2	0.1	<0.1	0.1	0.3
10	2,5-Dimethoxytetra hydrofuran	-	-	<0.1	-	0.2	0.2	0.1	0.3	0.1	0.1	<0.1	0.1	0.3
11	Succindialdehyde	-	-	-	0.1	0.2	0.3	<0.1	<0.1	-	-	0.1	0.3	0.1
12	Butanoic acid	-	-	-	<0.1	0.1	0.2	<0.1	0.1	-	-	0.1	0.1	0.1
13	Furfural	0.9	0.2	0.2	0.4	0.2	0.4	0.3	0.5	4.6	2.3	2.5	1.5	3.4
14	α-Angelicalactone	0.3	0.1	<0.1	<0.1	<0.1	-	0.1	0.2	0.1	0.3	0.4	0.3	0.7
15	2-Furanmethanol	0.1	<0.1	<0.1	<0.1	0.1	0.1	<0.1	-	-	-	0.1	0.1	-
16	2-Methylcyclopent-2-enone	-	-	-	<0.1	<0.1	0.1	0.0	0.2	<0.1	0.1	0.2	0.1	0.4
17	Acetylfuran	0.1	0.5	0.6	<0.1	0.5	0.2	0.5	0.7	-	-	0.1	2.1	1.4
18	4-Cyclopentene-1,3-dione	0.1	0.1	0.1	<0.1	0.1	0.1	0.1	0.1	0.1	0.1	<0.1	0.1	0.4
19	4-Hydroxydihydro furan-2(3H)-one	0.2	0.3	0.4	0.3	0.2	<0.1	0.3	0.4	-	-	0.6	0.7	1.9
20	2-Hydroxycyclopent-2-enone	0.2	0.3	0.3	0.5	0.9	0.9	0.6	1.9	1.3	1.3	1.7	1.2	3.9
21	5-Methylfurfural	0.2	0.1	0.1	0.1	0.1	0.1	0.2	1.0	1.3	0.6	1.4	1.1	1.7
22	Butyrolactone	<0.1	<0.1	<0.1	0.1	0.1	0.2	0.1	0.1	0.2	0.1	0.2	0.1	0.4
23	2(5H)-Furanone	0.1	0.1	0.1	0.1	0.2	0.2	0.1	0.3	0.2	0.2	0.4	0.3	1.0
24	5-Methyl-2(5H)-furanone	0.1	<0.1	<0.1	<0.1	0.1	<0.1	0.1	0.2	0.3	0.1	0.2	0.2	0.8
25	3-Methylcyclopent-2-enone	0.4	0.4	0.3	0.2	0.1	-	0.2	0.3	0.7	0.4	0.7	0.7	2.1
26	2H-Pyran-2-one	<0.1	<0.1	<0.1	<0.1	0.1	0.2	0.1	0.2	0.1	0.1	0.2	0.1	0.4
27	4H-Pyran-4-one	-	-	-	<0.1	0.1	0.3	<0.1	0.1	-	-	0.1	0.1	0.1
28	Corylon	0.2	0.2	0.1	0.1	0.1	0.1	0.2	1.5	0.5	0.6	2.3	2.0	2.3

29	3-Methyl-2(5H)-furanone	0.1	0.1	0.1	0.1	<0.1	0.1	0.1	0.4	-	-	0.4	0.4	1.0
30	Phenol	<0.1	<0.1	<0.1	<0.1	0.1	0.2	0.1	<0.1	-	-	0.3	0.2	0.8
31	Furaneol	0.2	0.2	0.2	0.1	<0.1	<0.1	0.1	0.1	0.4	0.3	0.5	0.5	1.1
32	2-Methylphenol	-	-	-	<0.1	0.1	<0.1	<0.1	<0.1	-	-	0.2	0.1	0.3
33	Methyl 2-furoate	0.2	0.1	<0.1	0.1	0.1	<0.1	0.2	0.2	-	-	2.5	1.2	2.0
34	4-Methyl-2(5H)-furanone	0.1	0.1	0.1	0.1	<0.1	<0.1	0.1	0.2	<0.1	0.2	0.4	0.2	1.1
35	LGO	3.2	0.7	0.4	0.2	0.1	0.1	1.3	4.3	74.3	82.6	67.0	64.2	21.6
36	5-Hydroxymaltol	0.3	0.2	0.1	<0.1	<0.1	0.1	0.1	3.5	<0.1	0.1	0.3	0.3	1.0
37	LAC	0.6	1.1	1.4	2.0	2.2	1.7	2.2	3.6	10.8	6.2	4.9	5.5	17.6
38	DGP	3.8	1.7	0.9	0.6	0.4	0.2	1.1	1.2	0.2	0.1	3.7	6.7	16.6
39	MAGF	0.1	<0.1	<0.1	0.1	0.1	<0.1	0.1	0.1	-	-	<0.1	0.1	0.2
40	5-Hydroxymethyl furfural	1.2	0.6	0.5	0.7	0.3	0.4	0.5	0.5	-	-	0.1	0.7	0.7
41	DH	0.7	0.6	0.5	0.1	0.3	0.1	0.7	1.3	-	-	0.2	0.5	0.6
42	ADGH	5.2	5.0	2.9	1.6	0.2	0.0	1.5	1.4	-	-	4.2	5.4	2.6
43	Resorcinol	-	<0.1	<0.1	<0.1	<0.1	0.1	<0.1	0.1	-	-	0.7	0.3	
44	2-Butene-1,4-diol	<0.1	0.1	0.1	0.2	0.2	0.1	0.3	0.2	-	-	0.1	0.2	0.9
45	D-Allose	0.2	0.1	0.1	0.1	0.0	-	0.1	0.1	-	-	-	-	-
46	AXP	0.2	0.1	0.1	0.1	<0.1	<0.1	0.4	0.1	-	-	-	-	-
47	LGA	78.2	83.8	85.8	86.2	85.8	86.5	81.4	66.7	-	-	-	-	-
48	AGF	3.2	3.0	3.7	4.3	2.7	2.5	5.2	4.8	-	-	-	0.1	-

(LAC) 1-Hydroxy, (1R)-3,6-dioxabicyclo[3.2.1]octan-2-one, (DGP) 1,4:3,6-Dianhydro-α-D-glucopyranose, (MAGF) Methyl 3,6-anhydro-b-D-glucopyranoside, (DH) 6,8-Dioxabicyclo[3.2.1]octane-2,4,4-triol, (ADGH) 1,5-Anhydro-4-deoxy-*D-glycero*-hex-1-en-3-ulose, (AXP) 1,4-Anhydro-D-xylopyranose, (AGF) 1,6-Anhydro-β-D-glucofuranose.

The volatiles from cellulose pyrolysis contained various organics, for example, organic acids, furans, anhydrosugars, and anhydrosugar oligomers. On the other hand, as shown in **Table 2-2** and evidenced in many past studies, the primary component was always LGA regardless of the pyrolysis temperature (350–600 °C). The yield of LGA showed a trend similar to the bio-oil yield. The maximum LGA yield of 38.4 wt%-C was observed at pyrolysis temperature of 500 °C. Above this temperature, LGA can be decomposed to small fragmented products, such as C_{1-3} organics and non-condensable gases [36]. Because LGA was a main feedstock for LGO in the catalytic reforming

section, the best pyrolysis temperature was thus determined to be 500 °C.

As recently discussed by Maduskar et al. in their report [29], LGA yield reported in literatures varies over a wide range of 5–80%. Although the reason has not been fully understood, analytical pyrolysis using small reactors loaded with a tiny amount of cellulose, such as CDS pyroprobe and frontier micropyrolyzer, generally provide high LGA yields. This indicates the importance of suppression of interaction between solid (unpyrolyzed, pyrolyzing, and pyrolyzed cellulose) and the volatiles [37]. In our previous study [21], the yield of LGA was only 12.7% when 0.5 g of cellulose loaded in a quartz tube was pyrolyzed at a slow heating rate. On the other hand, the volatiles had little opportunity to have a contact with solid (only with diluted falling cellulose) in the updraft fixed bed reactor of the present study, which likely resulted in the relatively high LGA yield of 38.4%. To the best of our knowledge, this is the first study that examined updraft fixed bed reactor for producing LGA with the purpose of LGO production. A fluidized bed reactor also enables high yield production of LGA (e.g., 40% [38]) but is not necessarily suitable for the two-step reaction system of this study because a high flow rate of carrier gas is required in the pyrolyzer for the fluidization of bed material and necessitates the use of more amount of catalyst in the reformer.

The cellulose pyrolysis also produced LGO but with the low yield below 1.2 %-C (350 °C). LGO decomposed in the gas phase more easily than LGA because of the high reactivity of α,β-unsaturated ketone and protected aldehyde functionality [13]. Therefore, the LGO yield decreased to less than <0.1% at >350 °C. The result indicated

that the temperature of catalytic reforming in the reactor following the pyrolysis should not be higher than 350 °C.

2.3.3 Catalytic reforming of volatiles from cellulose pyrolysis

The volatiles from updraft fixed bed pyrolyzer operated at 500 °C were reformed over several types of catalysts, i.e., P/AC, S/AC, IL/AC, IL/Al_2O_3, and IL/SiO_2, at 350 °C. The products from the two-step conversion are compared in the left part of **Fig. 2-6**. The yield of coke deposited over catalyst (coke-CR) was determined from the difference in the weight of catalyst before and after the experiment. In the case of supported IL phase catalysts, the weight difference was calculated from the weight of solid after removing IL with ethanol and the following filtration and drying. A considerable amount of coke was deposited over catalysts with the yield in the range of 14.0–20.4 wt%. This is problematic since it can deactivate catalyst and cause plugging of reactor tube. One of the objectives of this study is to identify and quantitatively show such operational problems for solving them in a future work. The coke formation caused difference in the bio-oil yield (60.0–68.6 wt%), depending on the catalyst type. The yield of gaseous product was little affected by the type of catalyst (8.0–9.9 wt%).

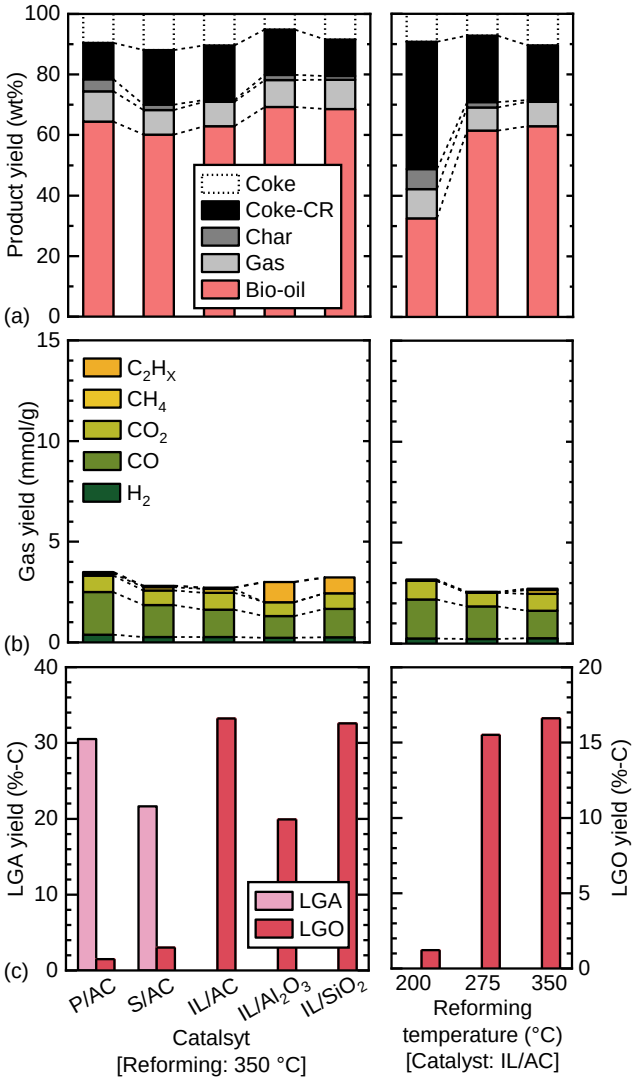

Fig. 2-6 Yields of products from the two-step cellulose conversion with catalytic reforming. Temperature for the pyrolysis in updraft fixed bed was fixed at 500 °C.

The composition of bio-oil was significantly affected by the catalyst type. The major component was LGA in the reforming with P/AC and S/AC while LGO in that with supported IL phase catalysts. This was in contrast to the result of catalytic rapid pyrolysis, where all the catalysts (P/AC, S/AC, and IL) showed the activity toward LGO formation. The clear difference in the bio-oil composition can be confirmed from FT-IR spectra (**Fig. 2-7**). The bio-oils prepared with supported IL phase catalysts had a

prominent absorbance at 1697 cm−1, which is assigned to CO stretching vibration, suggesting the presence of LGO. On the other hand, the spectra of bio-oils prepared without catalyst and with P/AC and S/AC did not present clear absorbance for the ketone group. It is seen from the detailed composition of the bio-oils (**Table 2-2**) that no LGA could survive the reforming over supported IL phase catalysts. The bio-oils prepared with P/AC and S/AC contained compounds similar to that without catalyst.

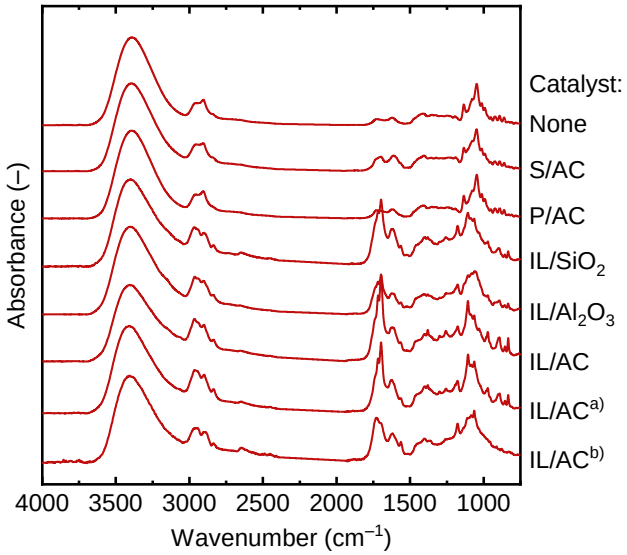

Fig. 2-7 FT-IR spectra of bio-oils obtained from the two-step cellulose conversion. Temperatures for pyrolysis and catalytic reforming were 500 °C and 350 °C, respectively. [a)] reforming at 275 °C and [b)] reforming at 200 °C.

The mechanism of LGO formation should be essentially same between the catalytic rapid pyrolysis and catalytic reforming of volatiles from cellulose pyrolysis. Nevertheless, the result was thus very different. The most plausible explanation on this result is that P/AC and S/AC was quickly deactivated in the reforming. The yields of coke-CR were 14.0 and 20.4 wt%, respectively. The pyrolysis volatiles were absorbed over the acid sites, deposited as coke and deactivated them at the initial stage of

experiment. Apparently, the catalyst bed after the deactivation was nearly inert even to the coke deposition. Thus, P/AC and S/AC, which showed good performances in catalytic rapid pyrolysis of this work and studies in literature [19], were unavailable to the continuous reforming of volatiles from cellulose pyrolysis.

The maintenance of catalytic activity of supported IL phase catalysts clearly shows that the active sites are IL itself. These catalysts also suffered from the coke deposition at the level similar to those of P/AC and S/AC. In fact, the surface area of support material decreased significantly after the reforming (e.g., from 1322 to 201 m^2/g in the case of AC (reforming at 350 °C)). TG and DTG curves of fresh and spent AC (**Fig. 2-8**) revealed the presence of newly added carbonaceous material (coke) deposited from the volatiles. However, the coke deposition mainly occurred over the support surface and did not necessarily influence the catalytic activity of IL. Due to the mobile characteristic, IL freely shuttled in the pore of support and moved to the coke surface to present its catalysis.

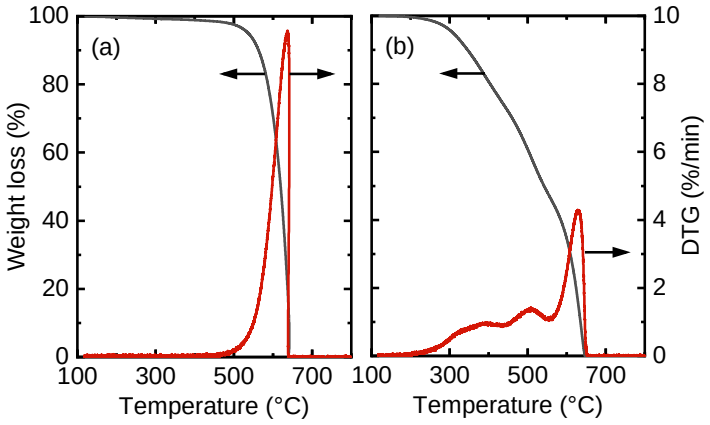

Fig. 2-8 TG analysis of (a) fresh and (b) spent AC. The spent AC was from the reforming at 350°C, and it was washed with ethanol for removing IL, filtered and then dried before the TG analysis.

Because the same amount of IL was used in the reforming, and the pores of support were filled with IL, it was expected that the type of support material had little influence on the product yield. IL/AC and IL/SiO_2 indeed resulted in similar yields, but IL/Al_2O_3 showed lower LGO yield. This was possibly attributed to the relatively strong acidity of Al_2O_3 (γ-type), which showed catalysis toward LGA, precursor of LGO, to form by-products such as gas and coke, though the coke-CR yield was similar to others. Alternatively, the acidic catalysis may promote decomposition of IL that is gradually decomposed to volatiles at this temperature even under inert atmosphere [21]. The IL maintained in IL/Al_2O_3, IL/SiO_2, IL/AC during the reforming test was 47.3, 69.5, and 73.9%, respectively. The IL decomposition is also highly problematic in the continuous operation and should be suppressed by applying lower temperatures, although 350 °C was employed for better comparison with P/AC and S/AC in this test. The loss of IL was indeed scarcely observed in the reforming at 275 and 200 °C.

The influence of reforming temperature is presented in the right part of **Fig. 2-6** for IL/AC, which showed the best performance along with IL/SiO_2 among the catalysts examined in this study. Decrease in the reforming temperature resulted in lower LGO yield and higher coke-CR yield at 200 °C in particular. At 200 °C, the LGO yield was only 1.2 %-C with considerable coke deposition (47.7 wt%). The result indicates that, when the reforming temperature is not sufficiently high, major portion of LGA polymerizes and deposits as coke before or after the conversion into LGO. It is to be noted that the IL employed in this study ([BMMIM]OTf) has catalysis for dehydration

of saccharides even below 200 °C [23].

The highest LGO yield obtained in this study is 16.6 %-C with IL/AC. Considering the LGA yield in the updraft fixed bed pyrolyzer (38.4 %-C), the selectivity from LGA to LGO is less than half (43.3%). In our previous study [21] with a small scale reactor (cellulose feed: 0.5−1.2 g), the highest LGO yield was 31.6 %-C from volatiles containing LGA with the yield of 22.6 %-C from cellulose. It was concluded that the yield of LGO higher than that of LGA was caused by depolymerization of anhydrosugar oligomers and their conversion to LGO. Based upon this previous data, the lower LGO yield, compared to LGA yield, indicates that the catalytic activity of IL/AC (and other supported IL phase catalysts) deteriorated during the operation. Nonetheless, this is the first report for the LGO production with the catalytic reforming system, which can be continuously operated, and the yield of 16.6 %-C is not necessarily low, compared to the yields reported in literatures for catalytic rapid pyrolysis, e.g., 18.1 wt% with P/AC [19].

A possible reaction pathway from LGA to LGO under catalysis of IL ([BMMIM]OTf) is proposed on the basis of our experiments with various ILs for reactions relevant to LGO formation [23] and presented in **Fig. 2-9**. At first, triflate anion, which has hydrogen-bond basicity, interacts with hydroxyl group on C_4 of LGA, resulting in dehydration to form an enol structure. Subsequently, triflate anion induces a keto-enol tautomerism reaction to form a keto structure. At last, the C_2 hydroxyl group is dehydrated to form carbon double bond. The cation interacts with -OH group and

helps dehydration induced by the anion. The catalysis highly depends on the type of anion. According to our previous results [23], ILs bearing sulfonate anions generally show good performance. On the other hand, the cation also contributes to the catalysis, and the type significantly influences thermal stability of IL. Tuning properties of cation/anion and their combination are problems leading to catalyst deactivation such as coke accumulation and IL decomposition.

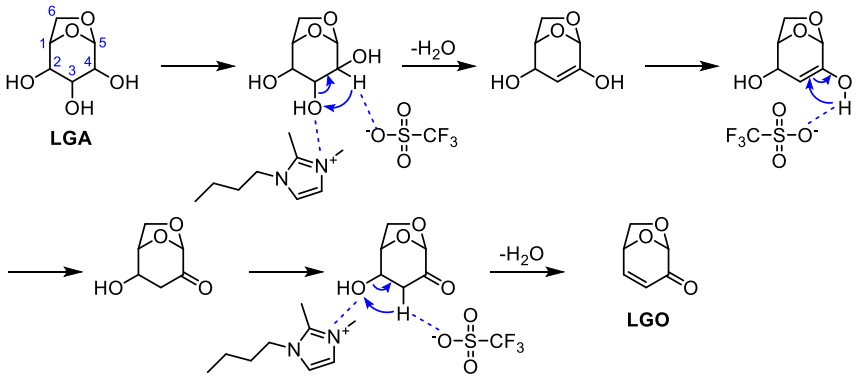

Fig. 2-9 The possible reaction pathway from LGA to LGO with IL ([BMMIM]OTf).

2.4 Conclusions

The two-step conversion of cellulose to LGO was performed with updraft fixed bed pyrolyzer and catalytic reformer with several types of packed bed catalysts. All the catalysts examined in this study (P/AC, S/AC, IL/Al_2O_3, IL/SiO_2, and IL/AC) presented the activity toward LGO formation in catalytic rapid pyrolysis of cellulose, but the catalysts available for the two-step process were limited to the supported IL phase catalysts. Active sites of P/AC and S/AC were deactivated by coke deposition at the initial stage of the reforming and could produce little LGO in the reforming. Due to the richness in active sites (IL itself), the supported IL phase catalysts did not allow LGA,

which was supplied from the pyrolyzer at the yield of 38.4 %-C, to survive the reforming during the operation of 0.5 h. The continuous production of LGO with a relatively high yield of 16.6 %-C was demonstrated. However, the supported IL phase catalysts also suffered from the coke deposition. The coke precursor included LGA, resulting in the low selectivity of LGO from LGA at 43.3 %-C. Furthermore, another problem of IL decomposition was quantitatively identified. For avoiding the IL decomposition, the employment of AC and SiO_2 as the support material rather than Al_2O_3, having acidity, was effective, and lower reforming temperature was recommended, although the coke deposition was promoted when it was too low (e.g., 200 °C).

2.5 References

[1] G.W. Huber, S. Iborra, A. Corma, Synthesis of transportation fuels from biomass: chemistry, catalysts, and engineering, Chem. Rev., 106 (2006) 4044-4098.

[2] Y. Muranaka, H. Nakagawa, I. Hasegawa, T. Maki, J. Hosokawa, J. Ikuta, K. Mae, Lignin-based resin production from lignocellulosic biomass combining acidic saccharification and acetone-water treatment, Chem. Eng. J., 308 (2017) 754-759.

[3] X. Huang, J.P. Cao, X.Y. Zhao, J.X. Wang, X. Fan, Y.P. Zhao, X.Y. Wei, Pyrolysis kinetics of soybean straw using thermogravimetric analysis, Fuel, 169 (2016) 93-98.

[4] M.A. Akhtar, S. Zhang, X. Shao, H. Dang, Y. Liu, T. Li, L. Zhang, C. Z. Li, Kinetic compensation effects in the chemical reaction-controlled regime and mass

transfer-controlled regime during the gasification of biochar in O_2, Fuel Process. Technol., 181 (2018) 25-32.

[5] Q. Lu, H.Q. Guo, M.X. Zhou, M.S. Cui, C.Q. Dong, Y.P. Yang, Selective preparation of monocyclic aromatic hydrocarbons from catalytic cracking of biomass fast pyrolysis vapors over Mo_2N/HZSM-5 catalyst, Fuel Process. Technol., 173 (2018) 134-142.

[6] K.G. Kalogiannis, S.D. Stefanidis, A.A. Lappas, Catalyst deactivation, ash accumulation and bio-oil deoxygenation during ex situ catalytic fast pyrolysis of biomass in a cascade thermal-catalytic reactor system, Fuel Process. Technol., 186 (2019) 99-109.

[7] S. Papari, K. Hawboldt, A review on condensing system for biomass pyrolysis process, Fuel Process. Technol., 180 (2018) 1-13.

[8] R. Rinaldi, F. Schüth, Acid hydrolysis of cellulose as the entry point into biorefinery schemes, ChemSusChem, 2 (2009) 1096-1107.

[9] R. Rinaldi, F. Schüth, Design of solid catalysts for the conversion of biomass, Energy Environ. Sci., 2 (2009) 610-626.

[10] M. Zavrel, D. Bross, M. Funke, J. Buchs, A.C. Spiess, High-throughput screening for ionic liquids dissolving (ligno-)cellulose, Bioresour. Technol., 100 (2009) 2580-2587.

[11] C. Liu, H. Wang, A.M. Karim, J. Sun, Y. Wang, Catalytic fast pyrolysis of lignocellulosic biomass, Chem. Soc. Rev., 43 (2014) 7594-7623.

[12] S.H. Krishna, T.W. Walker, J.A. Dumesic, G.W. Huber, Kinetics of levoglucosenone isomerization, ChemSusChem, 10 (2016) 129-138.

[13] A. Flourat, A. Peru, A. Teixeira, F. Brunissen, F. Allais, Chemo-enzymatic synthesis of key intermediates (S)-γ-hydroxymethyl-α, β-butenolide and (S)-γ-hydroxymethyl-γ-butyrolactone via lipase-mediated Baeyer-Villiger oxidation of levoglucosenone, Green Chem., 17 (2015) 404-412.

[14] S.H. Krishna, D.J. McClelland, Q.A. Rashke, J.A. Dumesic, G.W. Huber, Hydrogenation of levoglucosenone to renewable chemicals, Green Chem., 19 (2017) 1278-1285.

[15] C. Paris, M. Moliner, A. Corma, Metal-containing zeolites as efficient catalysts for the transformation of highly valuable chiral biomass-derived products, Green Chem., 15 (2013) 2101-2109.

[16] M.B. Comba, Y.h. Tsai, A.M. Sarotti, M.I. Mangione, A.G. Suárez, R.A. Spanevello, Levoglucosenone and its new applications: valorization of cellulose residues, Eur. J. Org. Chem., 2018 (2018) 590-604.

[17] P. Ray, T. Hughes, C. Smith, G.P. Simon, K. Saito, Synthesis of bioacrylic polymers from dihydro-5-hydroxylfuran-2-one (2H-HBO) by free and controlled radical polymerization, ACS Omega, 3 (2018) 2040-2048.

[18] H.Y. Zhang, X. Meng, C. Liu, Y. Wang, R. Xiao, Selective low-temperature pyrolysis of microcrystalline cellulose to produce levoglucosan and

levoglucosenone in a fixed bed reactor, Fuel Process. Technol., 167 (2017) 484-490.

[19] X.N. Ye, Q. Lu, X. Wang, H.Q. Guo, M.S. Cui, C.Q. Dong, Y.P. Yang, Catalytic fast pyrolysis of cellulose and biomass to selectively produce levoglucosenone using activated carbon catalyst, ACS Sustainable Chem. Eng., 5 (2017) 10815-10825.

[20] S. Kudo, Z. Zhou, K. Norinaga, J. Hayashi, Efficient levoglucosenone production by catalytic pyrolysis of cellulose mixed with ionic liquid, Green Chem., 13 (2011) 3306.

[21] S. Kudo, N. Goto, J. Sperry, K. Norinaga, J. Hayashi, Production of levoglucosenone and dihydrolevoglucosenone by catalytic reforming of volatiles from vellulose pyrolysis using supported ionic liquid phase, ACS Sustainable. Chem. Eng., 5 (2016) 1132-1140.

[22] H. Kawamoto, S. Saito, W. Hatanaka, S. Saka, Catalytic pyrolysis of cellulose in sulfolane with some acidic catalysts, J. Wood Sci., 53 (2007) 127-133.

[23] S. Kudo, Z. Zhou, K. Yamasaki, K. Norinaga, J. Hayashi, Sulfonate ionic liquid as a stable and active xatalyst for levoglucosenone production from saccharides via catalytic pyrolysis, Catalysts, 3 (2013) 757-773.

[24] A.I. Casoni, M.L. Nievas, E.L. Moyano, M. Álvarez, A. Diez, M. Dennehy, M.A. Volpe, Catalytic pyrolysis of cellulose using MCM-41 type catalysts, Appl. Catal., A, 514 (2016) 235-240.

[25] X.W. Sui, Z. Wang, B. Liao, Y. Zhang, Q.X. Guo, Preparation of levoglucosenone through sulfuric acid promoted pyrolysis of bagasse at low temperature, Bioresour. Technol., 103 (2012) 466-469.

[26] J.E. Camp, Bio-available Solvent Cyrene: Synthesis, Derivatization, and applications, ChemSusChem, 11 (2018) 3048-3055.

[27] V. L. Budarin, K. J. Milkowski, P. Shuttleworth,B.Lanigan, J. H. Clark, D. J. Macquarrie, A. Wilson (University of York), US20110219679A1, 2011.

[28] A.V. Bridgwater, Progress in thermochemical biomass conversion, John Wiley & Sons, 2008, pp. 1500-1508.

[29] S. Maduskar, V. Maliekkal, M. Neurock, P.J. Dauenhauer, On the yield of levoglucosan from cellulose pyrolysis, ACS Sustain. Chem. Eng., 6 (2018) 7017-7025.

[30] X.L Wei, Z. Wang, Y. Wu, Z.M Yu, J. Jin, K. Wu, Fast pyrolysis of cellulose with solid acid catalysts for levoglucosenone, J. Anal. Appl. Pyrolysis, 107 (2014) 150-154.

[31] D. Fabbri, C. Torri, I. Mancini, Pyrolysis of cellulose catalysed by nanopowder metal oxides: production and characterisation of a chiral hydroxylactone and its role as building block, Green Chem., 9 (2007) 1374-1379.

[32] X. Mo, D.E. López, K. Suwannakarn, Y. Liu, E. Lotero, J.G. Goodwin Jr, C. Lu, Activation and deactivation characteristics of sulfonated carbon catalysts, J. Catal., 254 (2008) 332-338.

[33] S.C. Qi, L. Zhang, H. Einaga, S. Kudo, K. Norinaga, J. Hayashi, Nano-sized nickel catalyst for deep hydrogenation of lignin monomers and first-principles insight into the catalyst preparation, J. Mater. Chem. A, 5 (2017) 3948-3965.

[34] S. Kudo, Y. Hachiyama, Y. Takashima, J. Tahara, S. Idesh, K. Norinaga, J Hayashi, Catalytic hydrothermal reforming of lignin in aqueous alkaline medium, Energy Fuels, 28 (2013) 76-85.

[35] X. Huang, J.P. Cao, P. Shi, X.Y. Zhao, X.B. Feng, Y.P. Zhao, X. Fan, X.Y. Wei, T. Takarada, Influences of pyrolysis conditions in the production and chemical composition of the bio-oils from fast pyrolysis of sewage sludge, J. Anal. Appl. Pyrolysis, 110 (2014) 353-362.

[36] A. Fukutome, H. Kawamoto, S. Saka, Processes forming gas, tar, and coke in cellulose gasification from gas-phase reactions of levoglucosan as intermediate, ChemSusChem, 8 (2015) 2240-2249.

[37] N. Sonoyama, J. Hayashi, Characterisation of coal and biomass based on kinetic parameter distributions for pyrolysis, Fuel, 114 (2013) 206-215.

[38] X. Zhuang, H. Zhang, J. Yang, H. Qi, Preparation of levoglucosan by pyrolysis of cellulose and its citric acid fermentation, Bioresour. Technol., 79 (2001) 63-66.

Chapter 3

Conversion of Levoglucosan to Levoglucosenone and Glucose

3.1 Introduction

Lignocellulosic biomass has shown the potential to serve as a bio-renewable source of fine/commodity chemicals and fuels [1, 2]. The development of future greener bio-based industry necessitates a broad range of biomass conversion technologies, such as catalytic, enzymatic, fermentative, and thermochemical processes. Pyrolysis, an effectively thermochemical process with the advantage of high efficiency and technical feasibility, is an alternative process to substitute acid and enzymatic hydrolysis method to give anhydrosugars in high selectivity and yields from lignocellulosic biomass [3]. Levoglucosan (LGA), a prevalent anhydro-sugar, is commonly known as the predominated product in bio-oil by pyrolysis of cellulose-enriched biomass. LGA yield reported in literatures varied a wide range of 5-80% from cellulose pyrolysis [4], milligram scale reactors, such as CDS pyroprobe a frontier micropyrolyzer, generally produce substantial LGA.

Many researches have devoted to investigate the conversion of LGA, most of them focus on the hydration reaction over acid-catalyzed hydrolysis to readily produce glucose [5-7], which is a sustainable platform chemical for the production of biofuels (bioethanol) and bio-based chemicals. However, all of previous studies used the mineral acid to accelerate this reaction, which may need more capital and operating costs because of rigorous reaction conditions requiring special materials for reactor

construction and chemical recovery systems. Furthermore, the recovery process produces significant amounts of waste and cause environmental pollution. Considering these drawbacks, heterogeneous catalysts represent a viable alternative to homogeneous catalysts and may offer an environmental advantage due to their selective and easy to handle nature, reducing equipment corrosion issues and relatively low cost if the catalyst can be easily separated and recycled.

Dehydration of two water molecule of LGA could produce levoglucosenone (LGO), which has recently been obtained extensive concern in the application of asymmetric and enantiopure syntheses [8], polyols [9], polymers [10], solvent [11, 12], commodity/fine chemicals [13-14]. In 2016, LGO production in a large scale process, Furacel process, was launched by the Circa Group in Austria with lignocellulosic biomass as feedstock. Nonetheless, the process was operated by mineral acid and organic solvent, leading to an undesirable waste stream and additional costs for operation and recovery system. Addressing this disadvantage, LGO production from catalytic fast pyrolysis of cellulose has been under investigation. There have been proposed two effective processes for LGO production over pyrolysis, one is direct pyrolysis the mechanical mixture of cellulose and catalyst [15-18], the other is an indirect two-step process, firstly pyrolysis of cellulose and then catalytic reforming of primary volatiles [19]. Both the direct and indirect mechanisms involve the formation of main intermediate, i.e. LGA. The former direct process could result in a substantial yield of char, usually higher than 20% [20], and the interactions among char, volatiles

and catalysts are not unavoidable. Moreover, the separation of catalyst from char significantly complicates the reutilization of the catalyst. To address these challenges, the indirect two-step process was initially developed [21]. Unfortunately, when used a relatively large scale updraft fixed bed pyrolyzer and catalytic reformer, the coke formed severely on the catalyst surface at the initial stage of experiment and therefore hindered for long time reaction effectively, resulting in less LGO formation in the upper chapter. On the other hand, liquid phase reaction was reported to be able to significantly suppress the coke/humin formation [22], high concentration of polar aprotic solvents can stabilize protons and anions well and promote the dehydration of saccharide. Therefore, I would like to propose another modified two-step process for LGO production, firstly obtain LGA from cellulose pyrolysis, and secondly dehydrate it to LGO in the liquid phase reaction. The former one has been studied over the past few years, however, the latter one, to the best of our knowledge, has not been reported yet.

With the aim to contribute to the construction of a feasible chemical industry from LGA process, we here initiated a study employed LGA as the starting material to produce LGO or glucose in liquid phase reaction. The influence of parameters on the dehydration of LGA varied including solvent, catalyst, reaction temperature, and reaction time. Specifically, an anhydrosugar mixture from bio-oil, mainly containing LGA by cellulose pyrolysis, was used as the reagent for LGO and glucose production.

3.2 Experimental

3.2.1 Materials

LGA and LGO were purchased form Carbosynth (UK) and Circa group (Australia), respectively. Glucose was obtained from Sigma-Aldrich. The other reagents (5-hydroxymethylfurfural (HMF), levulinic acid (LA), 1,4-dioxane, 1,2-dimethoxyethane, THF, acetone, acetonitrile, DMF, sulfolane, and DMSO) were purchased from Wako Pure Chemical Industries. All the solvents were subjected to complementary removal of inherent water by addition of $MgSO_4$ before experiment. Bio-oil was prepared from cellulose pyrolysis at 500 ^oC using an updraft fixed bed pyrolyzer according to our previous method, the details are shown in the former chapter. Amberlyst 70 was purchased from Organo, before using it was prewashed with deionized water and ethanol, followed by drying at 105 °C overnight. ZSM-5 (CBV 3024E), mordenite (CBV 21A), beta zeolite (HSZ-980HOA), and Y zeolite (CBV 400) were purchased from Zeolyst International and Tosoh. Nafion NR50 (a perfluorosulfonated ionomer) was purchased from Sigma-Aldrich. Sulfonated carbon was prepared, according to a reported method [23], by sulfonating a palm shell-derived activated carbon (Wako Pure Chemical Industry). Triflic acid pretreated SBA15 (TFA-SBA15) was prepared based on a previous method [24], briefly, SBA 15 was firstly synthesized and then it was functionalized with triflic acid. Nb_2O_5 and $Cs_{2.5}H_{0.5}P_{12}WO_{40}$ were prepared based on a reported literature [25]. 1-Butyl-2,3-dimethylimidazolium triflate (BMMIM-OTf, > 99.0%) ionic liquid was purchased from Ionic Liquids Technologies.

3.2.2 Reaction and product analysis

The experiment of LGA conversion was conducted in a 15 or 35 screw-cap and thick-walled glass vials from Ace Glass. Typically, solvent, 0.1 M of LGA and solid catalyst with a LGA/catalyst mass ratio of 1 were loaded into the reactor. Then, a magnetic stir cane was introduced into the reactor and it was sealed with a PTFE septum. A modified continuous N_2 flow reactor was developed to flush the generated water during the reaction. The diagram of the reactor without and with N_2 flushing is shown in **Fig. 3-1**. The reactor was immersed in an isothermal oil bath and stirred at a constant rate of 700 rpm. After a prescribed time, the reactor was quenched in an ice batch to stop the reaction, followed by filtration with a 0.22 μm PTFE membrane filter, and then analyzed by a high-performance liquid chromatography (HPLC, Shimadzu LC-20 prominence series). For the experiment conducted in NaCl−H_2O/acetone biphasic phase. In a typical experiment, 2 mL of H_2O, 6 mL of acetone, 600 mg of NaCl, 32 mg of Amberlyst 70, 200 mM of substrate, 25 mM of $AlCl_3$ were successively introduced into a 30 mL of PTFE-lined autoclave reactor. The BioRad Aminex HPX-87H column was used to separate the reactant. The chromatography was operated at 35 °C, and 5 mM sulfuric acid was used as mobile phase with a flow rate of 0.6 mL/min. The reactants were quantified with a calibration curve obtained by the measurement of standard samples. Due to commercial unavailability of 1,6-Anhydro-β-D-glucofuranose (AGF), it was quantified using the calibration curve of LGA by assuming the equivalent sensitivity towards refractive index detector. Carbon balance (C bal) is defined as the total yield of identified compounds by HPLC. The Brunauer-Emmet-Teller surface area

(S_{BET}) and total pore volume (V_{total}) of the catalysts were calculated from N_2 isotherm at –196 °C, which were measured on a Quantachrome, NOVA 3200e.

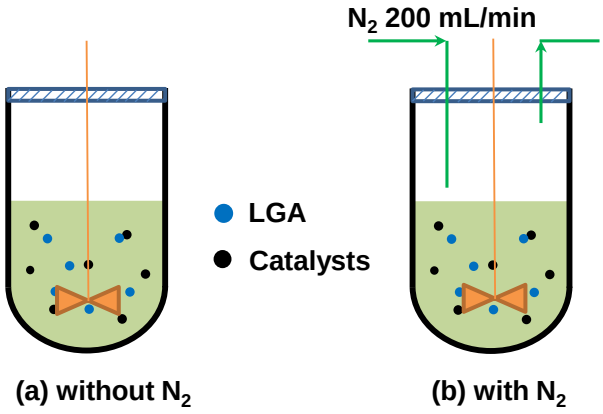

Fig. 3-1 A schematic of the batch reactor (a) without and (b) with N_2.

3.3 Results and discussion

3.3.1 Solvent effect

The primary products from LGA degradation are LGO, AGF and glucose. LGO was formed by dehydrating two water molecules while glucose was produced by hydrating one water molecule. AGF was formed by the rearrangement reaction. **Table 3-1** screened nine different solvents for the LGO conversion. Half of LGA conversion was achieved in 1,4-dioxane, a non-polar solvent, resulting to LGO, AGF and glucose in selectivity of *ca.* 3.3%, 5.7% and 3.0%, respectively. The polar aprotic solvents, such as 1,2-dimethoxyethane and THF significantly promoted LGA conversion to as much as *ca.* 90.6 and 95.6%, respectively. The C bal was, however, estimated to be much lower than that of in 1,4-dioxane, which was ascribed to the dominated polymerization reaction before or after LGA conversion as a possible result of the varied polarity of LGA with 1,2-dimethoxyethane and THF. As Hu et al. [26] suggested, LGA has a relatively low

solubility in solvent with weak dipole moment and shows high affinity with the Amberlyst 70 due to its high concentration of polar sulfo group. High LGA conversion of *ca.* 90% was also attained in sulfolane. The oligomer formation is obvious from C bal, as also evinced by the visible color change of the catalyst from brown to dark in merely 5 min. Compared to DMSO, the LGA conversion in DMF was much lower, probably because the acid-base reaction between Amberlyst 70 and DMF led to the deactivation of the catalyst [26]. It is important to highlight that both DMSO and NMP were effective to promote the dehydration reaction of LGA to LGO, leading to LGO selectivity of *ca.* 35.8 and 31.3%, respectively. NMP also favored the isomerization reaction of LGA to AGF, attaining selectivity of *ca.* 36.3%. Considering the LGO selectivity, DMSO performed as the most suitable solvent and was used in the following experiment.

Table 3-1 LGO conversion in different solvents.

Entry	Solvent	Dipole moment (D)	Time (h)	Conv. (%)	Selectivity (%)				C bal (%)
					LGO	AGF	Glucose	HMF	
1	1,4-Dioxane	0.45	1	49.4	13.3	5.7	3.0	1.0	61.9
2	1,2-Dimethoxyethane	0.86	1	95.6	8.2	1.7	0.4	0.5	14.8
3	THF	1.75	1	90.6	8.9	3.5	1.0	0.1	21.7
4	Acetone	2.88	1	71.8	3.5	4.7	14.5	1.8	45.8
5	DMF	3.82	12	26.0	4.3	2.8	9.8	1.1	78.7
6	Acetonitrile	3.92	4	37.6	2.0	2.7	2.7	0.3	65.3
7	DMSO	3.96	12	84.5	35.8	12.7	4.1	12.8	70.7
8	Sulfolane	4.35	1	90.0	4.1	3.4	12.1	7.2	34.1
9*	NMP	12.26	1	36.8	31.3	36.3	5.8	4.3	91.8

Reaction conditions: 140 ^{o}C, LGA 0.1 M, solvent 5 mL, LGA/Amberlyst 70 = 1 (*w/w*), * 160 ^{o}C.

3.3.2 Catalyst effect

It is commonly known that the heterogeneous catalysis reaction represents a viable alternative to homogeneous one due to the advantageous capabilities in tunable reactivity and chemical recovery and recyclability. Thus, various prepared heterogeneous catalysts were screened in LGA conversion, the characterization of the heterogeneous catalysts is shown in **Table 3-2** and **Fig. 3-2**. As shown in **Table 3-3**, it is clear to see that the LGA conversion and product selectivity significantly depended on the catalyst type. The sulfo functional group solid acid catalysts, including Amberlyst 70, Nafion NR 50, and sulfonated carbon, generally showed great performance to give substantial LGA conversion. However, the LGA conversion over sulfonated carbon was slightly lower than that of over resins, a possible reason is the lower total acid amount of sulfonated carbon. Amberlyst 70 favored a higher LGO selectivity and C bal compared to Nafion NR 50. Among the tested zeolites, mordenite promoted the highest LGO conversion while Y zeolite resulted to the lowest. This is in accordance with the acid amount in the order of mordenite > ZSM-5 > beta > Y, as reported in the later chapter. However, LGA conversion over beta zeolite was higher than that of over ZSM-5 zeolite with larger acid amounts, indicating that the reaction was influenced not only by the acid sites, but also their discrepancy in pore morphology. LGA shares a kinetic diameter of 6.7 Å, roughly same with the pore size of beta zeolite (5.6–6.7 Å) but beyond that of ZSM-5 (5.1–5.6 Å) [27], demonstrating that the pore and cage diameter of ZSM-5 are not large enough to allow LGA to diffuse and convert. Other solid acid catalysts, including TFA-SBA15 and Nb_2O_5, have low acid sites and thus

were incompetent for converting LGA to LGO. The base catalyst, $Cs_{2.5}H_{0.5}PW_{12}O_{40}$, lead to a similar LGA conversion in comparison of over beta zeolite, but 2-fold higher in LGO selectivity. Our previous studies suggested that BMMIM-OTf was effective in the gas phase reforming of LGA to LGO during cellulose pyrolysis [15,19], giving complete conversion of LGA accompanied with 43.3% LGO in selectivity in Chapter 2. Nevertheless, only 8.2% of LGA was converted in the liquid phase reaction, probably due to the low proton transfer efficiency of DMSO. Considering the LGA conversion and LGO selectivity, Amberlyst 70 performed best among the tested solid acid catalysts.

Table 3-2 Characteristics of the catalysts.

Catalyst	S_{BET} (m^2/g)	V_{total} (cm^3/g)	V_{micro} (cm^3/g)	Acid sites (mmol/g)
Amberlyst 70	36	-	-	2.65
Nafion NR50 [a]	0.02	-	-	0.900
Sulfonated carbon	1242	0.558	0.496	0.44
Mordenite	501	0.361	0.219	0.717
Beta	508	0.290	0.186	N.A.
ZSM-5	419	0.264	0.155	0.325
Y	705	0.356	0.249	N.A.
TFA-SBA15	682	1.651	-	0.33
Nb_2O_5	40	0.086	-	0.242
$Cs_{2.5}H_{0.5}PW_{12}O_{40}$	124	0.154	0.023	0.15

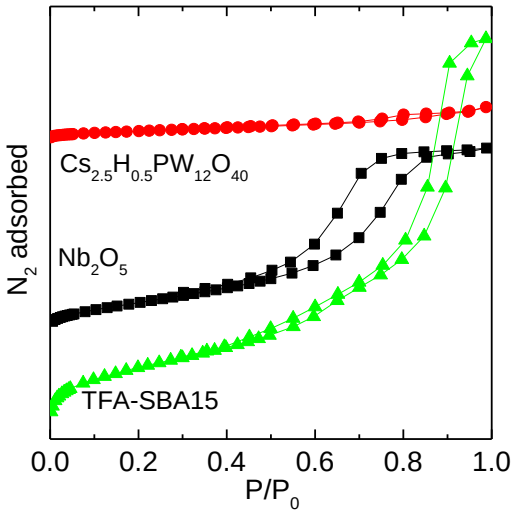

Fig. 3-2 N_2 ad/desorption isotherms.

Table 3-3 LGA conversion with different catalysts.

Entry	Catalysts	Conversion (%)	Selectivity (%)				C.bal
			LGO	AGF	Glucose	HMF	
7	Amberlyst70	84.5	35.8	12.7	4.1	12.8	70.7
10	Nafion NR50	85.5	24.6	12.3	4.1	12.9	60.6
11	Sulfonated carbon	66.0	10.1	25.3	13.0	6.5	70.2
12	Mordenite	31.8	6.0	19.9	20.3	2.3	83.6
13	Beta	16.1	10.2	16.5	32.2	1.7	93.6
14	ZSM-5	2.3	5.6	-	44.5	0.4	98.9
15	Y	0.4	-	-	-	0.1	99.6
16	TFA-SBA15	3.7	-	-	-	0.1	95.5
17	Nb_2O_5	7.3	1.7	-	8.4	2.1	93.6
18	$Cs_{2.5}H_{0.5}PW_{12}O_{40}$	15.6	22.5	31.9	39.3	4.2	99.7
19	BMMIM-OTf	8.2	9.8	8.4	26.2	0.6	95.5

Reaction conditions: LGA 0.1 M, DMSO 5 mL, LGA/catalyst = 1 (*w*/*w*), 140 ^{o}C, 12 h.

3.3.3 Reaction temperature effect

The catalytic reactivity and durability of Amberlyst 70 was specifically investigated at varied temperatures and reaction times. The time-on-stream change in LGA conversion and product selectivity is presented in **Fig. 3-3**, intimating a temperature-dependent reaction. HMF formation was not pronounced at the beginning of reaction, while other products (LGO, AGF and glucose) were obtained in substantial

selectivity, indicating that LGO, AGF and glucose are the primary product from LGA. As to glucose, its yield increased at the beginning, and gradually decreased due to further conversion to HMF or degradation products (DPs). AGF followed a qualitatively similar trend to glucose, which would repolymerize to only DPs with extended times. LGO yield showed the maximum at 140 and 160 ^{o}C, attaining to 27.9 and 32.2%, respectively. An additional experiment was conducted using LGO as substrate in pure DMSO over Amberlyst 70 at 160 ^{o}C for 8 h, a very low HMF yield of *ca.* 16.2% with LGO conversion of *ca.* 86.1% was observed. A similar result was also obtained in pure THF, almost no HMF was observed and LGO was mainly converted to unidentified products, and the increase of water content in THF could significantly promote the HMF yield [13]. In the LGA conversion experiment, a substantial HMF yield of *ca.*18.2% was obtained at 160 ^{o}C for 8 h in DMSO. Regarding to the mechanism of glucose formation, the water molecule, reacted with LGA to form glucose, should come from the interactions of the reactants because no water was imported from external. A plausible source of the water molecule was from the dehydration of two water molecule of LGA to LGO, and the repolymerization reaction of the reactants. This result revealed that the water played an important role on the LGA conversion, and it is discussed in the later section.

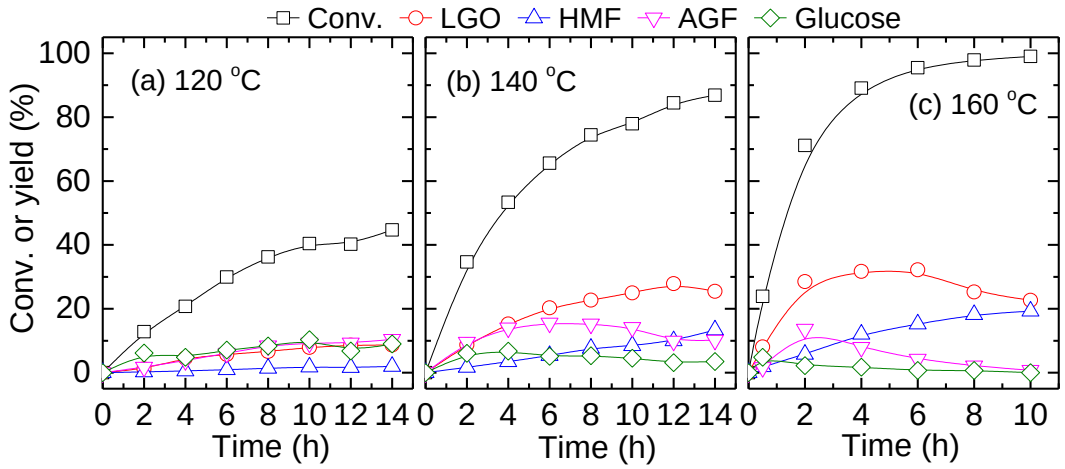

Fig. 3-3 LGA conversion in DMSO over Amberlyst 70: LGA 0.1 M, LGA/Amberlyst 70 = 1 (w/w).

Fig. 3-4(a) shows the C bal in the reaction of LGA conversion over Amberlyst 70 in DMSO at different reaction temperatures. In the range of reaction time employed, the C bal decreased with temporal evolution. LGA conversion conducted in high temperature could accelerate the formation of DPs, more than half of the total carbon formed to undetectable DPs after 8 h at 160 °C.

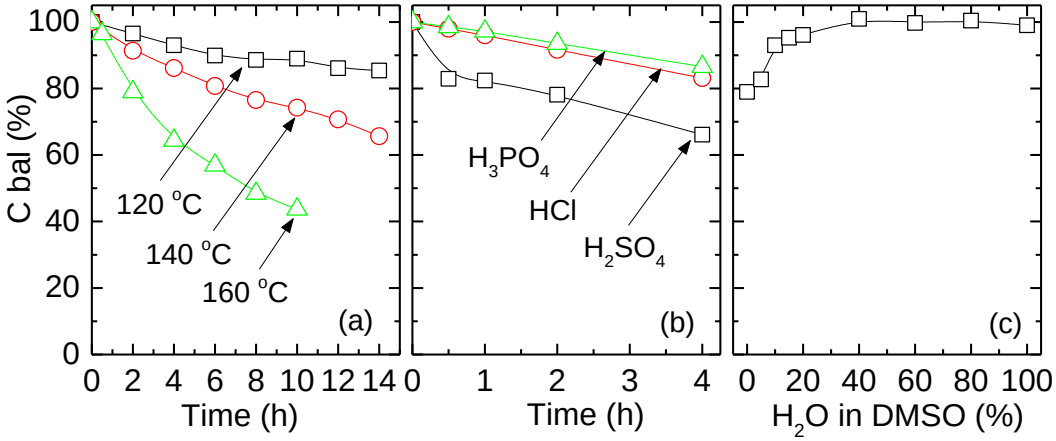

Fig. 3-4 Carbon balance (C bal) in LGA conversion over (a) Amberlyst 70, (b) mineral acids, (c) H_2O/DMSO solvent, and (d) continuous N_2.

3.3.4 Mineral acid effect

It has long been known that mineral acids are ubiquitously used in the dehydration

of mono- and polysaccharide. Cao et al. [28] converted cellulose over H_2SO_4 in tetrahydrofuran solvent, cellulose decomposed firstly to LGA, and then LGA was dehydrated to LGO by H_2SO_4, resulting in a LGO carbon yield of 51% based on cellulose. In order to investigate mineral acid effect, H_3PO_4, HCl, and H_2SO_4 were selected, respectively, and the result are seen in **Fig. 3-5**. In the reaction time employed, H_3PO_4 could not promote the conversion of LGA significantly, and accordingly, the product yield was very low, mainly because of its weak acid site. The pH values before reaction over H_3PO_4, HCl, and H_2SO_4 were 5.4, 3.0 and 2.9, respectively. Both HCl and H_2SO_4 were effective enough to convert LGA, but the reaction rate over H_2SO_4 was much faster than that of over HCl. The LGA conversion followed in the order of H_2SO_4 > HCl > H_3PO_4, this observation was in consistent with the C bal (**Fig. 3-4(b)**), which followed the regularity of the higher LGA conversion, the lower C bal LGO yield over H_2SO_4 showed the maximum yield of *ca.*30.4%, and it was comparable to the maximum yield (32.2%) over Amberlyst 70 when used an equivalent acid basis (0.04 mmol/mL H^+). Compared to Amberlyst 70, LA, formed from the rehydration of HMF, was observed in the reaction solution over HCl and H_2SO_4. Although the H^+ concentration over H_2SO_4 is 2-fold higher than that of over HCl, the LA yield over HCl is only slightly lower than that of over H_2SO_4 after 4 h (6.5 versus 7.9%), probably due to the promoted activity of protons of HCl [29]. Such H_2SO_4 or HCl induced catalysis, promoting the overreaction of HMF to LA, would be less likely to practical application due to the complex separation of reagents. Consequently, Amberlyst 70 seemed to be

more suitable than the mineral acids in the tested system.

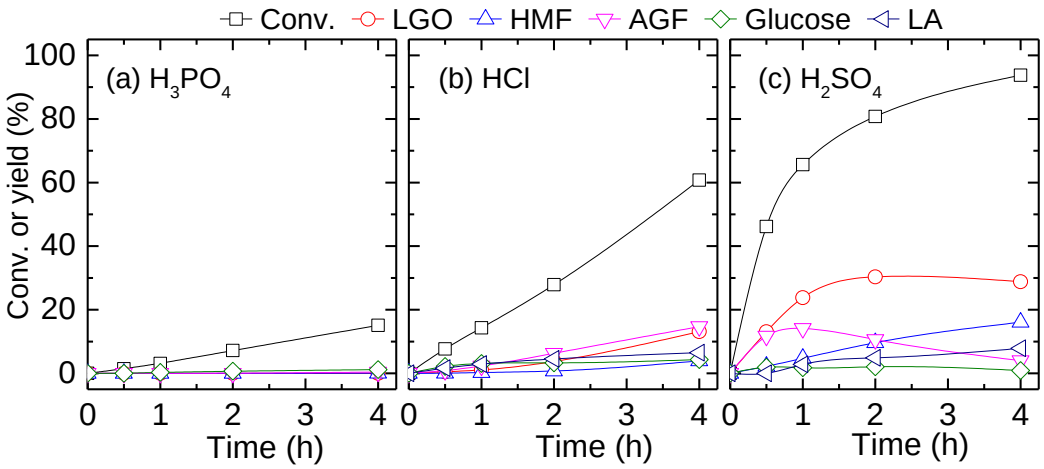

Fig. 3-5 LGA conversion in DMSO over mineral acids, (a) H_3PO_4, (b) HCl, and (c) H_2SO_4: 160 ^oC, LGA 0.1 M, mineral acid 20 mM.

3.3.5 Flushing generated water

Removing water from the reaction system in an efficient manner may provide an effective way to increase the LGO yield due to the water sensitivity of LGA to LGO/glucose. Consequently, a modified continuous N_2 flow reactor (**Fig. 3-1**) was developed to study the importance of water content formed from the LGA conversion itself. Different from the previously sealed system, the continuous N_2 was introduced to flush the generated water, and the result is shown in **Fig. 3-6**. LGO yield of *ca.* 39.3% was obtained after 4 h compared to that of *ca.* 31.7% (**Fig. 3-3(c)**) with the sealed system, while the LGA conversion is comparable, 87.9 versus 89.1% with and without flushing generated water, respectively. A steady increase in LGO yield from the flushing generated water system suggested that water should be continuously removed from the reaction system for a better LGO production. When substituted the solvent from DMSO to NMP, a quantitative similar trend of LGO could be observed (**Fig. 3-7**), however,

with slower reaction rate in NMP.

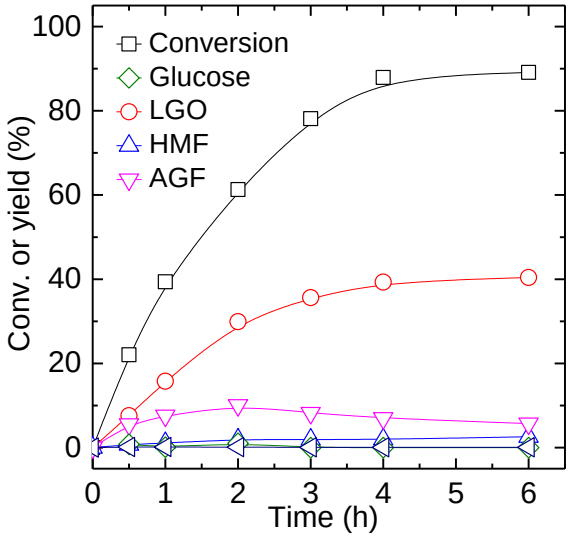

Fig. 3-6 LGA conversion in DMSO over Amberlyst 70 with N_2 flushing: 160 ^{o}C, LGA 0.1 M, LGA/Amberlyst 70 = 1 (w/w), N_2 200 mL/min.

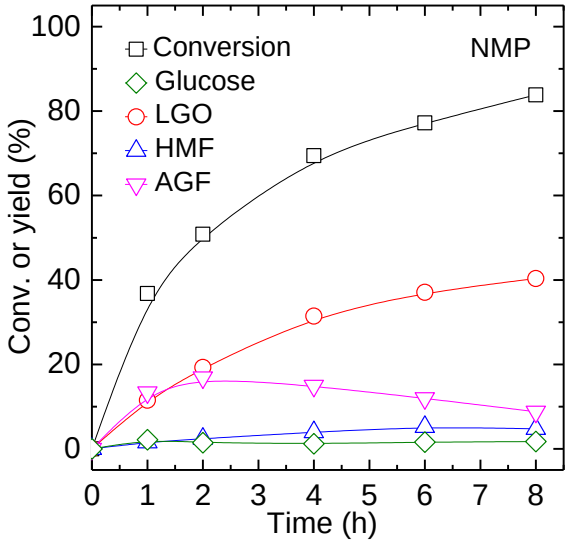

Fig. 3-7 LGA conversion in NMP over Amberlyst 70: 160 ^{o}C, LGA 0.1M, LGA/Amberlyst 70 = 1 (w/w).

To investigate catalytic stability, LGA conversion was further performed using the recovered catalyst, and the result is depicted in **Fig. 3-8**. For each cycle, the Amberlyst 70 was firstly separated from the product liquid by filtration, and then sequentially washed with acetone and water, followed by drying at 105 ^{o}C overnight. The conversion

of LGA decreased monotonically with consecutive runs, probably due to the aggregation of deposited carbonaceous materials on the catalyst surface [30], and subsequently inhibited the contact of reactants with the active sites over catalyst, as the catalyst weight increased after each run. On the other hand, the selectivity of LGO only changed slightly after five consecutive experiments, suggesting the high durability of the Amberlyst 70 catalyst.

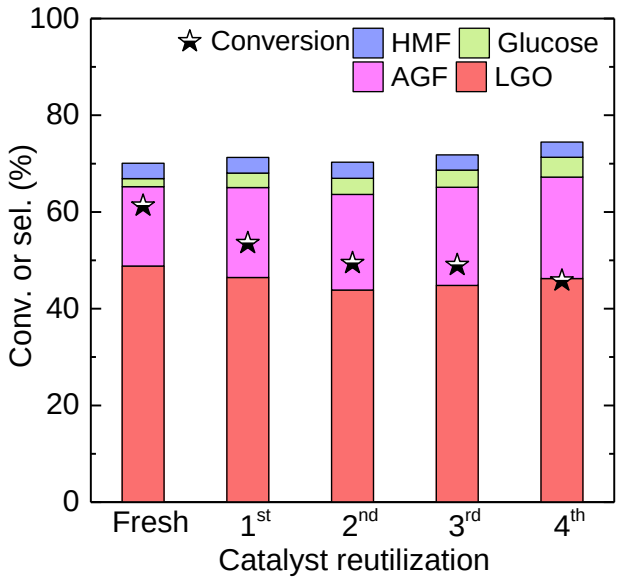

Fig. 3-8 Amberlyst 70 recyclability in LGO conversion reaction: 160 ^{o}C, 2 h, LGA 0.1M, LGA/Amberlyst 70 = 1 (w/w), N_2 200 mL/min.

3.3.6 LGO production from bio-oil

To further verify the possibility of LGO production form cellulose pyrolysis bio-oil, the bio-oil, prepared from an updraft fixed bed pyrolyzer at 500 ^{o}C pyrolysis, was used as the reagent, the detail information of the bio-oil production was presented in chapter 2. Before use, the water in bio-oil was removed by a rotary evaporator, and then the bio-oil was dissolved in DMSO. The bio-oil conversion experiment was conducted at 160 ^{o}C under N_2 flushing in DMSO solvent. Before reaction, LGA was the main

product together with a small amount of other anhydrosugars such 1,6-anhydro-β-D-glucofuranose, 1-Hydroxy (1R)-3,6-dioxabicyclo[3.2.1]octan-2-one, 1,4:3,6-Dianhydro-α-D-glucopyranose, and with nearly no LGO. However, the main compound changed to LGO after the acid dehydration reaction, suggesting the acid liquid reaction is effective to produce LGO. A quantitative analysis of LGO yield as a function of reaction time is depicted in **Fig. 3-9**. The conversion and product yield distribution from bio-oil followed a similar trend to the use of LGA as reagent, and the LGO yield reached a platform of *ca.* 53% after 4 h. This LGO yield is 14% higher than that of using standard LGA as reagent, mainly because the anhydrosugar oligomers, such as cellobisan, in bio-oil would significant convert to LGO. A similar result was observed for the glucose production form LGA and bio-oil [6], respectively. Glucose concentration was found higher than the initial LGA concentration in bio-oil after acid hydration reaction, mainly owing to the presence of anhydrosugar oligomers in bio-oil.

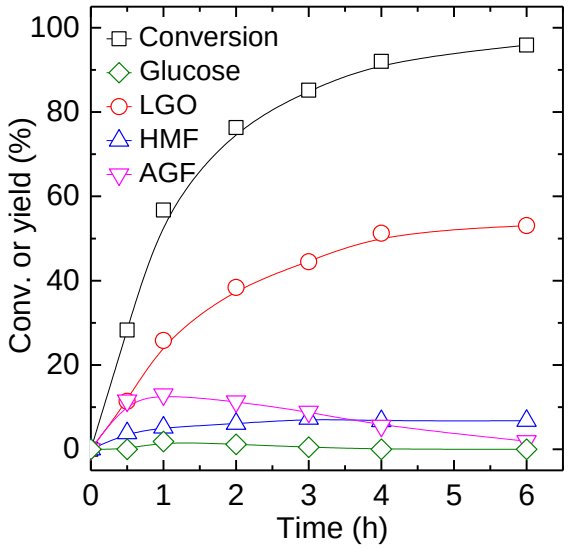

Fig. 3-9 Bio-oil conversion in DMSO over Amberlyst 70 with N_2 flushing: 160 ^{o}C, LGA 0.08 M, LGA/Amberlyst 70 = 0.8 (w/w), N_2 200 mL/min.

3.3.7 Water content effect

The above results stated that water content has a profound effect on the LGA conversion. Thus, the effect on water content in DMSO was investigated, and the result is depicted in **Fig. 3-10**. Without external importation of water, LGO *ca.* 28.5% was the dominated product, accompanying with the yield of AGF *ca.* 13.6 %, HMF *ca.* 5.8% and negligible glucose. Nevertheless, after introducing 5% of water in the reaction system, glucose with a yield of *ca.*31.4% dominated accompanying with an increase in HMF yield while a decrease in AGF yield. The glucose yield and LGA conversion increased monotonically with further increasing the water content in DMSO. When the water content in DMSO was higher than 40%, the selectivity of glucose was >95%. Almost 100% selectivity of glucose was obtained at 60% of water contend in DMSO. The C bal (**Fig. 3-4(c)**) followed a qualitatively similar trend to the increase of glucose yield, suggesting the presentence of water could significantly suppress the formation of DPs. This result is in accord with a previous literature [26]. It is noteworthy to mention that the HMF yield increased firstly and decreased progressively with the increase of water content. In the mixed water/DMSO solvent, we would like to propose that HMF was mainly formed from LGO. As we can see, the gradual increase in glucose yield should theoretically promote the HMF yield if HMF was formed from glucose in water/DMSO solvent. However, in fact, the HMF yield decreased. On the other hand, the low activation energy from LGO to HMF could also provide a plausible interpretation about this result. The activation energy of HMF formation from LGO was

reported to 65 kJ/mol in the following chapter, while that of from glucose was around 160 kJ/mol [31,32]. Such a big difference in activation energy rationalized this result well. In conclusion, increasing the water content in DMSO could significantly promote the hydration of LGA to glucose, while sharply suppress the dehydration to LGO.

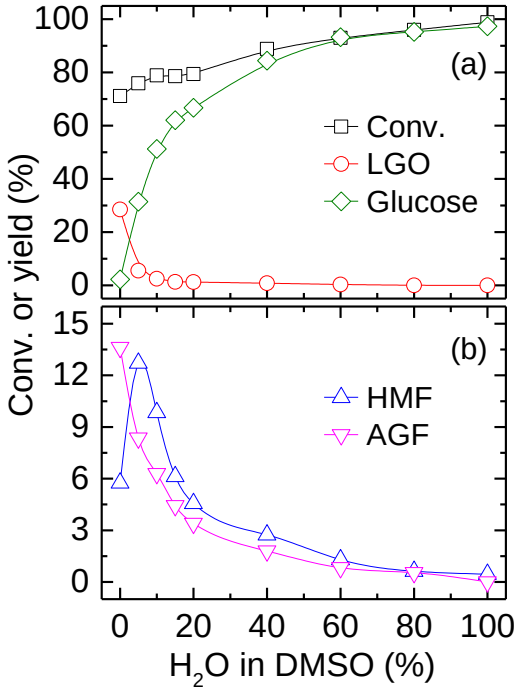

Fig. 3-10 LGA conversion in H_2O/DMSO over Amberlyst 70: 160 ^oC, 2 h, LGA 0.1 M, LGA/Amberlyst 70 = 1 (w/w).

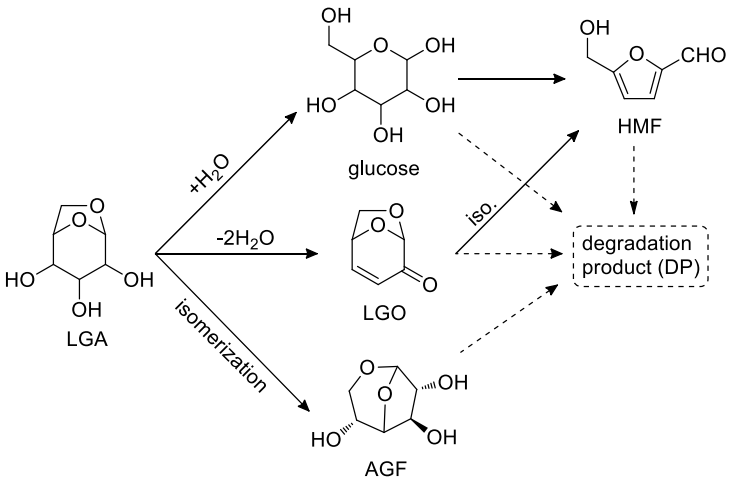

Scheme 3-1 Proposed reaction pathways of LGA conversion.

From the result of product analysis, a reaction network for the LGA conversion can be proposed as shown in **Scheme 3-1**. In the absence of water, LGA facilitates to form LGO and partly isomerize to AGF or hardly hydrate to glucose, simultaneously, substantially polymerize to DPs. All the products seem to undergo polymerization reactions after long reaction times. Besides, LGO conversion is quite sensitive to water. In the presence of water, LGA to glucose is predominant, accompanying with the significant suppression of LGO, AGF and DPs formation.

3.3.8 Glucose production

At first, the effect of reaction temperature on the LGA conversion was investigated, the reaction was conducted with a LGO concentration of 100 mM and LGA/Amberlyst 70 mass ratio of 1. **Fig. 3-11** depicts that reaction temperature has a profound influence on LGA conversion. In general, elevating reaction temperature could significantly accelerate the LGA conversion accompanying with the increase in glucose yield. For example, 98% of LGA conversion was observed at 140 °C after 112 min, whereas similar conversion was attainable after 345 min at 120 °C. At reaction temperature lower than 100 °C, LGA could not convert completely even at prolonged residence time and glucose yield is therefore rather low. Further prolonging the reaction time at 150 °C resulted in a slightly decrease in glucose yield, suggesting the overreaction of glucose to degradation products, such as HMF and polymers. Compared to temperature below 120 °C, relative high temperatures resulted in higher glucose selectivity, almost 100% at short reaction times at 140-180 °C, indicating that low temperatures would promote the

degradation of LGA to other soluble or insoluble polymers under acid conditions, whereas high temperatures favored to form glucose. This result can be explained by the reaction rate of LGA to glucose or polymers. The reaction rate of LGA → glucose was slower at low temperatures and much faster at high temperatures compared to that of LGA → polymers.

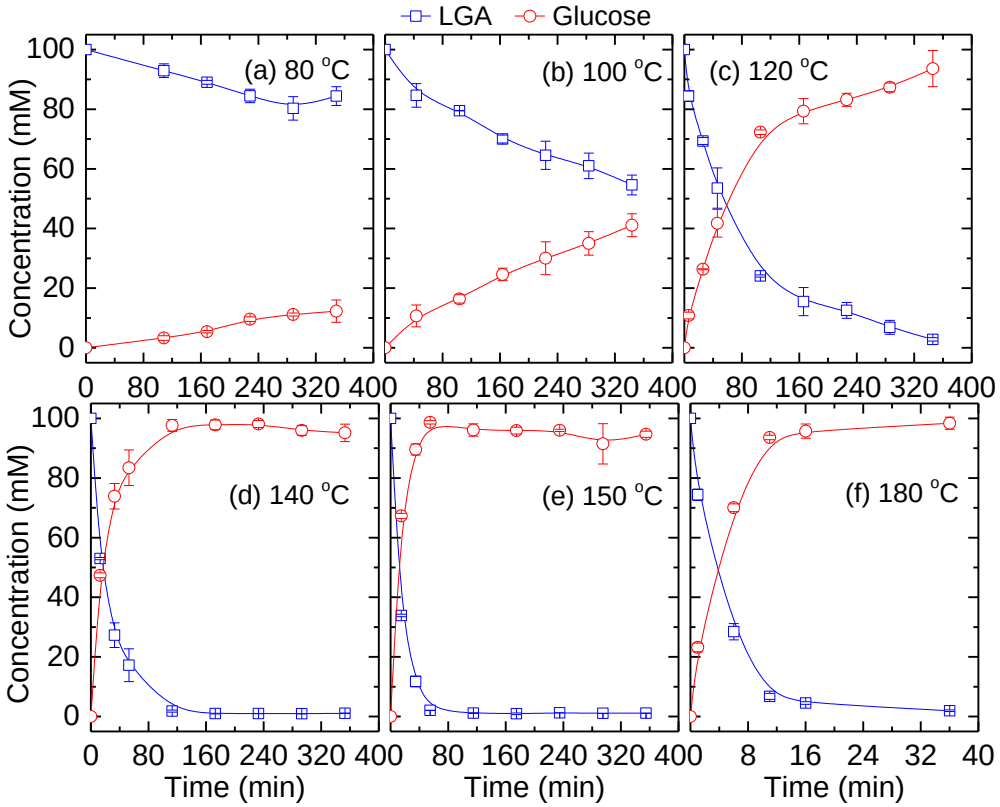

Fig. 3-11 LGA conversion in aqueous phase over Amberlyst 70: LGA 0.1M, LGA/Amberlyst 70 = 1 (w/w).

In order to highlight the performance of Amberlyst 70 and H_2SO_4, the H_2SO_4 was used as the catalyst with a concentration of 40 mM at 140 °C, which was under the equivalent acid concentration basis of Amberlyst 70 (40 mM). **Fig. 3-12** presents the LGA conversion and glucose yield over H_2SO_4, for example, > 98% LGA conversion was observed after 112 min, which was comparable to Ambelyst 70. Nevertheless, the

glucose was only 88% at 112 min, which is much lower than that of over Amberlyst 70 (98%). The selectivity of glucose ca. 90% over H_2SO_4 were also lower than that of using Amberlyst 70 (glucose selectivity > 96%). In combination the above results with the fact that almost no HMF was detected over H_2SO_4 and Amberyst 70, it demonstrates that glucose is easier to undergo degradation reactions to form soluble or insoluble polymers under H_2SO_4 conditions.

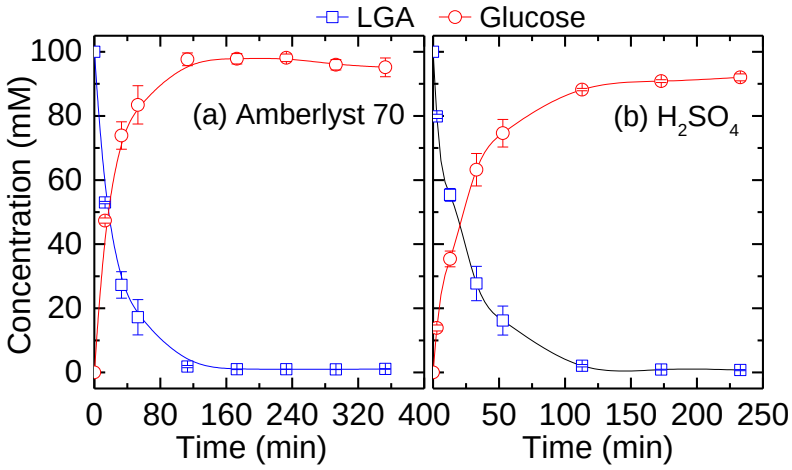

Fig. 3-12 LGA conversion and glucose yield over (a) Amberlyst 70 and (b) H_2SO_4: 140 °C H_2O 3 mL, LGA 100 mM, Amberlyst 70 or H_2SO_4 40 mM.

As we all know, a high concentration of reagent is usually preferred for the sake of industrial economics. Therefore, the effect of initial LGA concentration on its conversion and glucose yield was also studied, the reaction was conducted with a reaction temperature of 140 °C. Three different initial LGA concentrations, i.e. 100, 200, and 500 mM, were investigated, respectively, and the result is shown in **Fig. 3-13**. The initial LGA concentration of 100 and 200 mM did not exert as much influence on LGA conversion and glucose yield. However, when the initial LGA concentration increased to 500 mM, the glucose yield slightly decreased, suggesting a higher initial

concentration would have a higher rate of polymerization of LGA to polymers, eventually leading to a decrease of glucose yield.

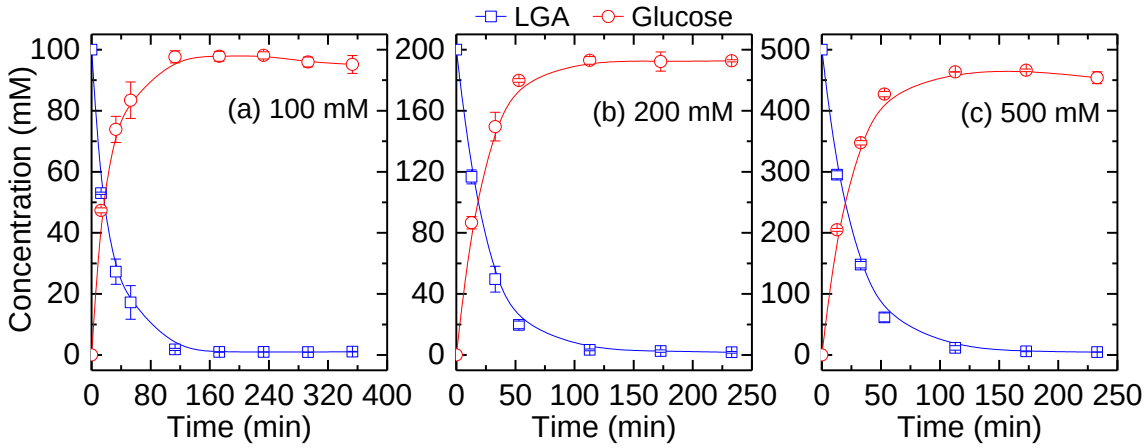

Fig. 3-13 LGA conversion at different initial concentration in aqueous phase over Amberlyst 70: 140 °C, H_2O 3 mL, Amberlyst 70 48.6 mg.

Next, cellobiose was chosen as one of anhydrosugars to investigate the glucose formation. Its dehydration product, cellobiosan, is commonly identified as a component of bio-oil from cellulose pyrolysis, but unfortunately, cellobiosan is commercial unavailable. Therefore, cellobiose was selected as the representative of cellobiosan. **Fig. 3-14** shows the effect of reaction temperature on cellobiose conversion and glucose yield under the condition of initial 100 mM of cellobiose and substrate/Amberlyst 70 mass ratio of 2. The reaction temperature and substrate/Amberlyst 70 mass ratio are selected based on the results of LGA conversion. The glucose yield from cellobiose followed a qualitatively similar trend to the effect of temperature on LGA conversion, lower temperature needed more time to get similar lever of cellobiose conversion. For example, reaching the cellobiose conversion around 73%, it took 16 min at 180 °C, while 73 min at 150 °C and 232 in at 140 °C, respectively. Glucose yield firstly

increased and attained the highest yield of 87% with cellobiose conversion of 94% at 180 °C. Further prolonging the reaction time would lead to a decrease in glucose yield, mainly due to the overreactions of glucose to degradation products.

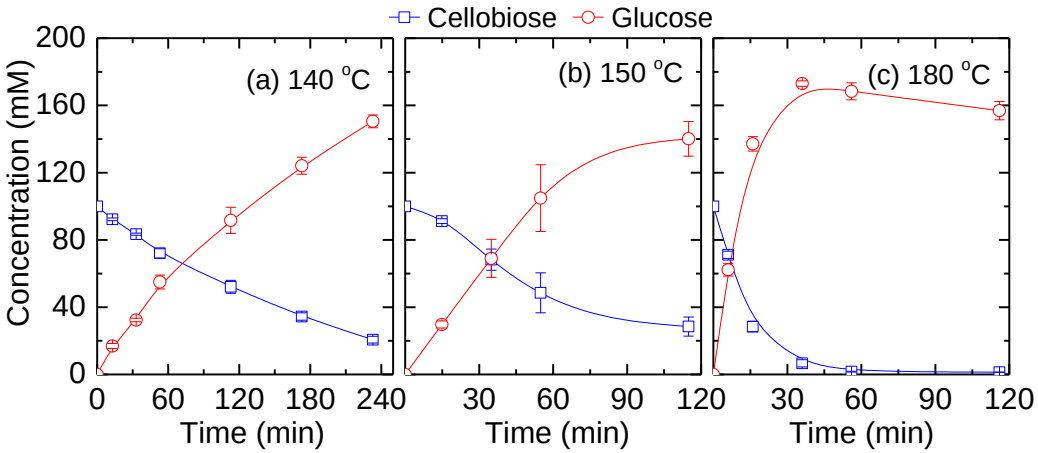

Fig. 3-14 Cellobiose conversion in aqueous phase over Amberlyst 70: cellobiose 0.1M, LGA/Amberlyst 70 = 1 (w/w).

For the purpose of identifying the difference in LGA and cellobiose conversion, we further simply constructed the kinetics profiles according to the reaction:

$$\text{LGA} \rightarrow \text{Glucose} \qquad (1)$$

$$\text{Cellobiose} \rightarrow 2\text{Glucose} \qquad (2)$$

The kinetics was analyzed by assuming the first order reaction for LGA or cellobiose to glucose, as described below.

$$kt = -\ln(1 - X_i) \qquad (3)$$

$$\ln(k) = -\frac{E_i}{RT} + \ln(A) \qquad (4)$$

(k: reaction rate, X: conversion, A: frequency factor, E_i: activation energy, R: gas constant, T: temperature, i = LGA or cellobiose)

The reaction rate at different temperatures can be calculated from the slope based on

equation 3, and activation energy can be determined from equation 4. The calculated activation energies and frequency factors for LGA and cellobiose are listed in **Table 3-4**. The activation energy for LGA or cellobiose in this study is 81.1 and 95.0 kJ/mol, respectively.

Table 3-4 Kinetic parameters for the glucose production from LGA or cellobiose over Amberlyst 70.

	LGA	Cellobiose
Frequency factor (mL/mol/s)	9.53×10^{6}	6.60×10^{9}
Activation energy (kJ/mol)	81.1	95.0

To further verify the possibility of glucose production from cellulose pyrolysis bio-oil, the bio-oil, prepared from an updraft fixed bed pyrolyzer at 500 °C pyrolysis, was also used as the reagent, and the detail information of the bio-oil was presented in Chapter 2. Before reaction, there is without any glucose in bio-oil. However, the main compound changed to glucose after the acid dehydration reaction over Amberlyst 70 and H_2SO_4, as shown in **Fig. 3-15**. The initial LGA concentration was 100 mM and the acid site was controlled to 40 mM both for Amberlyst 70 and H_2SO_4. The glucose yield is calculated based on the LGA. The use of Amberlyst 70 led to a higher reaction rate than H_2SO_4, this result is consistent with the observation using pure LGA as reagent. In general, the glucose yield from LGA-riched bio-oil followed a qualitatively similar trend to that of from pure LGA. At reaction time of 172 min, maximum glucose yield of 108 and 109% was observed using Amberlyst 70 and H_2SO_4, 13 and 15% higher than LGA conversion, respectively. In addition, it is obvious to see that the glucose yield was always higher that LGA conversion, suggesting the LGA selectivity is excess 100%, for

example, 114% selectivity to glucose at the maximum yield of 108% over Amberlyst 70. This can be explained by the presence of the anhydrosugar oligomers in bio-oil, which has a great possibility to hydrolyze to glucose.

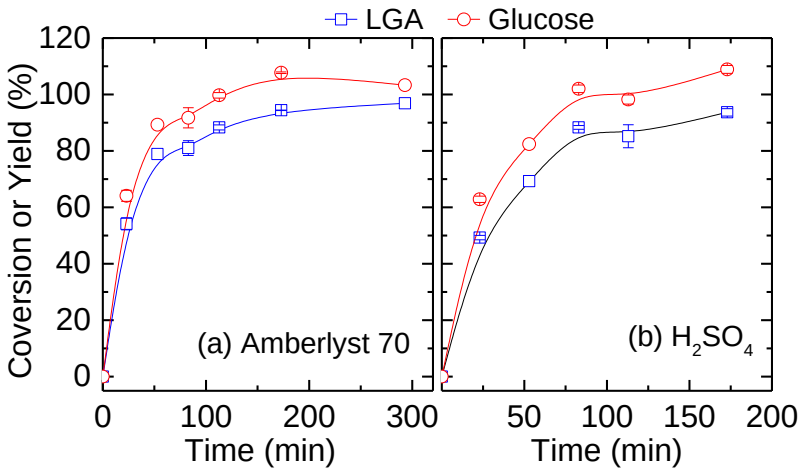

Fig. 3-15 Bio-oil conversion in aqueous phase over Amberlyst 70: 140 °C, LGA 90 mM, LGA/Amberlyst 70 = 0.8 (w/w).

3.3.9 HMF production

Table 3-5 Glucose conversion with different catalysts.

Entry	NaCl	Catalyst		Conv. (%)	Yield (%-C)		S_{HMF} (%)	C bal (%)
		$AlCl_3$	Amberlyst 70		fructose	HMF		
1	×	✓	✓	21	2	12	57	93.1
2	✓	×	✓	9	0	5	57	96.3
3	✓	✓	×	40	18	16	39	93.9
4	✓	✓	✓	15	1	12	81	97.9

Reaction conditions: 140 °C, 3 h, glucose 200 mM, H_2O 2 mL, H_2O/acetone = 1/3 (v/v), NaCl 600 mg, $AlCl_3$ 25 mM, glucose/Amberlyst 70 = 2 (w/w).

The catalytic performance in glucose conversion at 140 °C and 3 h are listed in **Table 3-5**. Without addition of NaCl, acetone and water are miscible to form a homogenous phase, resulted in 21% glucose conversion and 57% HMF selectivity. The absence of $AlCl_3$ led to a sharp decrease in glucose conversion, mainly because the

isomerization of glucose to fructose is dominated by the Lewis acid site. The absence of Amberlyst 70 promoted glucose conversion and decreased the HMF selectivity, suggesting that Brønsted and Lewis acid have a synergistic effect on fructose to HMF while have a negative effect on glucose to fructose. In the $AlCl_3$-Amberyst 70 catalyzed NaCl-H_2O/acetone biphasic system, the highest HMF selectivity was achieved in 81%, but the glucose conversion was relatively low due to the low reaction temperature.

Elevating reaction temperature to 180 °C could significantly enhance glucose conversion, as described in **Fig. 3-16(a)**. Glucose conversion increased from 60 to 97% with prolonging reaction time from 30 to 45 min, consequently resulted in the increase in HMF yield. Further prolonging the reaction time led to a sharp decrease in HMF yield while an increase in LA and FA yields, obviously due to the re-hydration reaction. The maximum HMF yield was achieved in 62% from glucose. When substituting the feedstock to LGA or glucose, similar yield of HMF was also observed (**Fig. 3-16 (b)** and **(c)**), suggesting the anhydrosugars derived from cellulose pyrolysis also have a potential for HMF production. Nevertheless, when the LGA-riched bio-oil was used as feedstock, the maximum HMF yield drastically decreased to 33%, probably because of the complexity of bio-oil which involved more polymerization reactions at the acid condition. This result indicated for the sake of massive HMF production from anhydrosugars, purification them from bio-oil before reaction is unavoidable. The partition coefficiency as the ratio of the HMF concentration in the acetone phase and aqueous phase ($C_{organic}/C_{H2O}$) is estimated to around 3.47 for all the experiments in the

NaCl-H_2O/acetone biphasic system (**Fig. 3-17(a)**), and about 92% of the HMF produced was extracted to the acetone layer (**Fig. 3-17(b)**).

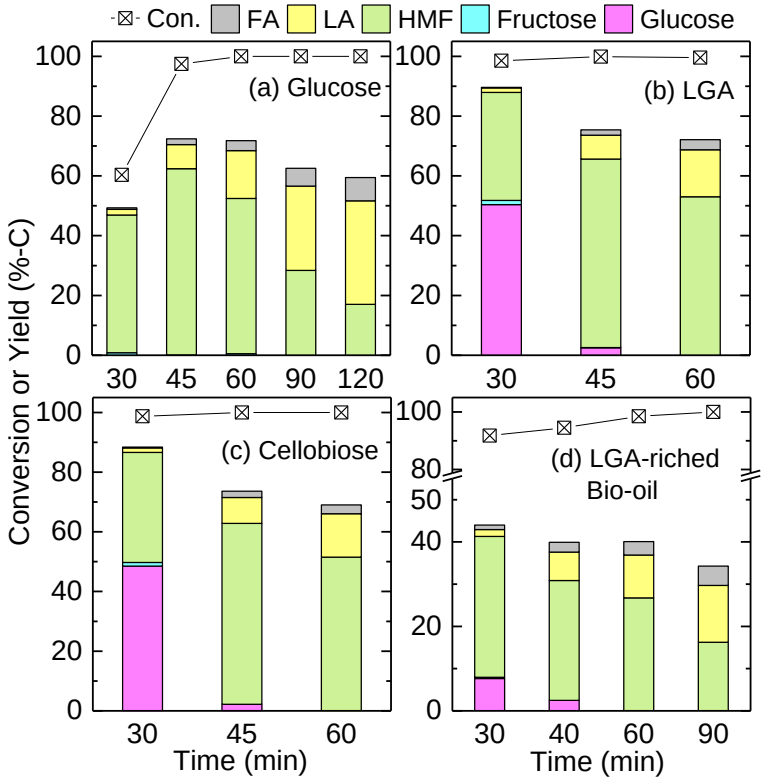

Fig. 3-16 HMF production in biphasic phase from (a) glucose, (b) LGA, (c) cellobiose and (d) LGA-riched bio-oil: 180 °C, glucose or LGA 200 mM, cellobiose or LGA-riched bio-oil 100 mM, H_2O 2 mL, H_2O/acetone = 1/3 (v/v), NaCl 600 mg, $AlCl_3$ 25 mM, Amberlyst 70 32 mg.

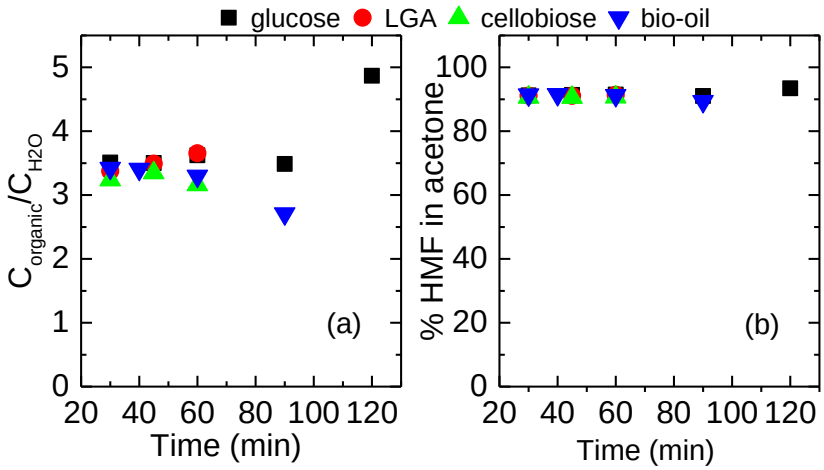

Fig. 3-17 (a) HMF concentration ration in organic phase and aqueous phase and (b) percentage of HMF on organic phase.

3.4 Conclusions

An acid-catalyzed reaction of LGA to LGO has been carried out for the first time. Among the parameters employed in this study, the best performance of LGO production is in DMSO over Amberlyst 70. Removing water from the reaction system by flushing the generated water could increase the maximum LGO yield from *ca.* 32 to 39%. Furthermore, LGO yield attained *ca.*53% from cellulose pyrolysis bio-oil due to the additional presence of anhydrosugar oligomers. After introducing water into the DMSO phase, the dominated LGA conversion reaction was adding one water molecule to form glucose, attaining almost 100% yield and selectivity. In aqueous phase, when using cellobiose as substrate, the maximum glucose yield of 87% with cellobiose conversion of 94% was obtained. When using LGA-riched bio-oil as substrate, the maximum glucose yield of 108% with a 13% higher than LGA conversion was observed. In a second stage, the $AlCl_3$-Amberyst 70 catalyzed NaCl-H_2O/acetone biphasic system was elaborated for HMF production from the anhydrosugars, leading to total HMF yield of 61-63% by the use of glucose, LGA and cellobiose as a substrate, respectively. However, HMF yield drastically decreased to 33% from LGA-riched bio-oil because the complexity of bio-oil aggravated the polymerization reactions, suggesting further purification of anhydrodugars from bio-oil is unavoidable for the sake of high HMF yield.

3.5 References

[1] J.C. Serrano-Ruiz, R. Luque, A. Sepúlveda-Escribano, Transformations of

biomass-derived platform molecules: from high added-value chemicals to fuels via aqueous-phase processing, Chem. Soc. Rev., 40 (2011) 5266-5281.

[2] V. Kumar, P. Binod, R. Sindhu, E. Gnansounou, V. Ahluwalia, Bioconversion of pentose sugars to value added chemicals and fuels: recent trends, challenges and possibilities, Bioresour. Technol., 269 (2018) 443-451.

[3] L. Jiang, A. Zheng, Z. Zhao, F. He, H. Li, N. Wu, The comparison of obtaining fermentable sugars from cellulose by enzymatic hydrolysis and fast pyrolysis, Bioresour. Technol., 200 (2016) 8-13.

[4] S. Maduskar, V. Maliekkal, M. Neurock, P.J. Dauenhauer, On the yield of levoglucosan from cellulose pyrolysis, ACS Sustainable Chem. Eng., 6 (2018) 7017-7025.

[5] R. Abdilla, C. Rasrendra, H. Heeres, Kinetic Studies on the conversion of levoglucosan to glucose in water using brønsted acids as the catalysts, Ind. Eng. Chem. Res., 57 (2018) 3204-3214.

[6] P.H. Blanco, J.B. Lad, A.V. Bridgwater, M.S. Holm, Production of glucose from the acid hydrolysis of anhydrosugars, ACS Sustainable Chem. Eng., 6 (2018) 12872-12883.

[7] S. Helle, N.M. Bennett, K. Lau, J.H. Matsui, S.J. Duff, A kinetic model for production of glucose by hydrolysis of levoglucosan and cellobiosan from pyrolysis oil, Carbohydr. Res., 342 (2007) 2365-2370.

[8] M.B. Comba, Y.H. Tsai, A.M. Sarotti, M.I. Mangione, A.G. Suarez, R.A. Spanevello,

Levoglucosenone and its new applications: valorization of cellulose residues, Eur. J. Org. Chem., 2018 (2018) 590-604.

[9] S.H. Krishna, Z.R. Schmidt, B.M. Weckhuysen, J.A. Dumesic, G.W. Huber, Catalytic production of hexane-1, 2, 5, 6-tetrol from bio-renewable levoglucosanol in water: effect of metal and acid sites on (stereo)-selectivity, Green Chem., 20 (2018) 4557-4565.

[10] A.L. Flourat, A.A.M. Peru, A.R.S. Teixeira, F. Brunissen, F. Allais, Chemo-enzymatic synthesis of key intermediates (S)-γ-hydroxymethyl-α,β-butenolide and (S)-γ-hydroxymethyl-γ-butyrolactone via lipase-mediated Baeyer-Villiger oxidation of levoglucosenone, Green Chem., 17 (2015) 404-412.

[11] J. Sherwood, A. Constantinou, L. Moity, C.R. McElroy, T.J. Farmer, T. Duncan, W. Raverty, A.J. Hunt, J.H. Clark, Dihydrolevoglucosenone (Cyrene) as a bio-based alternative for dipolar aprotic solvents, Chem. Commun., 50 (2014) 9650-9652.

[12] J. Zhang, G.B. White, M.D. Ryan, A.J. Hunt, M.J. Katz, Dihydrolevoglucosenone (Cyrene) as a green alternative to N, N-dimethylformamide (DMF) in MOF synthesis, ACS Sustainable Chem. Eng., 4 (2016) 7186-7192.

[13] S.H. Krishna, T.W. Walker, J.A. Dumesic, G.W. Huber, Kinetics of levoglucosenone isomerization, ChemSusChem, 10 (2016) 129-138.

[14] S.H. Krishna, D.J. McClelland, Q.A. Rashke, J.A. Dumesic, G.W. Huber, Hydrogenation of levoglucosenone to renewable chemicals, Green Chem., 19 (2017)

1278-1285.

[15] S. Kudo, Z. Zhou, K. Norinaga, J. Hayashi, Efficient levoglucosenone production by catalytic pyrolysis of cellulose mixed with ionic liquid, Green Chem., 13 (2011) 3306-3311.

[16] X.N. Ye, Q. Lu, X. Wang, H.Q. Guo, M.S. Cui, C.Q. Dong, Y.P. Yang, Catalytic fast pyrolysis of cellulose and biomass to selectively produce levoglucosenone using activated carbon catalyst, ACS Sustainable Chem. Eng., 5 (2017) 10815-10825.

[17] X.W. Sui, Z. Wang, B. Liao, Y. Zhang, Q.X. Guo, Preparation of levoglucosenone through sulfuric acid promoted pyrolysis of bagasse at low temperature, Bioresour. Technol., 103 (2012) 466-469.

[18] Q. Lu, X.N. Ye, Z.B. Zhang, C.Q. Dong, Y. Zhang, Catalytic fast pyrolysis of cellulose and biomass to produce levoglucosenone using magnetic SO_4^{2-}/TiO_2-Fe_3O_4, Bioresour. Technol., 171 (2014) 10-15.

[19] S. Kudo, N. Goto, J. Sperry, K. Norinaga, J. Hayashi, Production of levoglucosenone and dihydrolevoglucosenone by catalytic reforming of volatiles from cellulose pyrolysis using supported ionic liquid phase, ACS Sustainable Chem. Eng., 5 (2016) 1132-1140.

[20] Z. Wang, Q. Lu, X.F. Zhu, Y. Zhang, Catalytic fast pyrolysis of cellulose to prepare levoglucosenone using sulfated zirconia, ChemSusChem, 4 (2011) 79-84.

[21] S. Kudo, N. Goto, J. Sperry, K. Norinaga, J. Hayashi, Production of Levoglucosenone and Dihydrolevoglucosenone by Catalytic Reforming of Volatiles

from Cellulose Pyrolysis Using Supported Ionic Liquid Phase, ACS Sustainable Chem. Eng., 5 (2016) 1132-1140.

[22] X. Fu, J. Dai, X. Guo, J. Tang, L. Zhu, C. Hu, Suppression of oligomer formation in glucose dehydration by CO_2 and tetrahydrofuran, Green Chem., 19 (2017) 3334-3343.

[23] X. Mo, D.E. López, K. Suwannakarn, Y. Liu, E. Lotero, J.G. Goodwin Jr, C. Lu, Activation and deactivation characteristics of sulfonated carbon catalysts, J. Catal., 254 (2008) 332-338.

[24] P. Kalita, A.V. Baskar, J.H. Choy, K.S. Lakhi, M. El-Newehy, G. Lawrence, S.S. Al-deyab, V.V. Balasubramanian, A. Vinu, Preparation of highly active triflic acid Functionalized SBA-15 Catalysts for the Synthesis of coumarin under solvent-free conditions, ChemCatChem, 8 (2016) 336-344.

[25] R. Liu, T. Wang, C. Liu, Y. Jin, Highly selective and stable $CsPW/Nb_2O_5$ catalysts for dehydration of glycerol to acrolein, Chin. J. Catal., 34 (2013) 2174-2182.

[26] X. Hu, L. Wu, Y. Wang, D. Mourant, C. Lievens, R. Gunawan, C.Z. Li, Mediating acid-catalyzed conversion of levoglucosan into platform chemicals with various solvents, Green Chem., 14 (2012) 3087-3098.

[27] J. Jae, G.A. Tompsett, A.J. Foster, K.D. Hammond, S.M. Auerbach, R.F. Lobo, G.W. Huber, Investigation into the shape selectivity of zeolite catalysts for biomass conversion, J. Catal., 279 (2011) 257-268.

[28] F. Cao, T.J. Schwartz, D.J. McClelland, S.H. Krishna, J.A. Dumesic, G.W. Huber,

Dehydration of cellulose to levoglucosenone using polar aprotic solvents, Energy Environ. Sci., 8 (2015) 1808-1815.

[29] V. Tarabanko, M.Y. Chernyak, S. Aralova, B. Kuznetsov, Kinetics of levulinic acid formation from carbohydrates at moderate temperatures, React. Kinet. Catal. Lett., 75 (2002) 117-126.

[30] X. Hu, C. Lievens, D. Mourant, Y. Wang, L. Wu, R. Gunawan, Y. Song, C.Z. Li, Investigation of deactivation mechanisms of a solid acid catalyst during esterification of the bio-oils from mallee biomass, Appl. Energy, 111 (2013) 94-103.

[31] F.S. Asghari, H. Yoshida, Kinetics of the decomposition of fructose catalyzed by hydrochloric acid in subcritical water: formation of 5-hydroxymethylfurfural, levulinic, and formic acids, Ind. Eng. Chem. Res., 46 (2007) 7703-7710.

[32] R. Weingarten, J. Cho, R. Xing, W.C. Conner Jr, G.W. Huber, Kinetics and reaction engineering of levulinic acid production from aqueous glucose solutions, ChemSusChem, 5 (2012) 1280-1290.

Chapter 4

Clean Synthesis of 5-Hydroxymethylfurfural and Levulinic Acid from Levoglucosenone

4.1 Introduction

Fossil fuel depletion requires the development of sustainable chemical industries with a renewable source, biomass. Addressing this challenge, researchers have identified several sugar-derived platform chemicals that serve as the feedstock for a diverse selection of commodity and fine chemicals [1, 2] 5-Hydroxymethylfurfural (HMF) and levulinic acid (LA) are typical platform chemicals with great industrial potential. Derivatives from these chemicals cover a broad range of applications in both current petrochemical and future greener industries as frequently discussed in the literature [3–9]. Although HMF and LA have been the subject of research for a long time, their production is now on the brink of entering a new stage. During these few years, several companies have commenced commercial production in large-scale plants [10]. Nevertheless, the technology readiness levels of HMF and LA in a report from E4tech (UK) Ltd to the European Commission (DG-ENER) are ranked as being at the large-scale prototype stage and prototype-demonstration system stage, respectively [10]. They are still "premium" chemicals, which necessitates their application in high-value-added products with limited markets. A widely-studied route to access HMF is dehydration of three water molecules from glucose, which is a hydrolysis product of starch and cellulose as the feedstock. LA is produced by subsequent rehydration of

HMF along with formic acid (FA). The dehydration of glucose proceeds in multiple steps via intermediates such as fructose, the kinetics of which have not been fully clarified. This complex conversion chemistry eludes to the difficulty of the efficient production of HMF and LA from glucose or cellulose, as evidenced by the reported insufficient yields, and requires the use of costly solvents and catalysts, rendering the production process uneconomical and even environmentally unfriendly [6].

An alternative approach to synthesis of HMF and LA from cellulose has recently been proposed, which employs levoglucosenone (LGO) as feedstock or intermediate instead of glucose [11-13]. LGO is a product of pyrolytic conversion of cellulose. The presence of catalyst, typically mineral acids, over cellulose or in pyrolysis medium drastically enhances the selectivity and yield of LGO [14-19]. The commercialization status of the LGO production process is similar to HMF and LA. A large-scale production plant with lignocellulosic biomass as feedstock has been operated by Norske Skog and Circa for the commercial demonstration since 2016. LGO is not yet cheaply available, while studies are ongoing for the development of more economical production processes like that of our previous study which demonstrated the possibility of solvent free LGO production by reforming of volatiles from cellulose pyrolysis over a packed bed catalyst [20]. Because of its highly-functionalized structure, LGO has been used for synthesis of many natural and synthetic compounds as the platform, but the application has been limited mainly to those specialty chemicals [21–24]. Recent studies have opened up new ways to reach chemicals with potential heavy demand, e.g.,

polyols, Cyrene (green solvent), and, notably, HMF/LA [11–13, 25–28]. The formation of furanic compounds from LGO with substantial yields was identified in the catalytic pyrolysis of cellulose in sulfolane with sulfuric acid ten years ago [14], and a recent series of works [11, 12] by Huber's group demonstrated selective production of HMF and LA with cellulose conversion via LGO in a mixture of tetrahydrofuran and water containing sulfuric acid as catalyst. The reaction system is clearly superior to using glucose as intermediate or feedstock in terms of chemicals required for the conversion and the product yield, but it is not yet an economically viable and green production process. The homogenous acid-catalyzed reaction needs additional capital and operating costs for reactor construction and chemical recovery systems. Moreover, the use of organic solvent and mineral acid creates an undesirable waste stream.

With the aim to contribute to the construction of a feasible chemical industry with LGO as the platform, a study examining its clean conversion into HMF and LA was initiated. Specifically, we chose to investigate the conversion of LGO into HMF and LA in water using solid acid catalysts, a process that should enable catalyst recycling and generates no undesirable waste stream.

4.2 Experimental

4.2.1 Materials

LGO and LA were purchased from CIRCA and Tokyo Chemical Industry, respectively. All the other reagents (HMF, FA, and furfural (FF)) were purchased from Wako Pure Chemical Industries. The reagents were used as received without further

purification.

Zeolites ZSM-5 (CBV 3024E, ammonium form), mordenite (CBV 21A, ammonium form), beta (HSZ 980HOA, β-1, proton form; CP814N, β-2), and Y (HSZ 390HUA, Y-1, proton form; CBV 400, Y-2, proton form; CBV 100, Y-3, sodium form) were purchased from Zeolyst International and Tosoh. All the zeolites were calcined at 550 °C (heating rate = 10 °C/min) for 4 h in a muffle furnace before the use to generate the acidic form. A catalytic ion-exchange resin, Amberlyst 70, was purchased from Organo, and was prewashed with deionized water and ethanol, followed by drying at 105 °C overnight before the use. Sulfonated activated carbon (S-AC) was prepared, according to a reported method [29], by sulfonating a palm shell-derived activated carbon (Wako Pure Chemical Industry).

4.2.2 Catalyst characterization

The Brunauer-Emmet-Teller surface area (S_{BET}) and total pore volume (V_{total}) of zeolites were calculated from N_2 isotherm at –196 °C, which were measured on a Quantachrome, NOVA 3200e. The micro pore volume was calculated with the *t*-plot method. X-ray diffraction (XRD) measurement was performed on a Rigaku TTR-III X-ray diffractometer with Cu Kα radiation at 50 kV and 300 mA. Scanning electron microscopy (SEM) analysis was operated by JEOL JSM-6700F. Transmission electron microscope (TEM) images were taken with JEOL JEM-2100F. Ammonia temperature-programmed desorption (NH_3-TPD) was employed for characterizing acid sites of zeolites. The zeolite sample of 100 mg was packed in a quartz tube, set in a

catalyst analyzer (MicrotracBEL, BELCAT-II), and pretreated at 500 °C for 1 h under helium with a flow rate of 50 mL/min. For NH_3 adsorption, 5% NH_3 (helium balance) with a flow rate of 50 mL/min was fed into the tube at 100 °C for 30 min. After purging with 50 mL helium at 100 °C for 30 min, NH_3 was thermally-desorbed by ramping the temperature from 50 °C to 700 °C at 10 °C/min under 50 mL/min helium. The desorbed NH_3 was quantified by an online mass spectrometer (MicrotracBEL, BELMass) with m/z = 16. The total acid sites amount of S-AC was analyzed by standard acid-base back-titration [29].

4.2.3 Reaction and product analysis

The LGO conversion experiment was performed with a 30 mL autoclave. Typically, 5 mL of water, 50 mg of LGO, and 50 mg-dry of solid catalyst were loaded into the reactor and heated to a desired temperature (heating rate: ca. 100 °C/min) under continuous stirring at 600 rpm by immersing the reactor into the oil bath. After the prescribed time, the reaction was quenched by cooling the reactor with an iced water bath. The product liquid was separated from the solid catalyst by filtration with a 0.45 μm PTFE membrane filter, and then analyzed by a high-performance liquid chromatography (HPLC, Shimadzu LC-20 prominence series) equipped with a BioRad Aminex 87H column. The chromatography was operated at 35 °C with 0.6 mL/min of 5 mM sulfuric acid as mobile phase. The separated compounds were quantified with refractive index detector for LA, FA, FF, and 6,8-dioxabicyclo[3.2.1]octane-2,4,4-triol (DH) and with photo diode array detector for LGO and HMF according to a method

reported by Krishna et al. [11] DH forms from LGO as the dihydrated product in the presence of water even at room temperature [30]. The ratio between DH and LGO is thermochemically determined and rapidly shifts to the equilibrium value with changes in the composition and condition of the solution. The calculation of LGO conversion (X_{LGO}) in this study, therefore, used the concentration of not only LGO, but also DH. It should be noted that the direct formation of HMF from DH unlikely occurs [11]. The HMF selectivity (S_{HMF}) was calculated on a carbon basis with the ratio of generated HMF to converted LGO. The carbon balance (C bal) is defined as the total yield of main compounds (LGO, DH, HMF, FF, LA, and FA) in product liquid. In other words, the value of "100 – C bal (%)" represents the yield of carbon lost as degradation products.

4.3 Results and discussion

4.3.1 Effect of solid acid catalyst type

Seven types of zeolites, ion-exchange resin (Amberlyst 70), and sulfonated activated carbon (S-AC) were tested for the aqueous phase conversion of LGO as catalysts. The catalysts were selected because of their different characteristics as solid acid catalyst. Zeolites are highly structured crystalline microporous aluminosilicates containing channels with very well-defined pores, where the active sites are located. The pore window size and shape select molecules that are allowed to reach the active sites. S-AC and Amberlyst 70 bear functional groups, which work mainly as Brønsted acid. Structural characteristics of the catalysts are summarized in **Table 4-1**, and **Figs. 4-1 to 4-5** present XRD patterns, SEM images, TEM images, N_2 ad/desorption isotherms, and

NH_3-TPD profiles of zeolites, respectively. The XRD patterns confirm the characteristic structure of each zeolite [31, 32]. SEM and TEM images provide typical depictions of crystal structures of all the tested zeolites. All zeolites are porous with large surface areas, while the structures differ, depending on the type, as discussed later. NH_3-TPD measurement was performed for the selected four samples (**Fig. 4-5**), but the quantification of acid site amount was possible only for ZSM-5 and mordenite. β-1 showed little NH_3 adsorption which was insufficient for the quantification. The largest amount of NH_3 desorption detected for Y-2 at low temperatures with the peak at 239 °C presents its weak acidity, causing the difficulty in separation of NH_3 desorptions from proton over the catalyst and the adsorbed NH_3. It is reasonable from the profiles that the acid strength and amount are higher in the order of mordenite > β-2 > ZSM-5 > Y-1 > β-1, Y-2, Y-3. This trend agrees with a reported acidity order [33]. The carbonaceous catalysts, S-AC and Amberlyst 70, had comparable or more acid sites than zeolites. Amberlyst 70 consisted of relatively large pores with the average size of 22 nm. The S-AC was rich in micropores with larger surface areas, compared to those of zeolites.

Table 4-1 Structural properties of solid acid catalysts used in this study.

Zeolites

	SiO_2/Al_2O_3[a] (–, mol/mol)	S_{BET} (m^2/g)	V_{total} (cm^3/g)	V_{micro} (cm^3/g)	Acid sites[b] (mmol/g)
ZSM-5	30	419	0.264	0.155	0.325
Mordenite	20	501	0.361	0.219	0.717
β-1	500	508	0.290	0.186	N.A.[c]
β-2	18	617	0.721	0.154	1.419
Y-1	500	861	0.596	0.297	0.01
Y-2	5.1	705	0.356	0.249	N.A.[c]
Y-3	5.1	832	0.384	0.298	1.11

Ion-exchange resin

	Acid sites[a] (mmol/g)	S_{BET}[a] (m^2/g)	D_{pore}[a,d] (Å)	T_{max}[a,e] (°C)
Amberlyst 70	2.65	36	220	190

Sulfonated activated carbon

	Acid sites (mmol/g)	S_{BET} (m^2/g)	V_{total} (cm^3/g)	V_{micro} (cm^3/g)
S-AC	0.44	1242	0.558	0.496

[a] Data provided by manufacturer. [b] Measured by NH3-TPD. [c] Not available because of low acidity. [d] Average pore diameter. [e] Maximum operating temperature.

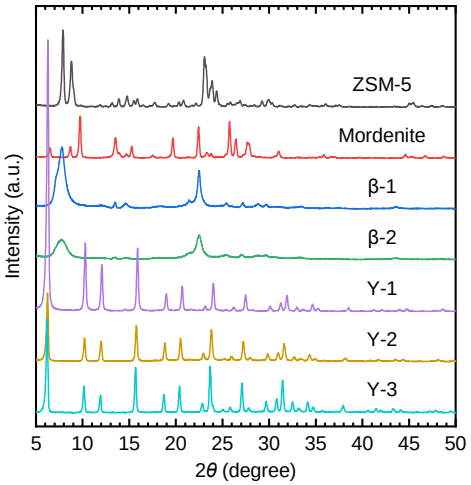

Fig. 4-1 XRD patterns of zeolites.

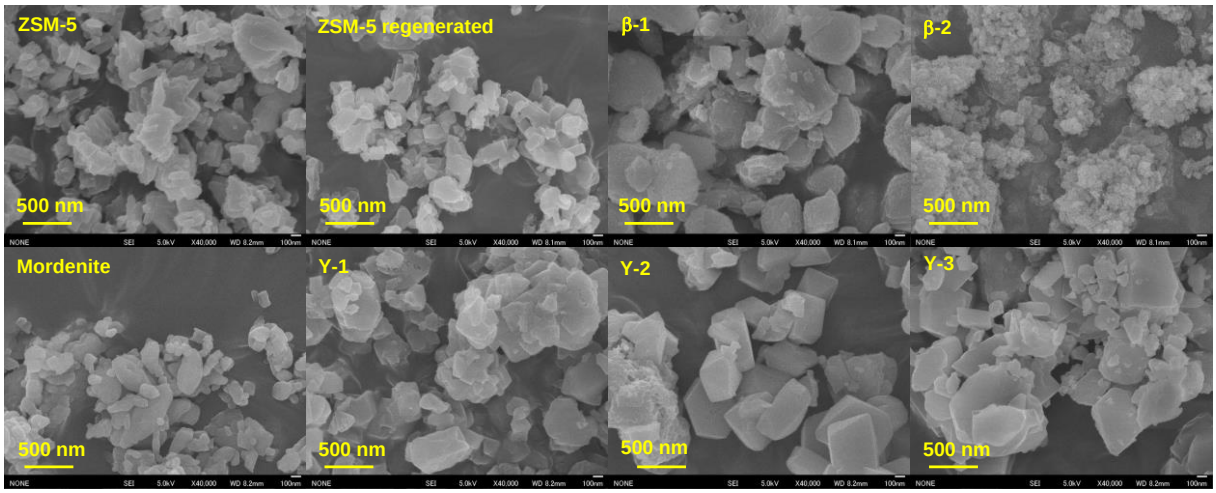

Fig. 4-2 SEM images of zeolite catalysts used in this study.

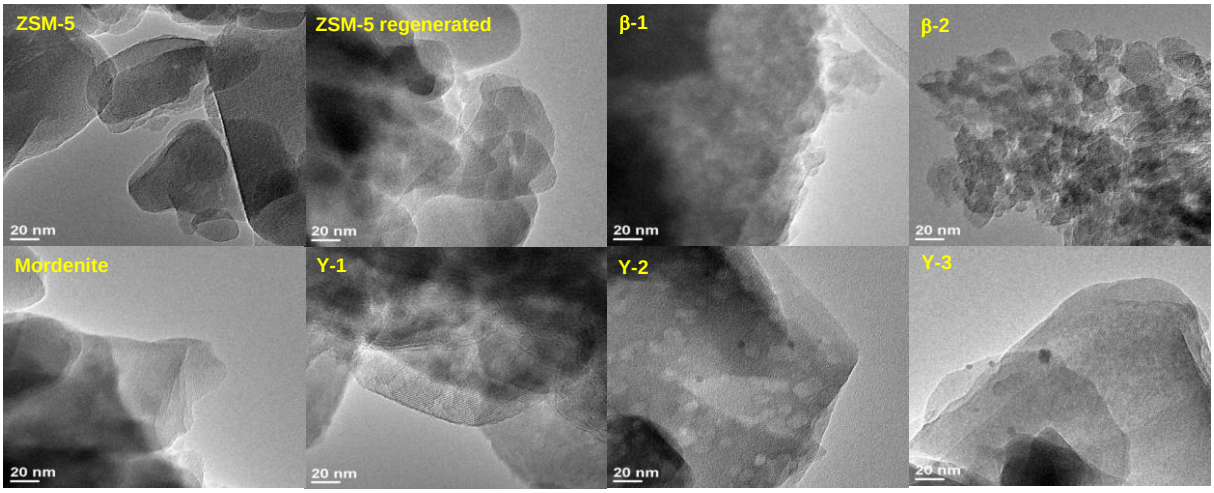

Fig. 4-3 TEM images of zeolite catalysts used in this study.

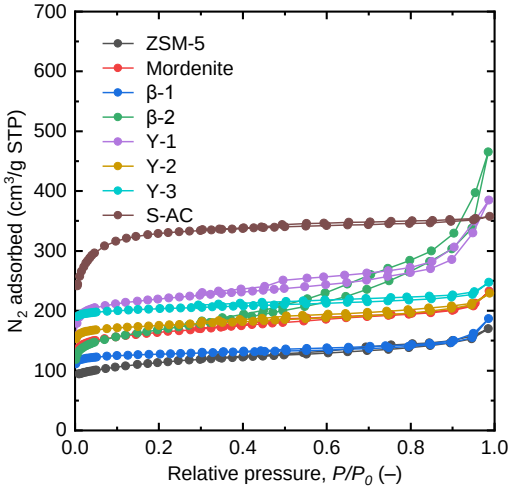

Fig. 4-4 N_2 ad/desorption isotherms of zeolites and S-AC.

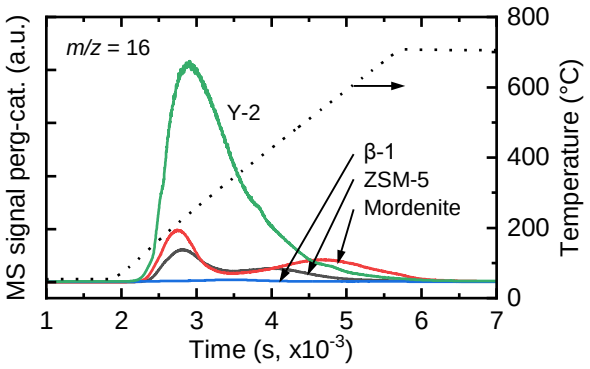

Fig. 4-5 NH_3-TPD profiles of ZSM-5, mordenite, β-1, Y-2.

The catalytic performances in LGO conversion at 150 °C and 1 h are listed in **Table 4-2**. As mentioned above, recent reports [11, 12] have revealed that LGO sequentially converts into HMF and then LA (+ FA) in an aqueous homogeneous condition with sulfuric acid as catalyst. The first step is isomerization of LGO to HMF, and the second step is hydration of HMF to LA and FA. The main compounds contained in the product liquids after all experiments were HMF, LA, FA, unconverted LGO (+ DH), and, in addition, FF. These were only compounds detectable with HPLC under employed conditions, excluding trace amounts of formaldehyde in some experiments. Because the second step of the reaction hardly progresses in this experiment (150 °C and 1 h), the catalytic selectivity toward the target reaction is compared in terms of S_{HMF}. The C bal was not sufficiently high with the detected compounds, largely due to the degradation to large molecular weight products such as humins, which was clear from the color of the recovered solution and catalyst.

Table 4-2 Aqueous phase conversion of LGO over various solid acid catalysts.

Catalyst	X_{LGO} (%-C)	Yield (%-C)				S_{HMF} (%-C)	C bal (%)
		HMF	FF	LA	FA		
None	3.2	<0.1	<0.1	<0.1	<0.1	0.0	96.8
ZSM-5	56.6	29.2	6.7	1.2	<0.1	51.6	79.2
ZSM-5[a]	65.3	33.7	6.0	1.6	0.1	51.6	76.2
Mordenite	16.1	4.2	1.1	0.6	0.1	25.7	89.1
β-1	29.3	5.5	1.6	<0.1	<0.1	18.7	77.8
β-2	23.2	5.9	1.1	<0.1	<0.1	25.4	83.8
Y-1	25.2	0.5	0.1	<0.1	<0.1	2.1	75.4
Y-2	19.5	0.0	0.1	<0.1	<0.1	0.2	80.6
Y-3	37.0	0.0	0.1	<0.1	<0.1	0.1	63.1
Amberlyst 70[a]	46.2	29.6	0.5	2.4	0.4	64.0	86.7
S-AC	44.0	0.5	<0.1	<0.1	<0.1	1.1	56.5
S-AC[a]	28.1	0.6	0.1	<0.1	<0.1	2.2	72.6

Reaction conditions: 150 °C, 1 h, LGO 50 mg, H_2O 5 mL, LGO/catalyst = 2 (w/w). [a] LGO/catalyst = 1 (w/w).

The comparison with the catalyst-free experiment showed the effect of solid acid catalysts on LGO conversion, although the product selectivity strongly depended on the catalyst type. Among zeolites, ZSM-5 showed the best performance. The S_{HMF} of mordenite and β zeolites were less than half of that of ZSM-5, and Y zeolites produced little HMF. Considering the order of acid strength and amount of tested zeolites, the results indicated that reaction selectivity was influenced by not only acidic characteristics, but also the pore morphology. Detailed information on the pore structure is supplemented in **Table 4-3**. ZSM-5 had the smallest pores and internal pore space, and, accordingly, the highest steric hindrance represented by constraint index (C.I.). The sizes are likely not large enough to allow LGO and HMF, which have a kinetic diameter ($\sigma = 1.234Mw^{1/3}$) [34] of 6.2 Å, to enter into the structure, if based on the sizes

calculated with commonly-used atomic radii. On the other hand, ZSM-5 was in fact effective for the HMF production in this study as well as production of the other compounds, e.g., BTX (σ > 5.9 Å) [34, 35]. Therefore, reactions only occurring on the outer surface of ZSM-5 were not a sufficient explanation. The disagreement in the sizes may be modified by employing the pore sizes calculated using Norma radii [34]. In this case, the pore sizes are the same or slightly higher than those of LGO and HMF. The other zeolites (mordenite, β, and Y), showing lower S_{HMF}, had larger pores and lower steric hindrance. Since the low S_{HMF} is caused mainly by the formation of degradation products (humins), this result indicates that extra space inside the zeolite pores provides opportunities for LGO and HMF to undergo side reactions. The acid strength and quantity are also important properties for the catalysis, but, in this comparison, the pore morphology is considered as the main reason for difference in the reaction selectivity because all the zeolites showed considerable LGO conversion with the acid catalysis. The influence of acid type (Brønsted or Lewis) is discussed in the next section.

Table 4-3 Additional information on structural characteristics of zeolites[1–5].

	ZSM-5	Mordenite	β	Y
IZA code	MFI	MOR	BEA	FAU
Pore dimension	3	2	3	3
Pore size (Å)	5.1×5.5, 5.3×5.6	6.5×7.0, 3.4×4.8, 2.6×5.7	6.6×6.7, 5.6×5.6	7.4×7.4
Internal pore space (Å)	6.36	6.70	6.68	11.24
C.I.	6.9	0.5	0.6–2.0	0.4
Max. pore diameter (atomic radii) d_A (Å)	5.5–5.6	4.8–7.0	5.6–6.7	7.4
Max. pore diameter (Norman radii) d_N (Å)	6.2–6.3	5.5–7.7	6.3–7.4	8.1

[1] Jae, J.; Tompsett, G. A.; Foster, A. J.; Hammond, K. D.; Auerbach, S. M.; Lobo, R. F.; Huber, G. W. J. Catal. **2011**, 279, 257–268. [2] Treacy, M. M. J.; Foster, M. D. *Micropor. Mesopor. Mater.* **2009**, 118, 106-114. [3] International Zeolite Association (http://www.iza-structure.org/) [4] Japan Zeolite Association (https://jza-online.org/) [5] van Bekkum, H., Flanigen, E. M., Jacobs, P. A., Jansen, J. C., Eds. Introduction to Zeolite Science and Practice, 2nd ed.; Elsevier Science, Amsterdam, The Netherlands.

Amberlyst 70 and S-AC also showed good performance to give substantial LGO conversion, although much higher HMF yield was observed for Amberlyst 70. For S-AC, possible factors decreasing the S_{HMF} are the pore structure and richness in functionality. S-AC is basically microporous, but the pore size distribution is rather broad as seen in the isotherm (**Fig. 4-4**). Accordingly, as with the case of zeolites, the pores slightly larger than the molecular size of LGO could cause the occurrence of side reactions. The sulfo group selectively works toward the LGO conversion as evidenced in the result of Amberlyst 70, but the support, activated carbon, also has other acidic functional groups. The multiplicity of acidic function can enhance the rate of LGO

conversion while decreasing the reaction selectivity. Thus, among the solid acid catalysts employed in this study, ZSM-5 and Amberlyst 70 were the best for the LGO conversion to HMF. In the next section, the catalytic activities are investigated in more detail.

4.3.2 Catalysis of ZSM-5 and Amberlyst 70

The aqueous phase LGO conversion over ZSM-5 and Amberlyst 70 was carried out at different temperatures and reaction times. Data points in **Figs. 4-6 and 4-7** present the experimentally obtained conversion and yield profiles. In the range of reaction time employed, LA formation was not pronounced at 120 °C. HMF yield showed the maximum at 150 and 180 °C, and LA yield exceeded the HMF yield at 180 °C at a prolonged reaction time. With Amberlyst 70, the total yield of HMF, LA, and FA, indicating the reaction selectivity, was over 70%-C at 8 h (150 °C) and >2 h (180 °C), and the highest yield of 72.2%-C was achieved at 180 °C for 2 h. This is comparable to the reported yield for the homogeneous reaction system with sulfuric acid (*ca.* 80 %-C: LGO 50 mM, H_2SO_4 50 mM, 125 °C, and > 2 h) [11]. Severer reaction conditions (temperature or time) were required for the present study with tested Amberlyst 70 amount (acid sites concentration = 26 mM), but, nonetheless, it was notable that the highly selective reaction was possible with a cleaner reaction system using the solid acid catalyst, having the potential for a simple recyclability. Regarding LGO as the feedstock, it was likely superior to glucose for this reaction system because, for example, a study by Weingarten et al. [36] has shown that aqueous phase glucose conversion over

Amberlyst 70 (at 150–180 °C and 80–100 %-C conversion) produced humins at the yield of 50–55 %-C, which was much higher than that observed in this study (less than 30 %-C at 150 and 180 °C).

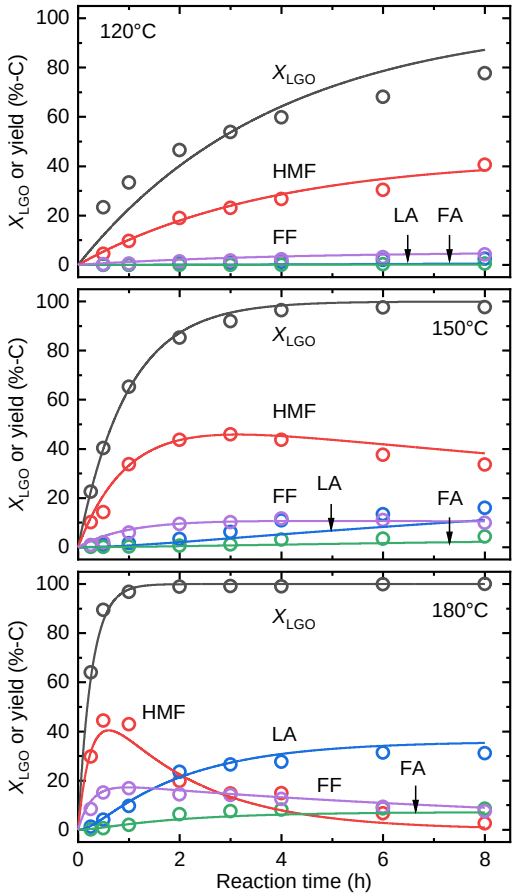

Fig. 4-6 LGO conversion over ZSM-5: LGO 50 mg, H_2O 5 mL, LGO/ZSM-5 = 1 (w/w). Data points represent the experimentally obtained results. Lines represent the conversion and yields calculated with kinetic parameters.

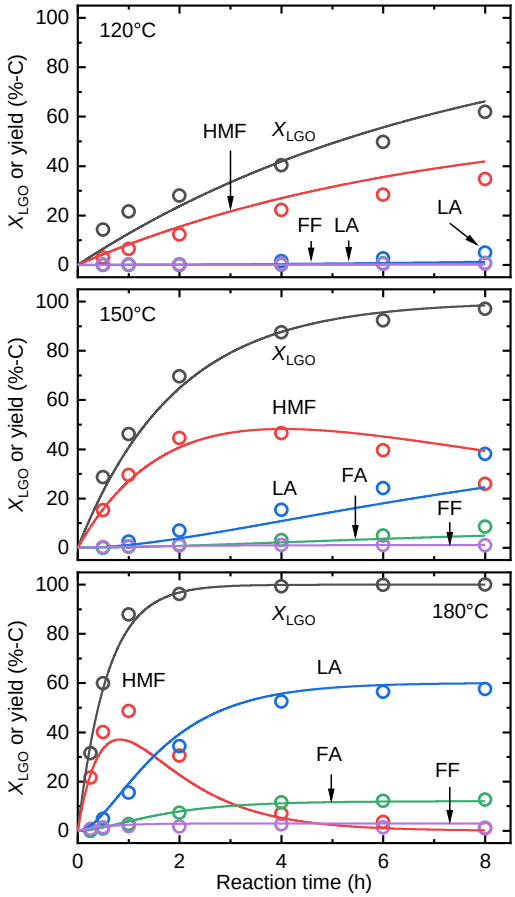

Fig. 4-7 LGO conversion over Amberlyst 70: LGO 50 mg, H_2O 5 mL, LGO/Amberlyst 70 = 1 (w/w). Data points represent the experimentally obtained results. Lines represent the conversion and yields calculated with kinetic parameters.

Compared to Amberlyst 70, ZSM-5 enabled faster LGO conversion, but lower reaction selectivity. The highest total yield of HMF, LA, and FA was 57.6 %-C at 150 °C and 4 h. The most important factor decreasing the reaction selectivity was the preference for humins formation. As shown in **Fig. 4-8**, ZSM-5 showed lower C bal than Amberlyst 70 within the entire range of reaction time and temperature. Moreover, the formation of FF, another by-product, was more apparent in the reaction with ZSM-5. The highest FF yields were 16.8 and 2.6 %-C for ZSM-5 and Amberlyst 70, respectively. The influence of LGO/ZSM-5 ratio on the reaction selectivity was investigated (**Fig.**

4-9), but apparent improvement in the total yield was not confirmed (46.6–54.4 %-C at LGO/ZSM-5 = 0.3–3.0 (w/w)). An additional experiment was carried out using citric acid for the pretreatment of ZSM-5 to improve the catalysis (**Table 4-4**). The citric acid pretreatment, as an alternative to simple calcination, has been reported to be effective to increase acid sites by producing extraframework of aluminum [37]. However, the change in pretreatment method did not alter the product yields, suggesting the presence of a causative factor in the inherent characteristics of the catalyst.

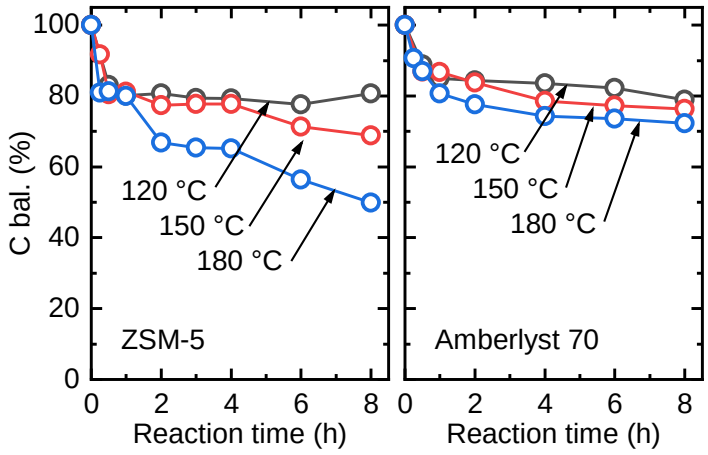

Fig. 4-8 Carbon balance (C bal) in LGO conversion over ZSM-5 and Amberlyst 70: LGO 50 mg, H_2O 5 mL, LGO/Amberlyst 70 = 1 (w/w).

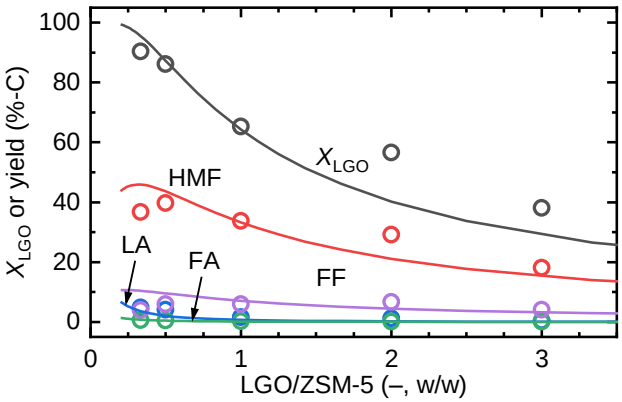

Fig. 4-9 Effect of ZSM-5 loading amount on X_{LGO} and product yields: 150 °C, 1 h, LGO 50 mg, H_2O 5 mL. Data points represent the experimentally obtained results. Lines represent the conversion and yields calculated with kinetic parameters.

To clearly describe the difference in reaction selectivity, the experimental results with ZSM-5 and Amberlyst 70 (**Figs. 4-6 and 4-7**) were kinetically analyzed with the reaction pathway consisting of six first-order reactions (r_1– r_6), shown in **Fig. 4-10**. The kinetics was analyzed using the reaction pathway in **Fig. 4-10** and assuming first order for reactions r_1–r_6 with respect to the reactant (LGO, HMF, and FF for "r_1, r_4, r_6", r_2, and r_5, respectively):

$$r_i = k_{0,i}\exp(-E_i/\mathrm{R}T)C_j \quad (1)$$

(r_i: reaction rate, $k_{0,i}$: frequency factor, E_i: activation energy, R: gas constant, T: temperature, C_j: concentration, i = 1–6, j = LGO, HMF, LA, FA, FF, or DP1–DP3)

$$\mathrm{d}C_{\mathrm{LGO}}/\mathrm{d}t = -r_1 - r_4 - r_6 \quad (C_{\mathrm{LGO}}\text{: total concentration of LGO and DH}) \quad (2)$$

$$\mathrm{d}C_{\mathrm{HMF}}/\mathrm{d}t = r_1 - r_2 - r_3 \quad (3)$$

$$\mathrm{d}C_{\mathrm{LA}}/\mathrm{d}t = 5 \cdot \mathrm{d}C_{\mathrm{FA}}/\mathrm{d}t = r_2 \quad (4)$$

$$\mathrm{d}C_{\mathrm{FF}}/\mathrm{d}t = r_4 - r_5 \quad (5)$$

$$\mathrm{d}C_{\mathrm{DP1}}/\mathrm{d}t = r_3 \quad (6)$$

$$\mathrm{d}C_{\mathrm{DP2}}/\mathrm{d}t = r_5 \quad (7)$$

$$\mathrm{d}C_{\mathrm{DP3}}/\mathrm{d}t = r_6 \quad (8)$$

The concentration of each component was calculated with equations (1)–(8) and optimized by regression analysis to the best fit with experimental data. The analysis did not consider the influence of catalyst deactivation and mass transfer. **Table 4-5** lists the obtained kinetic parameters, and **Fig. 4-11** describes the product yields calculated with the parameters as functions of reaction time and temperature. The calculation data in **Fig. 4-9** on the effect of ZSM-5 loading amount was obtained by changing the value of frequency factor, $k_{0,i}$, proportionally to the loading amount. For example, when LGO/ZSM-5 = 2 w/w, $k_{0,i}$ was doubled. All the reactions are catalyzed by the employed catalysts. An additional experiment confirmed that HMF was stable in the absence of catalyst even at 180 °C for 3 h (98% yield). Potential reactants to form humins, denoted

by degradation products (DP1–DP3), were assumed to be LGO, HMF, and FF. This assumption was reasonable, according to carbon balance in the consumption of each reactant (LGO → HMF and HMF → LA + FA). FF formed from LGO, but not from HMF, and then gradually converted into degradation products, which was confirmed in an experiment using HMF and FF as reactants (**Fig. 4-12**). LA and FA were stable under the present reaction conditions as shown in **Fig. 4-8**. The other assumptions, calculation method, and the obtained parameters of kinetic analysis are described in the supporting information. Determined activation energy for the conversion of HMF to LA was 121 and 115 kJ/mol for the reactions with ZSM-5 and Amberlyst 70, respectively. These are roughly consistent with the reported values [11, 36, 38]. On the other hand, the activation energy for the LGO conversion to HMF was less than the value reported in above mentioned study [11] on the reaction with sulfuric acid (130 kJ/mol). This possibly indicates a difference in the sensitivity of catalysis toward reaction temperature, while being partially attributed to the introduction of two additional reaction pathways of LGO, the conversion into FF and DP3, in the present study.

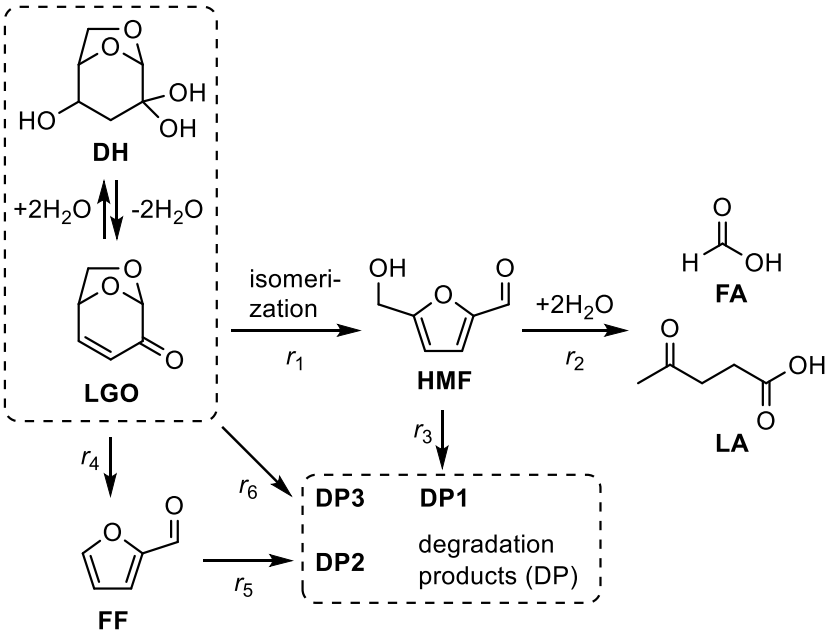

Fig. 4-10 Proposed reaction pathways from LGO to HMF, LA, FA, FF, and degradation products.

Table 4-5 Kinetic parameters for the LGO conversion over ZSM-5 and Amberlyst 70 at LGO 50 mg, H_2O 5 mL, and LGO/catalyst = 1 w/w.

	ZSM-5	Amberlyst 70
Frequency factor, $k_{0,i}$ (L/mol/min, × 10^{-10})		
$k_{0,1}$	6.72×10^{-4}	6.83×10^{-5}
$k_{0,2}$	6.14×10	2.79×10
$k_{0,3}$	1.30×10^{6}	1.29×10^{6}
$k_{0,4}$	3.06×10^{-1}	2.15×10
$k_{0,5}$	6.50×10^{2}	4.55×10^{2}
$k_{0,6}$	3.28×10^{-7}	1.35×10^{-6}
Activation energy, E_i (kJ/mol)		
E_1	71.8	65.2
E_2	121.1	115.5
E_3	163.3	207.3
E_4	98.2	115.6
E_5	135.4	160.8
E_6	46.6	54.5

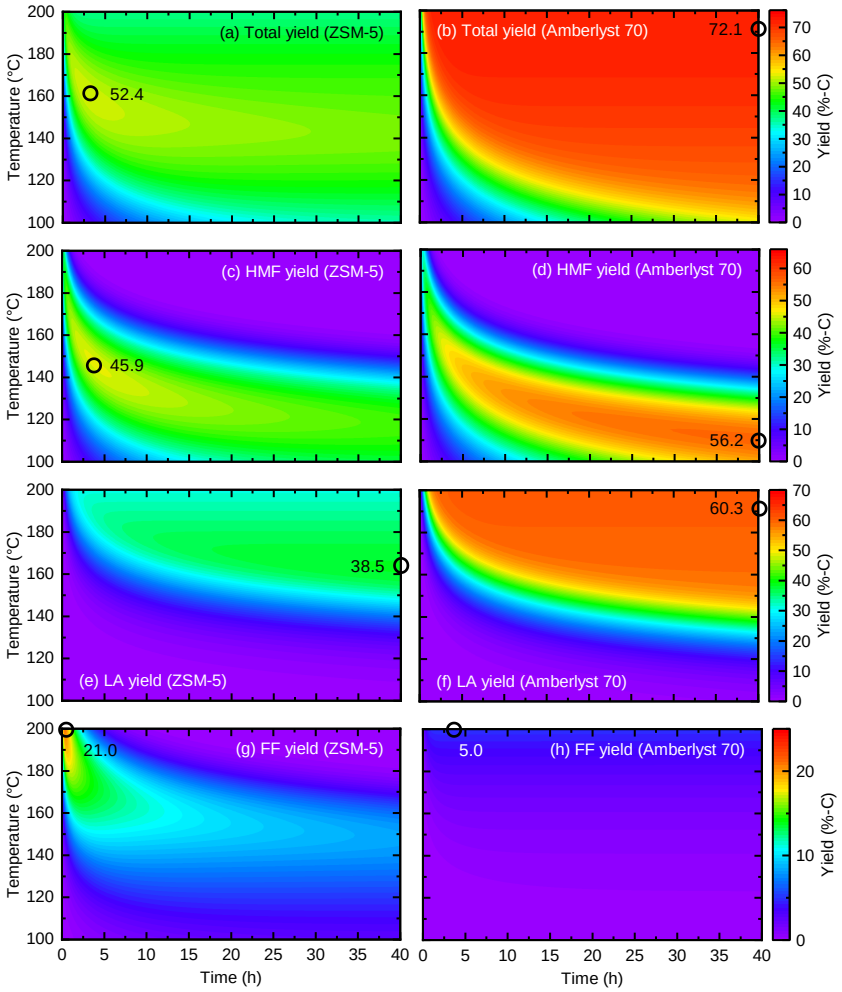

Fig. 4-11 Yield map calculated with kinetic parameters. (a, b) total yield of HMF, LA, and FA, (c, d) HMF yield, (e, f) LA yield, (g, h) FF yield for ZSM-5 and Amberlyst 70. Plots represent the highest yield in the presented reaction time and temperature ranges.

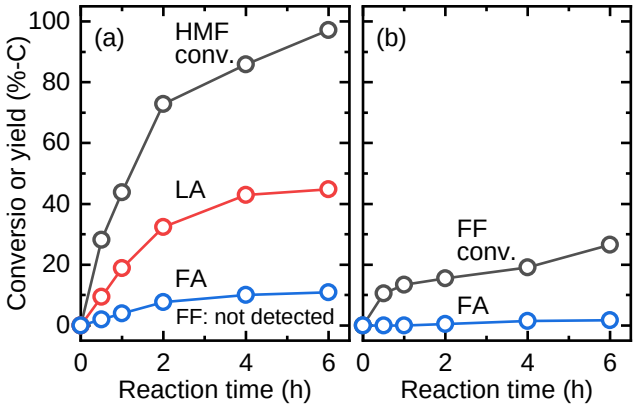

Fig. 4-12 Aqueous phase conversion of HMF (a) and FF (b) over ZSM-5: 180 °C, HMF or FF 50 mg, H_2O 5 mL, HMF or FF/ZSM-5 = 1 (w/w).

Fig. 4-13 describes the carbon distribution in the product during the reaction, calculated with kinetic parameters. The calculation was carried out for the reaction of 40 h under the assumption that the catalysis did not change over this time period. The significance of DPs formation is clear from the result. In the presented cases, the DPs were derived mostly from LGO (DP3), which was in contrast with the reported pathway [11] that considered only HMF-derived DP (DP1). It is noteworthy that the formation of DP3 was suppressed at higher temperatures. The reason was kinetically clear because the reaction rate of LGO → HMF was slower at low temperatures and faster at high temperatures than that of LGO → DP3. Given that DP3 derives mainly from DH, this trend can also be explained by the shift of equilibrium between LGO and DH toward LGO with increases in the temperature. The comparison between ZSM-5 and Amberlyst 70 confirms that ZSM-5 had higher catalytic activity toward the LGO conversion but with lower selectivity. ZSM-5 produced a considerable amount of FF (up to 21.0 %-C yield (**Fig. 4-11**), DP1, and FF-derived DP (DP2). Ambetlyst 70 hardly showed any catalysis resulting in these by-products. In the comparison of zeolites (**Table 4-2**), the catalyst with larger pores showed lower S_{HMF}. Amberlyst 70 had much larger pores (220 Å) than the zeolites, but it showed good selectivity. This result indicates the importance of acid type. Zeolites generally contain both Brønsted and Lewis acids [31, 39, 40]. According to a study [31] that measured the distribution of these acids with FT-IR using pyridine as a probe molecule, zeolites used in this study with SiO_2/Al_2O_3 = 12–25 had 45-256 μmol/g of Lewis acid sites in addition to Brønsted acid sites. Because Amberlyst

70 has only Brønsted acidity, the present result suggests that Lewis acid sites have a catalysis toward the formation of DP1, DP2, and FF. In fact, the LGO conversion with sulfuric acid [11] did not produce FF, and the selectivity to HMF was high. A similar conclusion regarding the unfavorable catalytic role of Lewis acid sites over solid acid catalysts is apparent for the conversion of xylose to FF [41], fructose to HMF [42], and furfuryl alcohol to levulinic acid [43]. FF is likely formed by the catalysis of Lewis acid sites for removing alcohol functional group in the course of LGO pyranose ring opening to form furan ring [14]. A similar reaction pathway has been reported for the conversion of fructose to FF under catalysis of Lewis acid sites [44]. In view of the low selectivity to side reactions, it seemed that the large pore size of Amberlyst 70 did not have predominant influence over the formation of DPs. In other words, the large pores allowed LGO and the products to enter and leave the catalyst matrix, and the dense Brønsted acid over the surface, formed by the high acid site amount (2.65 mmol/g) in a small area (S_{BET} = 36 m^2/g), contributed to the suppression of side reactions.

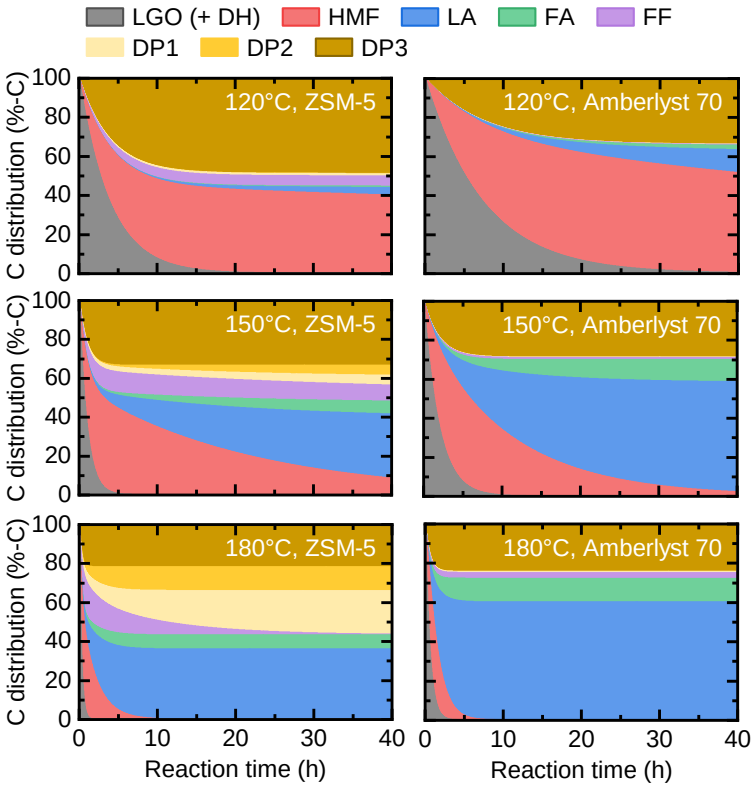

Fig. 4-13 Carbon distribution in product of reaction, calculated with kinetic parameters.

As a result of the inhibiting effect on DP3 formation, the highest total yield of HMF, LA, and FA with Amberlyst 70 was observed at a high temperature of 191 °C in the calculation (**Fig. 4-11**), although the temperature was slightly outside the range of T_{max} (190 °C). The influence of DP1 formation was remarkable above this temperature and decreased the yield. ZSM-5 showed the highest total yield at a middle temperature of 161 °C because the formations of DP1 and FF were pronounced at higher temperatures (**Figs. 4-11** and **4-13**). Thus, for both catalysts, higher temperature was not necessarily preferred to show the best reaction selectivity. On the other hand, the highest HMF yields were found at lower temperatures of 146 °C and 110 °C for ZSM-5 and Amberlyst 70, respectively (**Fig. 4-11(c)** and **(d)**). This was because of weaker catalysis

toward the conversion of HMF to LA and DP1 at lower temperatures, compared to the catalysis to LGO → HMF.

Deposition of carbonaceous materials derived from humins is generally one of the main reasons for decrease in catalytic activity of the present reaction system. The majority of DPs was present in the liquid phase, but the deposition was clear from the color of catalyst, even at an early stage of the reaction. For example, the carbon yield from LGO over ZSM-5 was 5.0 %-C in the reaction at 150 °C for 0.5 h, and the yield gradually increased with the reaction time (**Fig. 4-14**). Supposedly, the sharp decrease in C bal at < 1 h (**Fig. 4-8**) was caused mainly by this reaction. To investigate the influence on catalytic activity, the LGO conversion experiments were carried out using the catalyst recovered by separation from the product liquid after rinsing with pure water at room temperature. Catalyst regeneration was also performed by recalcination at 550 °C for 2 h for ZSM-5 and by sequential washing with acetone and water at 60 °C, followed by vacuum drying, for Amberlyst 70. **Fig. 4-15** compares the catalyst activities with HMF and LA yields in the reaction at 180 °C. Considerable decreases in the yields were confirmed when the catalyst was directly reused, for ZSM-5 in particular. This showed that the deposited carbonaceous materials inhibited the contact of reactants with the active sites over catalyst. The S_{BET} of spent ZSM-5 was in fact very low, 82 m^2/g. On the other hand, the result with regenerated catalyst revealed that the deposits could be removed by simple recalcination at the temperature identical to the pretreatment temperature (S_{BET} = 407 m^2/g after regeneration). There is no significant change for the

fresh, spent and regenerated ZSM-5 from the XRD patterns (**Fig. 4-14(c)**). As shown in TG curves of the spent catalyst combustion (**Fig. 4-14**), the removal of deposits started below 200 °C and gradually progressed with temperature, suggesting that the deposits were rather volatile and not like coke, its removal requiring harsh conditions. The activity of Amberlyst 70 suffered less from the deposits. Over 90% of the HMF and LA total yields in fresh catalysts were reproduced with the regenerated catalysts for both ZSM-5 and Amberlyst 70.

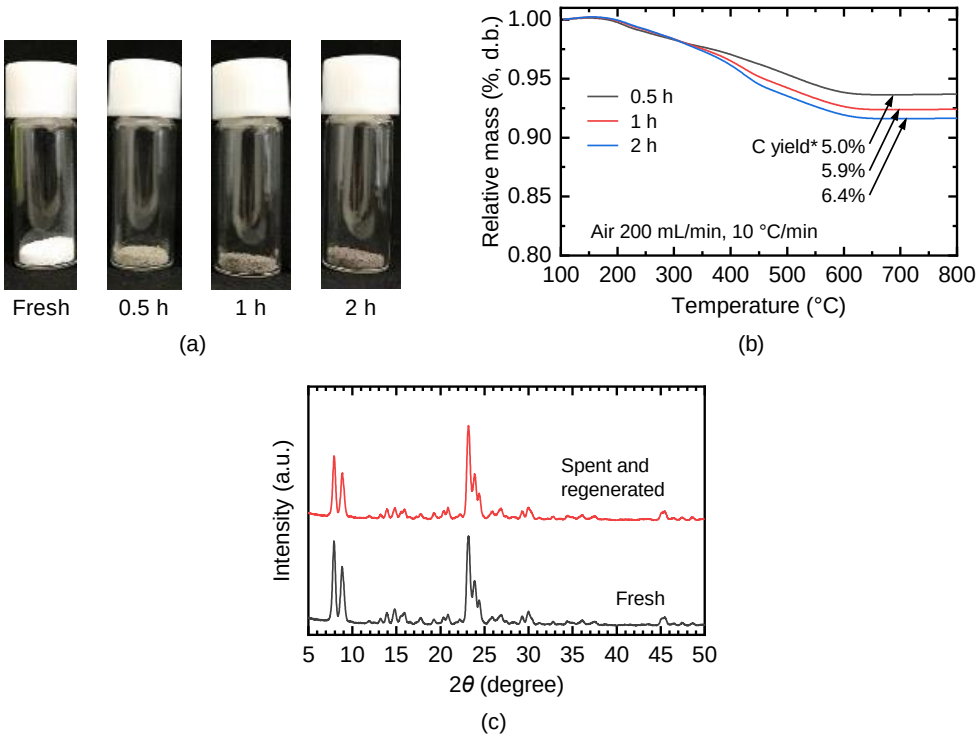

Fig. 4-14 ZSM-5 after the LGO conversion at 150 °C, LGO 50 mg, H_2O 5 mL, and LGO/ZSM-5 = 1 w/w: (a) images of fresh and spent catalysts. (b) TGA analysis under a flow of air. C yield (carbon yield) in the figure (b) represents the yield of carbon deposited from LGO over ZSM-5. The analysis was carried out on a PerkinElmer 2400 Series II CHNS/O Elemental Analyzer. (c) XRD patterns of fresh and spent-regenerated catalysts.

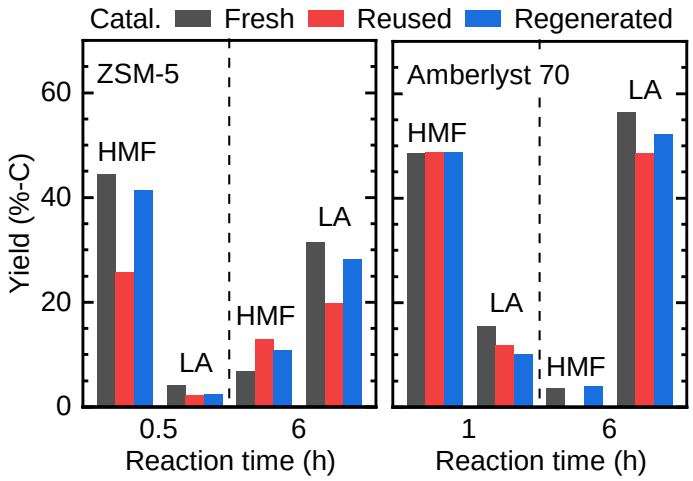

Fig. 4-15 HMF and LA yields in LGO conversion at 180°C and LGO/catalyst = 1 (w/w) using fresh, recovered by separation from the product liquid after reaction (reused), and regenerated catalysts.

4.4 Conclusions

A simple and clean reaction of LGO in water with solid acid catalyst produced HMF and LA with a substantial yield. The solid acid catalysts, employed in this study, all promoted the LGO conversion, but the selectivity to HMF and LA was significantly affected by the pore structure and acid type. ZSM-5, having pore sizes close to the molecular sizes of LGO and HMF, showed the best rate of LGO conversion (per mass of catalyst) and selectivity among zeolites, and Amberlyst 70, having dense Brønsted acid sites, showed best selectivity. The highest total yields of HMF and LA were 57.6 and 72.2 % on a molar basis, respectively. The kinetic analysis of experimental results revealed that DPs, causing the decrease in HMF and LA yields, were formed directly from LGO (and/or DH) rather than HMF and FF at an early stage of the reaction. Because of the increased formation of DP1 and FF, a high temperature was not necessarily preferred for achieving higher HMF and LA yields, and the best

temperatures were identified as 161 °C and 191 °C for ZSM-5 and Amberlyst 70, respectively, under the present experimental conditions. Despite the amount of DPs formed, they had a negligible effect on the performance of the recycled Amberlyst 70 and were readily removed by calcination from ZSM-5.

4.5 References

[1] R. A. Sheldon, Green and sustainable manufacture of chemicals from biomass: state of the art. Green Chem. 16 (2014) 950–963.

[2] F. H. Isikgor, C.R. Becer, Lignocellulosic biomass: a sustainable platform for the production of bio-based chemicals and polymers. Polym. Chem. 6 (2015) 4497–4559.

[3] J.J. Bozell, L. Moens, D.C. Elliott, Y. Wang, G.G. Neuenscwander, S.W. Fitzpatrick, R.J. Bilski, J.L. Jarnefeld, Production of levulinic acid and use as a platform chemical for derived products. Resour. Conserv. Recycl. 28 (2000) 227–239.

[4] Qi, L. Y.F. Mui, S.W. Lo, M.Y. Lui, G.R. Akien, I.T. Horváth, Catalytic conversion of fructose, glucose, and sucrose to 5-(hydroxymethyl)furfural and levulinic and formic acids in γ-valerolactone as a green solvent. ACS Catal. 4 (2014) 1470–1477.

[5] D.W. Rackemann, W.O.S. Doherty, The conversion of lignocellulosics to levulinic acid. Biofuels, Bioprod. Biorefin. 5 (2011) 198–214.

[6] R.J. Van Putten, J.C. Van der Waal, E. De Jong, C.B. Rasrendra, H.J. Heeres, J.G. De Vries, Hydroxymethylfurfural, a versatile platform chemical made from renewable resources. Chem. Rev. 113 (2013) 1499–597.

[7] Y. Román-Leshkov, J.N. Chheda, J.A. Dumesic, Phase modifiers promote efficient production of hydroxymethylfurfural from fructose. Science 312 (2006) 1933–1937.

[8] S. Van de Vyver, Y. Román-Leshkov, Emerging catalytic processes for the production of adipic acid. Catal. Sci. Technol. 3 (2013) 1465–1479.

[9] Z. Cao, Z. Fan, Y. Chen, M. Li, T. Shen, C. Zhu, H. Ying, Efficient preparation of 5-hydroxymethylfurfural from cellulose in a biphasic system over hafnyl phosphates. Appl. Catal. B: Environ. 244 (2019) 170–177.

[10] E4tech, RE-CORD and WUR (2015) "From the sugar platform to biofuels and biochemicals". Final report for the European Commission, contract No. ENER/C2/423-2012/SI2.673791"

[11] S.H. Krishna, T.W. Walker, J.A. Dumesic, G.W. Huber, Kinetics of levoglucosenone isomerization. ChemSusChem 10 (2016) 129–138.

[12] J. He, M. Liu, K. Huang, T.W. Walker, C.T. Maravelias, J.A. Dumesic, G.W. Huber, Production of levoglucosenone and 5-hydroxymethylfurfural from cellulose in polar aprotic solvent-water mixtures. Green Chem. 19 (2017) 3642–3653.

[13] S.H. Krishna, K. Huang, K.J. Barnett, J. He, C.T. Maravelias, J.A. Dumesic, G.W. Huber, M. De bruyn, B.M. Weckhuysen, Oxygenated commodity chemicals from

chemo-catalytic conversion of biomass derived heterocycles. AIChE J. 64 (2018) 1910–1922.

[14] H. Kawamoto, S. Saito, W. Hatanaka, S. Saka, Catalytic pyrolysis of cellulose in sulfolane with some acidic catalysts. J. Wood Sci. 53 (2006) 127–133.

[15] S. Kudo, Z. Zhou, K. Norinaga, J. Hayashi, Efficient levoglucosenone production by catalytic pyrolysis of cellulose mixed with ionic liquid. Green Chem. 13 (2011) 3306–3311.

[16] J. Zandersons, A. Zhurinsh, G. Dobele, V. Jurkjane, J. Rizhikovs, B. Spince, A. Pazhe, Feasibility of broadening the feedstock choice for levoglucosenone production by acid pre-treatment of wood and catalytic pyrolysis of the obtained lignocellulose. J. Anal. Appl. Pyrolysis 103 (2013) 222–226.

[17] F. Cao, T.J. Schwartz, D.J. McClelland, S.H. Krishna, J.A. Dumesic, G.W. Huber, Dehydration of cellulose to levoglucosenone using polar aprotic solvents. Energy Environ. Sci. 8 (2015) 1808–1815.

[18] X.W. Sui, Z. Wang, B. Liao, Y. Zhang, Q.X. Guo, Preparation of levoglucosenone through sulfuric acid promoted pyrolysis of bagasse at low temperature. Bioresour. Technol. 103 (2012) 466–469.

[19] X.N. Ye, Q. Lu, X. Wang, H.Q. Guo, M.S. Cui, C.Q. Dong, Y.P. Yang, Catalytic fast pyrolysis of cellulose and biomass to selectively produce levoglucosenone using activated carbon catalyst. ACS Sustainable Chem. Eng. 5 (2017) 10815–10825.

[20] S. Kudo, N. Goto, J. Sperry, K. Norinaga, J. Hayashi, Production of levoglucosenone and dihydrolevoglucosenone by catalytic reforming of volatiles from cellulose pyrolysis using supported ionic liquid phase. ACS Sustainable Chem. Eng. 5 (2017) 1132–1140.

[21] T. Nishikawa, D. Urabe, M. Isobe, An efficient total synthesis of optically active tetrodotoxin. Angew. Chem. Int. Ed. 43 (2004) 4782–4785.

[22] K.P. Stockton, C.J. Merritt, C.J. Sumby, B.W. Greatrex, Palladium-catalyzed Suzuki-Miyaura, Heck and hydroarylation reactions on levoglucosenone and application to the synthesis of chiral γ-butyrolactones. Euro. J. Org. Chem. 32 (2015), 6999–7008.

[23] M.B. Comba, Y.H. Tsai, A.M. Sarotti, M.I. A.G. Mangione, Suárez, R.A. Spanevello, Levoglucosenone and its new applications: valorization of cellulose residues. Euro. J. Org. Chem. 5 (2018), 590–604.

[24] S.W. Kim, E.T. Ledingham, S. Kudo, B.W. Greatrex, J. Sperry, Bio-based chiral amines via Aza-Michael additions to levoglucosenone under aqueous conditions. Euro. J. Org. Chem. 17 (2018), 2028–2038.

[25] J. Sherwood, M. De bruyn, A. Constantinou, L. Moity, C.R. McElroy, T.J. Farmer, T. Duncan, W. Raverty, A.J. Hunt, J.H. Clark, Dihydrolevoglucosenone (Cyrene) as a bio-based alternative for dipolar aprotic solvents. Chem. Commun. 50 (2014) 9650–9652.

[26] J.E. Camp, Bio-available solvent Cyrene: synthesis, derivatization, and applications. ChemSusChem 11 (2018) 3048–3055.

[27] S.H. Krishna, R.S. Assary, Q.A. Rashke, Z.R. Schmidt, L.A.Curtiss, J.A. Dumesic, G.W. Huber, Mechanistic insights into the hydrodeoxygenation of levoglucosanol over bifunctional platinum silica–alumina catalysts. ACS Catal. 8 (2018) 3743–3753.

[28] S.H. Krishna, M. De bruyn, Z.R. Schmidt, B.M. Weckhuysen, J.A. Dumesic, G.W. Huber, Catalytic production of hexane-1,2,5,6-tetrol from bio-renewable levoglucosanol in water: effect of metal and acid sites on (stereo)-selectivity. Green Chem. 20 (2018) 4557–4565.

[29] X. Mo, D.E. López, K. Suwannakarn, Y. Liu, E. Lotero, J.G. Goodwin, C. Lu, Activation and deactivation characteristics of sulfonated carbon catalysts. J. Catal. 254 (2008) 332–338.

[30] F. Shafizadeh, R.H. Furneaux, T.T. Stevenson, Some reactions of levoglucosenone. Carbohydr. Res. 71 (1979) 169–191.

[31] A. Aho, N. Kumar, K. Eränen, T. Salmi, M. Hupa, D.Y. Murzin, Catalytic pyrolysis of woody biomass in a fluidized bed reactor: Influence of the zeolite structure. Fuel 87 (2008) 2493–2501.

[32] J. Jae, G.A. Tompsett, A.J. Foster, K.D. Hammond, S.M. Auerbach, R.F. Lobo, G.W. Huber, Investigation into the shape selectivity of zeolite catalysts for biomass conversion. J. Catal. 279 (2011) 257–268.

[33] A. Auroux, Microcalorimetry Methods to Study the Acidity and Reactivity of Zeolites, Pillared Clays and Mesoporous Materials. Top. Catal. 19 (2002) 205–213.

[34] J. Jae, G.A. Tompsett, A.J. Foster, K.D. Hammond, S.M. Auerbach, R.F. Lobo, G.W. Huber, Investigation into the shape selectivity of zeolite catalysts for biomass conversion. J. Catal. 279 (2011) 257–268.

[35] K. Uemura, S. Appari, S. Kudo, J. Hayashi, H. Einaga, K. Norinaga, In-situ reforming of the volatiles from fast pyrolysis of ligno-cellulosic biomass over zeolite catalysts for aromatic compound production. Fuel Process. Technol. 136 (2015) 73–78.

[36] R. Weingarten, W.C. Conner, G.W. Huber, Production of levulinic acid from cellulose by hydrothermal decomposition combined with aqueous phase dehydration with a solid acid catalyst. Energy Environ. Sci. 5 (2012) 7559–7574.

[37] Y. Fan, X. Bao, X. Lin, G. Shi, H. Liu, Acidity adjustment of HZSM-5 zeolites by dealumination and realumination with steaming and citric acid treatments. J. Phys. Chem. B 110 (2006) 15411–15416.

[38] B. Girisuta, L.P.B.M. Janssen, H.J. Heeres, A kinetic study on the decomposition of 5-hydroxymethylfurfural into levulinic acid. Green Chem. 8 (2006) 701–709.

[39] B. Valle, A. G. Gayubo, A. Alonso, A.T. Aguayo, J. Bilbao, Hydrothermally stable HZSM-5 zeolite catalysts for the transformation of crude bio-oil into hydrocarbons. Appl. Catal. B: Environ. 100 (2010) 318–327.

[40] S. Saravanamurugan, M. Paniagua, J.A. Melero, A. Riisager, Efficient isomerization of glucose to fructose over zeolites in consecutive reactions in alcohol and aqueous media. J. Am. Chem. Soc. 135 (2013) 5246–5249.

[41] R. Weingarten, G.A. Tompsett, W.C. Conner, G.W. Huber, Design of solid acid catalysts for aqueous-phase dehydration of carbohydrates: The role of Lewis and Brønsted acid sites. J. Catal. 279 (2011) 174–182.

[42] V.V. Ordomsky, J. Van der Schaaf, J.C. Schouten, T.A. Nijhuis, Fructose dehydration to 5-hydroxymethylfurfural over solid acid catalysis in a biphasic system. ChemSusChem 5 (2012) 1812–1819.

[43] M.A. Mellmer, J.M.R. Gallo, D. Martin Alonso, J.A. Dumesic, Selective production of levulinic acid from furfuryl alcohol in THF solvent systems over H-ZSM-5. ACS Catal. 5 (2015) 3354–3359.

[44] Y. Wang, X. Yang, H. Zheng, X. Li, Y. Zhu, Y. Li, Mechanistic insights on catalytic conversion fructose to furfural on beta zeolite via selective carbon-carbon bond cleavage. Molecular Catal. 463 (2019) 130–139.

Chapter 5

Hydrodeoxygenation of γ-Valerolactone to 2-Methyltetrahydrofuran and Pentane

5.1 Introduction

In recent years, lignocellulosic biomass has been widely investigated as a sustainable carbon resource for the production of biofuels and platform chemicals to reduce the influence of dwindling fossil energy reserves [1, 2]. In this respect, conversion of biomass-derived compounds to alternative fuels and chemicals similar to those obtained from oil processing is of great significance [3]. However, biomass-derived feedstocks in general contain excess oxygen-containing functional group, reducing excess oxygen atom to the desired functionality in the final product via hydrodeoxygenation is a key step to successful establishment of bio-based chemical industry [4, 5], where heterogeneous catalysis exhibits an efficient methodology allowing for remarkable reaction rates and high selectivity of target products [6-8].

Initial dehydration of poly- or monosaccharide, such as cellulose, sucrose, cellobiose, glucose, fructose, etc., would produce a significant yield of 5-hydroxymethylfurfural (HMF), subsequently HMF further undergoes a ring-opening reaction under acid conditions to form levulinic acid (LA), a typical platform chemical with promising industrial potential. And then, LA can be converted into γ-valerolactone (GVL) under hydration conditions with a substantial yield (>95%) [9]. Recently, GVL, has been attracting intensive attention due to its potential utilization as fuels [10], an environmental solvent [11] and a precursor for other value-added chemicals [12, 13].

One of the most promising pathways is hydrodeoxygenation of GVL to produce 2-methyltetrahydrofuran (2-MTHF), involving the ring-opening reaction of tetrahydrofuran on the substituent of ketone functional group, and subsequently an intramolecular etherification. 2-MTHF is a promising alternative chemical as a renewable solvent [14] or a fuel additive in a more suitable biofuel compared to ethanol due to its higher hydrophobic property and a higher heating value and density [15].

Considerable research efforts have been devoted to produce a high yield of 2-MTHF from lignocellulose-derived chemicals, such as furfural [16], levulinic acid [17-20] and GVL [21, 22]. Al-Shaal et al. [6] showed that a full conversion of GVL with the maximum 2-MTHF yield of *ca.* 43% was observed over a Ru/C catalyst at 190 °C. Obregón et al. [21] reported that Ni-Cu/Al_2O_3 catalyst allowed a 2-MTHF yield of *ca.* 64% from GVL at 230 °C. They also found that this catalyst was effective enough to substitute the substrate from GVL to levulinic acid, attaining 2-MTHF yield of *ca.* 56% at 250 °C [15]. Moreover, Upare et al. [17] investigated the hydrocyclization of levunilic acid to 2-MTHF over nanocomposite Cu/SiO_2 catalysts, a full levunilic acid conversion with 2-MTHF yield of *ca.* 64% was obtained at 265 °C. Nonetheless, all the above mentioned catalysts need a relatively high temperature (> 190 °C), which would definitely lead to high energy consumptions, and the future bio-based chemical industry would highly appreciate economic viability regarding to low temperature conversion. Thus, it is of great significance to promote the 2-MTHF production at relatively low temperatures meanwhile a high yield. It is reported that *ca.* 87% 2-MTHF yield from

levunilic acid was attained at moderate temperature (150 °C) when using ruthenium-N-Triphos complexes [23]. Nevertheless, the complicate catalyst preparation may restrict its utilization. On the other hand, it has been reported that silica-supported Rh-based catalyst presented a high activity towards the C-O bond hydrodeoxygenation under mild conditions [24].

In the present study, silica-supported RhRe and RhMo bimetallic catalysts are synthesized with the aim to produce 2-MTHF from GVL with high (～80%) selectivity under mild conditions. The reaction conditions, such as solvent, reaction temperature, were optimized to construct a feasible chemical industry. Especially, a cleaner approach to produce 2-MTHF employing the aqueous phase conversion has been investigated.

5.2 Experimental

5.2.1 Materials

Standard samples (＞99%), including GVL, 2-MTHF, pentane, 2-butanol and 2-pentanol, were purchased from TCI company. Heptane (>99%), activated carbon (from palm shell, Wako Pure Chemical Industries)， Rhodium chloride hydrate, ammonium perrhenate, and ammonium molybdate tetrahydrate were obtained from Wako Pure Chemical Industries. Silicon dioxide (nanopowder, 99.5% trace metals basis,) and Nafion NR50 (a perfluorosulfonated ionomer) were supplied by Sigma-Aldrich. ZSM-5 (CBV 3024E), mordenite (CBV 21A), beta zeolite (HSZ-980HOA), and Y zeolite (CBV 400) were purchased from Zeolyst International and Tosoh. Amberlyst 70 was purchased from Organo Corporation.

5.2.2 Catalyst preparation

$RhRe/SiO_2$ and $RhMo/SiO_2$ catalysts were prepared by sequential impregnation with a reported method [25, 26]. Briefly, an aqueous solution of $RhCl_3 \cdot 3H_2O$ was added to SiO_2 (BET surface area 543 m^2/g and total pore volume 0.590 cm^3/g) and stirred for 4 h at room temperature. subsequently by evaporating the water and drying at 105 °C overnight, then the solid was added to an aqueous solution of NH_4ReO_4 or $(NH_4)_6Mo_7O_{24} \cdot 4H_2O$ and stirred for another 4 h. After evaporating the water and drying at 105 °C overnight again, the catalyst was calcined in air at 500 °C with a heating rate of 10 °C /min for 3 h and stored in an airtight container before use. The loading amount of Rh was controlled to 4 wt% Rh and a Re/Rh (or Mo/Rh) molar ratio of was 0.25 or 0.5, respectively. $PdMo/SiO_2$ and $PdRe/SiO_2$ catalysts were prepared with the same way.

To generate the acidic form of the zeolite, all the zeolites were calcined in ambient atmosphere at 550 °C for 4 h. Amberlyst 70 was prewashed with deionized water and ethanol followed by drying overnight while Nafion NR50 catalyst was directly used. Sulfonated activated carbon (S/AC) was prepared by immerging activated carbon in concentrated sulfuric acid at 150 °C for 15 h under N_2, followed by washing with water until no sulfate was detected in the filtrate [27].

5.2.3 Catalyst activity test

GVL (3.0 mmol) and cyclohexane (0.8 mmol, internal standard) was dissolved in 10 mL of heptane, which had been suspended with 100 mg of the catalyst. Diglyme (0.4

mmol) was used as internal standard when the reaction was conducted in aqueous phase. The suspension was transferred to a 100 mL of SUS-made stainless steel autoclave. After it was closed, the air in the headspace was purged by H_2 three times. Then the autoclave was heated to a prescribed temperature within a range of 120–180 °C with stirring at an impeller rotation rate of 400 rpm. Time zero was defined for the moment at which the inner temperature of the autoclave reached to the desired temperature. After the isothermal heated for a prescribed period of time, the autoclave was quenched with an iced water bath to ambient temperature, and then opened. The suspension was recovered and filtered with a 0.45 μm PTFE membrane filter. The filtrate was identified and quantified from the calibration curve of standard samples using an internal standard method by gas-chromatography mass-spectrometry (GC/MS, PerkinElmer, Clarus SQ 8), which is equipped with a capillary column coated with TC-1701 (GL Sciences, 60 m length, 0.25 μm inner diameter, 0.25 μm film thick-ness) and a quadrupole analyzer and operated in electron impact (70 eV) mode. As to catalyst regeneration test, the spent catalyst was repeatedly washed with acetone and water, and then dried at 105 °C overnight, followed by recalcination in the same way as the fresh one. Reagent conversion and product selectivity were defined as follows:

$$\text{Conversion [\%]} = \frac{\text{moles of reagent converted}}{\text{moles of reagent in feed}} \times 100$$

$$\text{Selectivity [\%]} = \frac{\text{moles of the product}}{\sum \text{moles of the product}} \times 100$$

5.2.4 Catalyst characterization

The Brunauer-Emmet-Teller surface area (S_{BET}) and total pore volume (V_{total}) were calculated from N_2 isotherm at -196 °C, which were measured on a Quantachrome, NOVA 3200e. H_2 temperature-programmed reduction (TPR) was conducted in a flow-type BELCAT-30 catalyst analyzer (BEL JAPAN, Inc) equipped with a U-shaped fixed bed reactor and a thermal conductivity detector as reported before [28]. Typically, 50 mg of the catalyst was loaded in the quartz tube and pretreated at 450 °C for 1 h with N_2 atmosphere. After cooling down to room temperature, 5.0 vol% H_2/N_2 with a total gas flow of 50 mL/min was introduced to the reactor, and then the reactor was heated from 30 to 800 °C at a ramp rate of 10 °C /min. CO chemisorption study was carried out by using BEL-CAT (BEL Japan Inc.). Prior to the CO pulse chemisorption, the catalysts were pretreated by reduction at 200 ^{o}C under a flow of 5 vol% H_2/N_2 (50 mL/min), and then CO chemisorption was conducted at 50 ^{o}C under a flow of 1.0 vol% CO/He (50 mL/min). X-ray diffraction (XRD) measurement was performed on a Rigaku TTR-III X-ray diffractometer with Cu Kα radiation at 50 kV and 300 mA. Before the XRD measurements, the catalysts were reduced at 200 °C for 1 h. X-ray photoelectron spectroscopy (XPS) was performed on Kratos AXIS-165 (Shimadzu) multi-technique electron spectrometer system equipped with a monochromatic Al Kα X-ray source and a charge neutralizer. The binding energy was calibrated by adjusting the C 1s peak to 284.6 eV. Transmission electron microscopy combined with energy dispersive spectrometry (TEM-EDS) analysis was taken with JEOL JEM-2100F. The samples were suspended in ethanol by supersonic wave and then dropped on a carbon-coated copper

grid.

5.3 Results and discussion

5.3.1 Catalyst characterization

The TPR traces of the bimetallic catalysts are plotted in **Fig. 5-1**. Reduction of Mo/SiO_2 and Re/SiO_2 take place at much high temperatures. The trace of Mo/SiO_2 presents two maxima at 530 and 760 °C, respectively. The former reduction peak is due to the reduction of MoO_3 species in polymolybdate structures to low valence of Mo species, while the later reduction peak is assigned to the reduction of all the Mo species in strong connection with the support [29]. The trace of Re/SiO_2 also shows two peaks, the first main one peaks at 345 °C and the second minor one peaks at 407 °C, corresponding to the reduction of Re_2O_7 and ReO_3, respectively. This result is consistent with the observation of a previous study [30], which demonstrated that the reducibility increases in the order: $NH_4ReO_4 < Re_2O_7 < ReO_3$. Moreover, Martínez et al. [31] proved that the valence of Re was main +7 with a small amount of +6 in Re/SiO_2 after calcination. The reduction temperature of Rh/SiO_2 starts at 45 °C and completes at 160 °C. Introducing Rh species would significantly lower the reduction temperature of the Mo or Re precursors, mainly due to hydrogen spillover from mental Rh to Re or Mo [32-34]. No peaks of separate Mo or Re species were observed during the reduction of the $RhMo/SiO_2$ and $RhRe/SiO_2$ catalysts, suggesting the well formation of metal alloys.

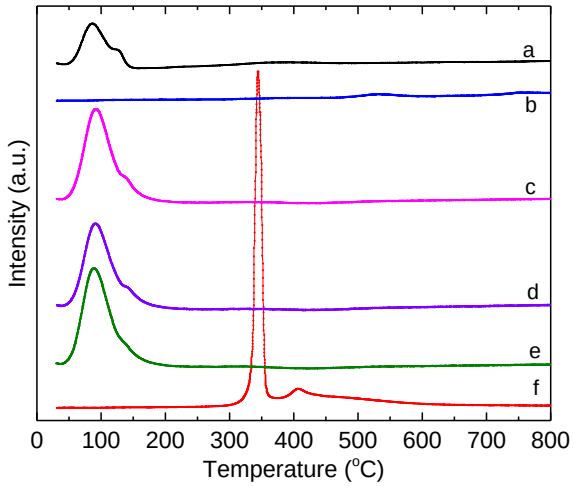

Fig. 5-1 TPR profiles of the catalyst. (a) Rh/SiO_2, (b) Mo/SiO_2, (c) $RhMo/SiO_2(0.25)$, (d) $RhRe/SiO_2(0.257)$, (e) $RhRe/SiO_2(0.5)$, (f) $Re/SiO_2(0.5)$.

Table 5-1 summarizes the CO chemisorption results of the Rh-based bimetallic catalysts. Rh/SiO_2 showed the highest CO uptake among the catalysts. Addition of Mo or Re caused decrease in the CO uptake, suggesting that part of surface Rh was covered by MoO_x or ReO_x species that does not have ability for the CO chemisorption. The particle diameter of active metals was estimated to be around 2 nm. Increasing the Re(Mo)/Rh ratio from 0.25 to 0.5, the particle size slightly increased, this results is consistent with the CO uptake. On the other hand, apparent dispersion of $RhMo/SiO_2$ and $RhRe/SiO_2$ decreased, suggesting the formation of alloys, in good agreement with the TPR results.

Table 5-1 Results of CO chemisorption of the catalysts.

Catalyst	M/Rh	Loading amount/mmol·g^{-1}–cat			Irreversible CO uptake /μmmol·g^{-1}	CO : Rh /mol : mol	Particle diameter /nm
		Rh	Mo	Re			
Rh/SiO_2	-	0.39	-	-	208	0.57	1.92
$RhMo/SiO_2$	0.25	0.39	0.10	-	164	0.45	2.43
$RhMo/SiO_2$	0.5	0.39	0.20	-	150	0.41	2.66
$RhRe/SiO_2$	0.25	0.39	-	0.10	200	0.55	1.99
$RhRe/SiO_2$	0.5	0.39	-	0.20	196	0.54	2.03

Fig. 5-2 shows the XRD patterns, the main peak at $2\theta = 23.5^{o}$ corresponds to SiO_2, while a weak peak appeared at $2\theta = 41.4^{o}$ is assigned to Rh metal. In addition, no Re or Mo species were observed in the $RhRe/SiO_2$ and $RhMo/SiO_2$, suggesting that Re and Mo species were finely dispersed on SiO_2. These results are well coinciding with Tomishige group's research [24].

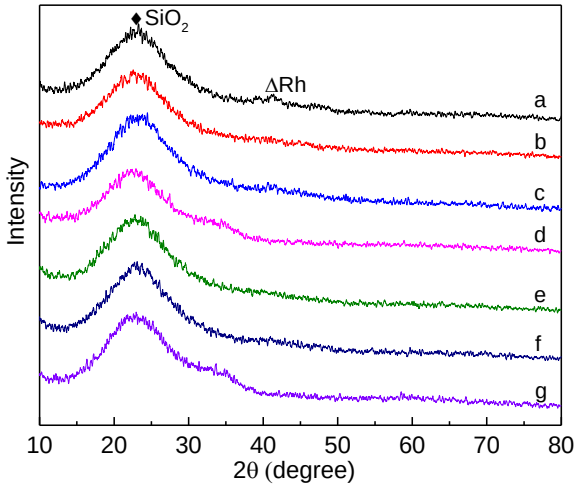

Fig. 5-2 XRD patterns of the Rh-based bimetallic catalysts. (a) Rh/SiO_2, (b) $RhRe/SiO_2$(0.257), (c) $RhRe/SiO_2$(0.5), (d) $RhRe/SiO_2$(0.5) after third run, (e) $RhMo/SiO_2$(0.25), (f) $RhMo/SiO_2$(0.5), (g) $RhMo/SiO_2$(0.25) after third run.

Fig. 5-3 depicts the XPS analysis of $RhRe/SiO_2$ and $RhMo/SiO_2$ catalysts. As to both $RhRe/SiO_2$ and $RhMo/SiO_2$ catalysts, Rh $3d_{5/2}$ and $3d_{3/2}$ binding energies were observed at 308.7 and 313.3 eV, corresponding to the presence of Rh_2O_3 species, no Rh^0 was detected mainly because after reduction the catalysts were exposed to air and re-oxidized due to its small particles. However, the reductions of Mo and Re species were observed. The deconvolution of the Mo species of $RhMo/SiO_2$ XPS data is described in **Fig. 5-3(b)**. The binding energy at 232.7 eV related to unreduced Mo^{+6} $3d_{5/2}$ species [35]. The binding energies at 231.1 and 229.1 eV correspond to Mo^{+5} $3d_{5/2}$

and Mo^{+4} $3d_{5/2}$, respectively, which is in accord with a reference book [36]. According to the reference book, the lines of the Mo 3d XPS data on the Mo-containing species in the range of 232.4-232.8, 230.8-231.2, and 229.1-229.5 eV were assigned to Mo^{+6}, Mo^{+5}, and Mo^{+4}, respectively. From **Fig. 5-3(b)**, it is obvious to know that the area ratio of Mo^{+4} to total Mo species is much smaller than that of Mo^{+5} species, suggesting that Mo^{+6} species were mainly reduced to Mo^{+5} species. **Fig. 5-3(b)** shows the XPS of the Re 4f region of $RhRe/SiO_2$. The Re $4f_{7/2}$ contributes to binding energy of 47.2 eV, corresponding to Re^{+7} of Re_2O_7 species [37, 38]. In addition, the binding energies at 45.4, 42.4, and 40.4 eV can be assigned to Re^{+6}, Re^{+4}, and Re^{0}, respectively [39-42].

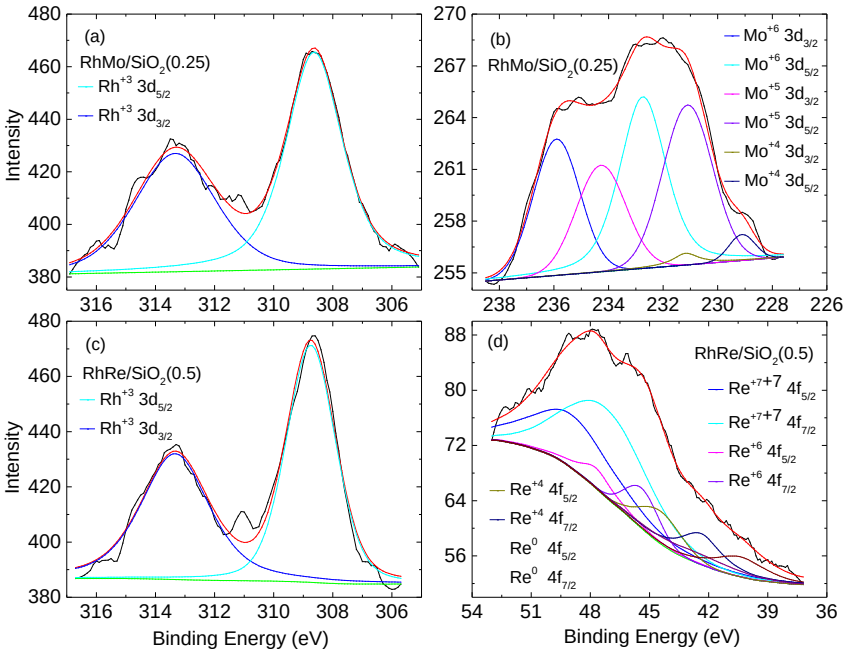

Fig. 5-3 XPS analysis of $RhRe/SiO_2$ and $RhMo/SiO_2$ catalysts. (a) Rh species of $RhMo/SiO_2$, (b) Mo species of $RhMo/SiO_2$, (c) Rh species of $RhRe/SiO_2$, (d) Re species of $RhRe/SiO_2$.

Fig. 5-4 exhibits TEM images and EDS analysis of the bimetallic $RhRe/SiO_2$ and $RhMo/SiO_2$ catalysts. the mapping images of Re, Mo, and Rh shows the same shape

with the Si images, indicating that the Re, Mo and Rh species were highly dispersed on the silica surface. Re or Mo species are also located very close to the Rh species, suggesting the interactions between Re or Mo and Rh species.

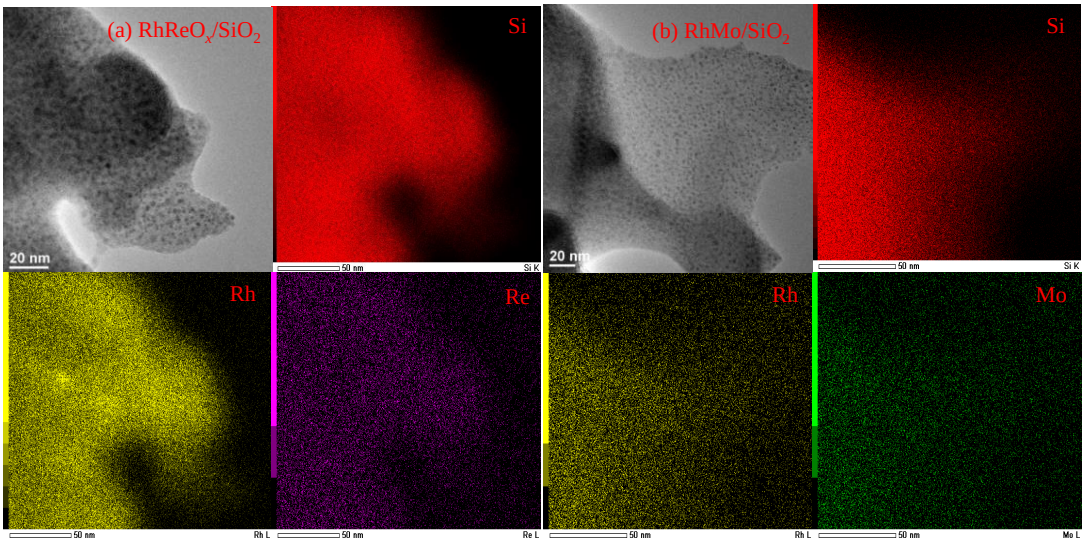

Fig. 5-4 TEM images and elemental mappings by TEM-EDS, (a) RhRe/SiO_2(0.5) and (b) RhMo/SiO_2(0.25).

5.3.2 Hydrodeoxygenation of GVL to 2-MTHF in alkane solvent

Initially, silicon dioxide supported Rh with Mo or Re catalysts were performed in the reaction of GVL to 2-MTHF in heptane solvent at 120 °C. As shown in **Table 5-2**, Rh/SiO_2 catalyst promoted complete conversion of GVL after 6 h, with 2-MTHF selectivity of *ca.* 51%. Decreasing the reaction time to 3 h (entry 1), 2-MTHF selectivity of *ca.* 63% and 2-PeOH selectivity of *ca.* 25% accompanying with GVL conversion of *ca.*77% were obtained, demonstrating that 2-MTHF was over-hydrogenolyzed by Rh/SiO_2 catalysts. After introducing the Re or Mo into Rh/SiO_2, both RhRe/SiO_2 and RhMo/SiO_2 are shown to be quite effective for the production of 2-MTHF, probably due to their acid sites [43, 44]. The RhMo/SiO_2 (0.25) catalyst showed the highest

catalytic performance among the catalysts, attaining 2-MTHF in *ca.* 86% selectivity, along with 2-BuOH, 2-PeOH and 1-PeOH in *ca.* 3%, 8% and 1% selectivity, respectively (entry 3). The $RhRe/SiO_2$ (0.5) catalyst also showed a good selectivity to 2-MTHF, resulting in *ca.* 83% selectivity. Noticeably, only small amounts of butane and pentane were observed at the reaction temperature of 120 °C, suggesting this temperature is not high enough for pentane production, as discussed in the following section.

Table 5-2 Hydrodeoxygenation of GVL to 2-MTHF[a].

Entry	Catalyst	M/Rh	Conv./%	Selectivity/%						
				Butane	Pentane	2-BuOH	2-MTHF	2-PeOH	1-PeOH	1,4-PDO
1[b]	Rh/SiO_2	-	77	1	6	4	63	25	1	-
2	Rh/SiO_2	-	100	1	7	2	51	37	2	-
3	$RhMo/SiO_2$	0.25	76	0.3	2	3	86	8	1	-
4	$RhMo/SiO_2$	0.5	73	0.1	0.4	3	84	11	1	-
5	$PdMo/SiO_2$	1	37	-	-	-	5	-	-	-
6[c,d]	$PdRe/SiO_2$	1	0.4	-	-	-	-	-	-	-
7	$RhRe/SiO_2$	0.257	55	0.2	2	3	79	15	1	-
8	$RhRe/SiO_2$	0.5	60	0.4	2	5	83	10	1	-
9[e]	$RhRe/SiO_2$	0.5	1	-	-	-	-	-	-	-
10[c]	$RhRe/SiO_2$	0.5	37	-	-	7	6	9	-	78

BuOH: butanol, MTHF: methyltetrahydrofuran, PeOH: pentanol. PDO: pentandiol. [a]Reaction conditions: 120 °C, 6 h, GVL 3 mmol, catalyst 100 mg, heptane 10 mL, H_2 4.5 MPa. [b]t = 3 h. [c]Water was used as a solvent. [d]160 °C. [e]Ethanol was used as a solvent.

In the solvent screening study, *ca.* 78% selectivity of 1,4-pentandiol (1,4-PDO) with *ca.* 37% conversion of GVL was obtained in aqueous phase. Further ramping the reaction temperature to 160 °C would promote the hydrodeoxygenation of 1,4-PDO, without promoting 2-MTHF formation, actually suppressed (**Table 5-3**). From the result, the heptane solvent was advantageous to aqueous phase for the 2-MTH production, a

plausible interpretation is because of the stronger acidity of the Re species and the stronger adsorption of substrate on catalyst surface in alkane phase than in aqueous phase [45, 46]. The GVL conversion and 2-MTHF selectivity were significantly higher in heptane than in ethanol solvent, this difference in catalytic performance could be as a result of competitive adsorption of between alcohol solvent and substrate on the Re clusters [47, 48].

Table 5-3 Hydrodeoxygenation of GVL Rh-based catalysts in aqueous phase.

Entry	Catalyst	M/Rh	Conv./%	Selectivity/%				
				2-BuOH	2-MTHF	2-PeOH	1,4-PDO	PA
1	Rh/SiO_2	-	11.0	58	9	12	7	14
2	$RhMo/SiO_2$	0.25	40	14	30	16	40	-
3	$RhMo/SiO_2$	0.5	38	23	26	13	38	-
4	$RhRe/SiO_2$	0.257	38	18	25	19	38	-
5	$RhRe/SiO_2$	0.5	37	23	35	5	37	-

BuOH: butanol, MTHF: methyltetrahydrofuran, PeOH: pentanol, PDO: pentandiol, PA: pentenoic acid. Reaction conditions: GVL 1 mmol, catalyst 100 mg, H_2O 10 mL, H_2 4.5 MPa, 160 °C, 6 h

5.3.3 Hydrodeoxygenation of GVL to 2-MTHF in aqueous phase

It is commonly known that water is used as a green solvent because of its advantageous properties such as sustainability, environmentally friendly, ready accessibility etc. Therefore, to achieve a good performance of biomass-derived chemical reactions in aqueous phase is rather important because most biomass-derived chemicals contain high oxygen content, and therefore are easily soluble in water. As previously reported, the acidic property of the Re species is rather weak in water [46]. Nevertheless, it is essential to maintain the acidic conditions during the reaction in case of hydrodeoxygenation of GVL to 2-MTHF, thus the solid acid co-catalyst was added to

the reaction system.

Fig. 5-5 displays the results of hydrodeoxygenation of GVL to 2-MTHF in aqueous phase over $RhRe/SiO_2$ in the presence of various solid acid co-catalysts. Seven types of solid acid catalysts (activated carbon, ion-exchange resins, and zeolites) were tested as co-catalyst with $RhRe/SiO_2$ (0.5) or $RhMo/SiO_2$ (0.25). The addition of S/AC and β/Y zeolites rather decreased the conversion of GVL. Multi-functionalities (S/AC) or scarce acid sites (β and Y) over highly porous structure likely caused competitive adsorption of GVL without catalysis. The other catalysts improved GVL conversion through the facilitation of 1,4-PDO dehydration. Amberlyst 70 and Nafion had large amount of acid sites but showed much less selectivities to 2-MTHF and the derivatives than ZSM-5 and mordenite. This may indicate that Lewis acidity is preferred for the 1,4-PDO dehydration, compared to Brøndted acidity. The reaction selectivity is thus affected by several structural factors of the solid acid catalysts such as pore morphology, acid type, and acid sites amount, and the acid sites of ZSM-5 with maximum pore diameter of 6.2−6.3 Å (Norman radii, Dn, **Table 4-3**) was the most effective among tested catalysts for the intramolecular dehydration of 1,4-PDO. The lower 2-MTHF selectivity of mordenite, compared to ZSM-5, is probably caused by smaller dN (5.5−7.7 Å, **Table 4-3**) against 1,4-PDO molecule, having kinetic diameter of 5.8 Å. On the other hand, 2-PeOH was obtained in high selectivity over mordenite, Amberlyst 70 and Nafion, suggesting 2-MTHF is easier to open oxolane-ring under relative higher acid sites conditions in the presence of the bimetallic catalyst. It is worth highlighting that the

selectivity of 2-MTHF reached 69% with ZSM-5 in water at 120 °C. When used RhMo/SiO2 (0.25), the reaction with ZSM-5 resulted in a slightly higher selectivity of 76%. The catalytic performances are comparable with that of Rh-based bimetallic catalyst in heptane.

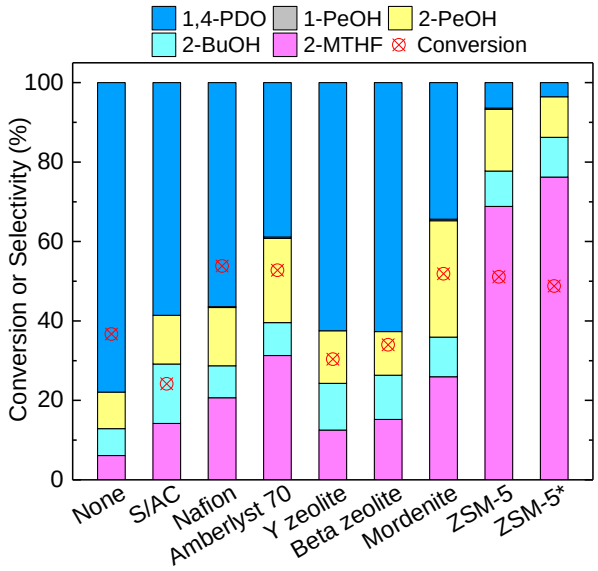

Fig. 5-5 Hydrodeoxygenation of GVL to 2-MTHF in aqueous phase over $RhRe/SiO_2$ in the presence of solid acid co-catalysts. BuOH: butanol, MTHF: methyltetrahydrofuran, PeOH: pentanol. PDO: pentandiol. Reaction conditions: 120 °C, 6 h, GVL 3 mmol, $RhRe/SiO_2$ (0.5) 100 mg, water 10 mL, H_2 4.5 MPa. *$RhMo/SiO_2$ (0.25).

5.3.4 Hydrodeoxygenation of GVL to pentane

In order to investigate the influence of reaction temperature on the product distribution, the reaction was performed at elevated temperatures, and the result is shown in **Fig. 5-6**. From the result, pentane selectivity presents as a function of temperature on the hydrodeoxygenation reaction of GVL. Ramping reaction temperature would significantly increase the selectivity of alkanes. The maximum pentane yield of *ca.* 84% together with butane yield of *ca.* 16% was observed at 160 °C over $RhRe/SiO_2$ catalyst. When using 2-MTHF as a reactant, *ca.* 94% yield of pentane

and *ca.* 6% yield of butane were observed. Considering the butane selectivity is *ca.* 16% from GVL, it suggests that the source of butane is not only 2-MTHF, but also others e.g. 2-butanol. When the reaction was conducted over $RhMo/SiO_2$ catalyst, *ca.* 80% pentane and *ca.* 12% butane yields were obtained, respectively, meanwhile there still existed a small amount of 2-MTHF and 2-PeOH in the reaction solution, illustrating that $RhMo/SiO_2$ catalyst was less effective for the production of alkanes compared to $RhRe/SiO_2$ catalyst.

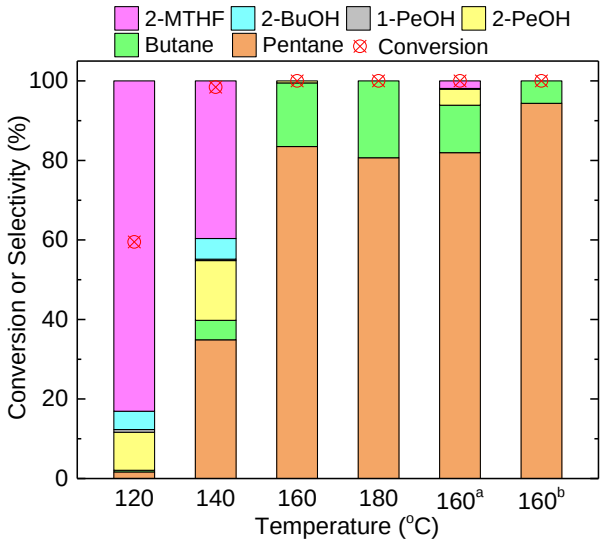

Fig. 5-6 Hydrodeoxygenation of GVL to pentane. BuOH: butanol, MTHF: methyltetrahydrofuran, PeOH: pentanol. PDO: pentandiol. Reaction conditions: 6 h, GVL 3 mmol, $RhRe/SiO_2$(0.5) 100 mg, heptane 10 mL, H_2 4.5 MPa. [a] $RhMo/SiO_2$(0.25). [b]2-MTHF was used as a reagent.

5.3.5 Catalyst recyclability

To evaluate the catalyst stability, the $RhMo/SiO_2$ (0.25) and $RhRe/SiO_2$ (0.5) catalysts were repeatedly used, respectively, and the results are presented in **Fig. 5-7**. Between each cycle, the method of catalyst regeneration was as follows: the catalyst was separated by filtration, washed with water and dried at 105 °C overnight, followed

by calcination at 500 °C for 3 h in air. In general, the catalytic performance after regeneration was comparable to that of the fresh catalyst. The selectivity of pentane almost not changed after three consecutive experiments (**Fig. 5-7(b)**). The selectivity of 2-MTHF decreased from *ca.* 86 to 73% after three consecutive runs (**Fig. 5-7(a)**), likely due to the aggregation of metals during recalcination, as shown in XRD patterns (**Fig. 5-2(d)** and **(g)**). After the third run, an obvious shoulder was detected at 2θ around 35^{o} in both $RhRe/SiO_2$ and $RhMo/SiO_2$ catalyst, respectively. On the other hand, when the spent catalyst was conducted without recalcination, GVL conversion was significantly decreased, as shown in **Table 5-4**. Only *ca.* 49 and 37 % GVL conversion was observed over $RhMo/SiO_2$ (0.25) and $RhRe/SiO_2$ (0.5) catalysts, respectively. It is also noteworthy to mention that without recalcination, the main compound changed to 2-MTHF rather than pentane over $RhRe/SiO_2$ (0.5). The reason could be mainly due to the carbon deposition on the catalyst surface during the reaction, and further leading to deactivity of active sides. On the other hand, the catalysts can be regenerated by simple recalcination.

Table 5-4 Recyclability of $RhMo/SiO_2$ (0.25) and $RhRe/SiO_2$ (0.5)[a].

Catalyst	Recalcination	Temp./ °C	Conv./ %	Selectivity/%					
				Butane	Pentane	2-BuOH	2-MTHF	2-PeOH	1-PeOH
$RhMo/SiO_2$	Without	120	49	0.1	0.3	6	90	4	0.4
	With	120	76	-	1	3	79	16	1
$RhRe/SiO_2$	Without	160	37	0.2	1	5	67	23	3
	With	160	100	17	83	-	-	-	-

BuOH: butanol, MTHF: methyltetrahydrofuran, PeOH: pentanol. PDO: pentandiol.
[a]Reaction conditions: 6 h, GVL 3 mmol, catalyst 100 mg, heptane 10 mL, H_2 4.5 MPa.

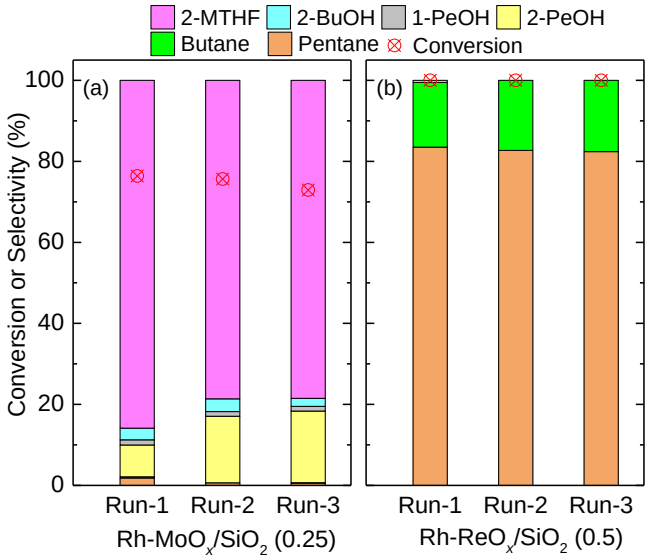

Fig. 5-7 Catalyst recyclability of (a) $RhMo/SiO_2$ (0.25) at 120 °C and (b) $RhRe/SiO_2$ (0.5) at 160 °C. BuOH: butanol, MTHF: methyltetrahydrofuran, PeOH: pentanol. PDO: pentandiol. Reaction conditions: 6 h, GVL 3 mmol, catalyst 100 mg, heptane 10 mL, H_2 4.5 MPa. The catalyst was recalcinated at 500 °C for 3 h in air after each run.

5.3.6 Reaction pathways

From the result of product analysis, a reaction network of the hydrodeoxygenation of GVL can be proposed, and is shown in **Scheme 5-1**. In the reaction pathway, GVL is firstly hydrogenated in an equimolar ratio to 4-hydroxpentanal. And then 4-hydroxpentanal undergoes a decarbonylation reaction to form 2-butanol with an equivalent mole of CO co-product, and 2-butanol can be further hydrodeoxygenated to butane. On the other hand, the main route is the hydrogenation of 4-hydroxpentanal to 1,4-PDO, and 1,4-PDO can further undergo an intramolecular etherification to form 2-MTHF in the presence of acid sites [6]. The fact that almost no 1,4-PDO were observed in the reaction solution infers that the rate controlling step is the hydrogenation of GVL to 1,4-PDO rather than the hydrogenation of 1,4-PDO to

2-MTHF. For the hydrodeoxygenation of 2-MTHF to pentane, there are two plausible reaction pathways. The side reaction involving ring-opening happens on the non-substituent tetrahydrofuran ring while the main reaction occurs on the substituent methyl group [49]. In both pathways, 1- or 2-pentananl are initially formed, and are rapidly hydrogenated to 1- or 2-pentanol, respectively, due to their high reactivity. It is noteworthy that a catalyst decarbonylation reaction of 1-pentananl can also lead to the formation of butane. Finally, pentane is formed as a result of hydrodeoxygenation of *n*-pentanol.

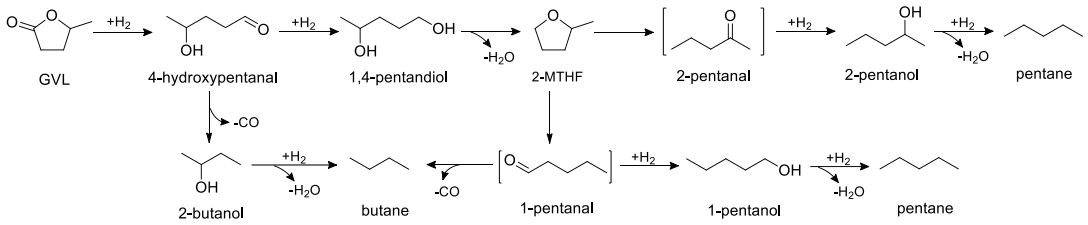

Scheme 5-1 Reaction pathways for the hydrodeoxygenation of GVL.

As for pentane formation, there are two plausible reaction pathways from *n*-pentanol in the presence of $RhRe/SiO_2$ catalyst (**Scheme 5-2 and 5-3**): one is the two-step indirect mechanism consisting of acid-catalyzed dehydration and following metal-catalyzed hydrogenation, the other is the direct mechanism involving the S_N-2-like attack of hydride to the Re alkoxide species [24, 46]. Tomishige et al. [46] considered that conversion of 1-momo-ols to corresponding alkanes catalyzed by $Ir\text{-}ReO_x/SiO_2$ catalyst was dominated by the direct mechanism, while dehydrogenation of 2-hexananol to hexane, analogy of 2-pentanol to pentane, corresponded to the two-step indirect mechanism. In the direct mechanism (**Scheme 5-2**), -OH group of

substrate molecule combines with the Re site of the catalyst and then the –ORe group is firstly formed. Meanwhile, active hydrogen species are formed from H_2 molecules on the Rh metal sites by the heterolytic dissociation of H_2 into hydride and proton ($H_2 \rightarrow H^- + H^+$), and then substrates are attacked by the hydride-like species, which was adsorbed on the interface between Rh and Re, from the backside to break down the C-O bond, ultimately leading to alkane formation [45, 46]. In the two-step indirect mechanism (**Scheme 5-3**), 2-pentanol is initially dehydrated to 2-pentene due to the acidity of Re species, and then 2-pentene is hydrogenated to pentane over of Rh species. It is worthwhile mentioning that the dehydration reaction is the rate controlling step rather than hydrogenation reaction as a result of no 2-pentene observed in the reaction solution. Regarding to butane formation, it can be formed from 2-butanol through the indirect mechanism, or from 2-MTHF through a hydrodeoxygenated reaction (**Scheme 5-1**).

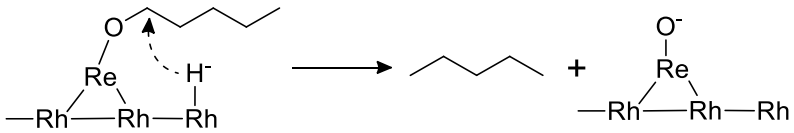

Scheme 5-2 Direct mechanism for the hydrodeoxygenation over $RhRe/SiO_2$ catalyst.

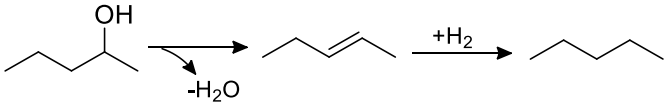

Scheme 5-3 Two-step indirect mechanism for the hydrodeoxygenation over $RhRe/SiO_2$ catalyst.

5.4 Conclusions

One-pot selective hydrodeoxygenation of cellulose-derived GVL to 2-MTHF was

performed over silica-supported RhRe and RhMo bimetallic catalysts under mild conditions. In heptane solvent, the highest selectivity of *ca.* 86% to 2-MTHF was observed at relatively low temperature (120 °C). On the other hand, when the reaction was conducted in aqueous phase, the precursor (1,4-pentandiol) of 2-MTHF was initially formed rather than 2-MTHF itself, mainly because of the weaker acidic property of Re species in aqueous phase than in alkane solvent. Introduction of solid acid co-catalysts in aqueous phase could significantly promote the intramolecular etherification of 1,4-PDO to form 2-MTHF. Among the tested sulfo functional group solid acid catalysts and zeolites, ZSM-5 performed best, attaining the highest 2-MTHF selectivity of *ca.*76% from GVL. Moreover, increasing the reaction temperature to 160 °C would substantially over-hydrogenolyze 2-MTHF to pentane with a yield of 94%. In addition, both the $RhMo/SiO_2$ and $RhRe/SiO_2$ bimetallic catalysts could be sequentially reused with little loss in activity by facile calcination.

5.5 References

[1] G.W. Huber, S. Iborra, A. Corma, Synthesis of transportation fuels from biomass: chemistry, catalysts, and engineering, Chem Rev, 106 (2006) 4044-4098.

[2] X. Jin, B. Yin, Q. Xia, T. Fang, J. Shen, L. Kuang, C. Yang, Catalytic transfer hydrogenation of biomass-derived substrates to value-added chemicals on dual-function catalysts: opportunities and challenges, ChemSusChem, 12 (2019) 71-92.

[3] J.C. Serrano-Ruiz, R. Luque, A. Sepulveda-Escribano, Transformations of

biomass-derived platform molecules: from high added-value chemicals to fuels via aqueous-phase processing, Chem. Soc. Rev., 40 (2011) 5266-5281.

[4] T. Prasomsri, T. Nimmanwudipong, Y. Román-Leshkov, Effective hydrodeoxygenation of biomass-derived oxygenates into unsaturated hydrocarbons by MoO_3 using low H_2 pressures, Energy Environ. Sci., 6 (2013) 1732-1738.

[5] D.M. Alonso, J.Q. Bond, J.A. Dumesic, Catalytic conversion of biomass to biofuels, Green Chem., 12 (2010) 1493-1513.

[6] M.G. Al-Shaal, A. Dzierbinski, R. Palkovits, Solvent-free γ-valerolactone hydrogenation to 2-methyltetrahydrofuran catalysed by Ru/C: a reaction network analysis, Green Chem., 16 (2014) 1358-1364.

[7] E. Gross, J.H.C. Liu, F.D. Toste, G.A. Somorjai, Control of selectivity in heterogeneous catalysis by tuning nanoparticle properties and reactor residence time, Nat Chem., 4 (2012) 947-952.

[8] P.L. Dhepe, A. Fukuoka, Cellulose conversion under heterogeneous catalysis, ChemSusChem, 1 (2008) 969-975.

[9] Y. Yi, H. Liu, L.P. Xiao, B. Wang, G. Song, Highly Efficient Hydrogenation of Levulinic Acid into γ-Valerolactone using an Iron Pincer Complex, ChemSusChem, 11 (2018) 1474-1478.

[10] J.S. Luterbacher, J.M. Rand, D.M. Alonso, J. Han, J.T. Youngquist, C.T. Maravelias, B.F. Pfleger, J.A. Dumesic, Nonenzymatic sugar production from biomass using biomass-derived γ-valerolactone, Science, 343 (2014) 277-280.

[11] S.G. Wettstein, D.M. Alonso, Y. Chong, J.A. Dumesic, Production of levulinic acid and gamma-valerolactone (GVL) from cellulose using GVL as a solvent in biphasic systems, Energy Environ. Sci., 5 (2012) 8199-8203.

[12] D.M. Alonso, S.G. Wettstein, J.A. Dumesic, Gamma-valerolactone, a sustainable platform molecule derived from lignocellulosic biomass, Green Chem., 15 (2013) 584-595.

[13] I.T. Horváth, H. Mehdi, V. Fábos, L. Boda, L.T. Mika, γ-Valerolactone—a sustainable liquid for energy and carbon-based chemicals, Green Chem., 10 (2008) 238-242.

[14] V. Pace, P. Hoyos, L. Castoldi, P. Domínguez de María, A.R. Alcántara, 2-Methyltetrahydrofuran (2-MeTHF): A biomass-derived solvent with broad application in organic chemistry, ChemSusChem, 5 (2012) 1369-1379.

[15] I. Obregón, I. Gandarias, N. Miletić, A. Ocio, P.L. Arias, One-pot 2-methyltetrahydrofuran poduction from levulinic acid in green solvents using Ni-Cu/Al_2O_3 Catalysts, ChemSusChem, 8 (2015) 3483-3488.

[16] H.Y. Zheng, Y.L. Zhu, B.T. Teng, Z.Q. Bai, C.H. Zhang, H.W. Xiang, Y.W. Li, Towards understanding the reaction pathway in vapour phase hydrogenation of furfural to 2-methylfuran, J. Mol. Catal. A: Chem., 246 (2006) 18-23.

[17] P.P. Upare, J.M. Lee, Y.K. Hwang, D.W. Hwang, J.H. Lee, S.B. Halligudi, J.S. Hwang, J.S. Chang, Direct hydrocyclization of biomass-derived levulinic acid to 2-methyltetrahydrofuran over nanocomposite copper/silica catalysts,

ChemSusChem, 4 (2011) 1749-1752.

[18] J.M. Bermudez, J.A. Menéndez, A.A. Romero, E. Serrano, J. Garcia-Martinez, R. Luque, Continuous flow nanocatalysis: reaction pathways in the conversion of levulinic acid to valuable chemicals, Green Chem., 15 (2013) 2786-2792.

[19] F.M. Geilen, B. Engendahl, M. Hölscher, J.r. Klankermayer, W. Leitner, Selective homogeneous hydrogenation of biogenic carboxylic acids with [Ru (TriPhos) H]$^{+}$: a mechanistic study, J. Am. Chem. Soc., 133 (2011) 14349-14358.

[20] T. Mizugaki, K. Togo, Z. Maeno, T. Mitsudome, K. Jitsukawa, K. Kaneda, One-pot transformation of levulinic acid to 2-methyltetrahydrofuran catalyzed by Pt-Mo/H-β in water, ACS Sustainable Chem. Eng., 4 (2016) 682-685.

[21] I. Obregón, I. Gandarias, A. Ocio, I. García-García, N.A. de Eulate, P.L. Arias, Structure-activity relationships of Ni-Cu/Al_2O_3 catalysts for γ-valerolactone conversion to 2-methyltetrahydrofuran, Appl. Catal., B, 210 (2017) 328-341.

[22] X.L. Du, Q.Y. Bi, Y.M. Liu, Y. Cao, H.Y. He, K.N. Fan, Tunable copper-catalyzed chemoselective hydrodeoxygenation of biomass-derived γ-valerolactone into 1,4-pentanediol or 2-methyltetrahydrofuran, Green Chem., 14 (2012) 935-939.

[23] A. Phanopoulos, A.J. White, N.J. Long, P.W. Miller, Catalytic transformation of levulinic acid to 2-methyltetrahydrofuran using ruthenium-N-triphos complexes, ACS Catal., 5 (2015) 2500-2512.

[24] S. Koso, H. Watanabe, K. Okumura, Y. Nakagawa, K. Tomishige, Comparative study of Rh-MoO_x and Rh-ReO_x supported on SiO_2 for the hydrogenolysis of ethers

and polyols, Appl. Catal., B, 111 (2012) 27-37.

[25] T. Buntara, S. Noel, P.H. Phua, I. Melián-Cabrera, J.G. de Vries, H.J. Heeres, Caprolactam from renewable resources: catalytic conversion of 5-hydroxymethylfurfural into caprolactone, Angew. Chem. Int. Ed., 50 (2011) 7083-7087.

[26] Y. Shinmi, S. Koso, T. Kubota, Y. Nakagawa, K. Tomishige, Modification of Rh/SiO_2 catalyst for the hydrogenolysis of glycerol in water, Appl. Catal., B, 94 (2010) 318-326.

[27] X. Mo, D.E. López, K. Suwannakarn, Y. Liu, E. Lotero, J.G. Goodwin, C. Lu, Activation and deactivation characteristics of sulfonated carbon catalysts, J. Catal., 254 (2008) 332-338.

[28] H. Einaga, A. Kiya, S. Yoshioka, Y. Teraoka, Catalytic properties of copper-manganese mixed oxides prepared by coprecipitation using tetramethylammonium hydroxide, Catal. Sci. Technol., 4 (2014) 3713-3722.

[29] K. Al-Dalama, A. Stanislaus, Temperature programmed reduction of SiO_2-Al_2O_3 supported Ni, Mo and NiMo catalysts prepared with EDTA, Thermochim. Acta, 520 (2011) 67-74.

[30] P. Arnoldy, E. Van Oers, O. Bruinsma, V. De Beer, J. Moulijn, Temperature-programmed reduction of Al_2O_3-, SiO_2-, and carbon-supported Re_2O_7 catalysts, J. Catal., 93 (1985) 231-245.

[31] N. Martínez, R. García, J. Fierro, C. Wheeler, R. Austin, J. Gallagher, J. Miller, T.

Krause, N. Escalona, C. Sepúlveda, Effect of Cu addition as a promoter on Re/SiO_2 catalysts in the hydrodeoxygenation of 2-methoxyphenol as a model bio oil compound, Fuel, 186 (2016) 112-121.

[32] A. Ciftci, D.M. Ligthart, E.J. Hensen, Aqueous phase reforming of glycerol over Re-promoted Pt and Rh catalysts, Green Chem., 16 (2014) 853-863.

[33] M. Chia, Y.J. Pagán-Torres, D. Hibbitts, Q. Tan, H.N. Pham, A.K. Datye, M. Neurock, R.J. Davis, J.A. Dumesic, Selective hydrogenolysis of polyols and cyclic ethers over bifunctional surface sites on rhodium-rhenium catalysts, J. Am. Chem. Soc., 133 (2011) 12675-12689.

[34] S. Koso, H. Watanabe, K. Okumura, Y. Nakagawa, K. Tomishige, Stable low-valence ReO x cluster attached on Rh metal particles formed by hydrogen reduction and its formation mechanism, J. Phys. Chem. C, 116 (2012) 3079-3090.

[35] N. Boufaden, R. Akkari, B. Pawelec, J. Fierro, M.S. Zina, A. Ghorbel, Dehydrogenation of methylcyclohexane to toluene over partially reduced Mo-SiO2 catalysts, Appl. Catal., A, 502 (2015) 329-339.

[36] J. Chastain, R.C. King, J. Moulder, Handbook of X-ray photoelectron spectroscopy: a reference book of standard spectra for identification and interpretation of XPS data, Physical Electronics Division, Perkin-Elmer Corporation Eden Prairie, Minnesota, 1992.

[37] K. Leiva, N. Martinez, C. Sepulveda, R. García, C. Jiménez, D. Laurenti, M. Vrinat, C. Geantet, J. Fierro, I. Ghampson, Hydrodeoxygenation of 2-methoxyphenol over

different Re active phases supported on SiO2 catalysts, Appl. Catal., A, 490 (2015) 71-79.

[38] A. Naor, N. Eliaz, L. Burstein, E. Gileadi, Direct experimental support for the catalytic effect of iron-group metals on electrodeposition of rhenium, Electrochem. Solid-State Lett., 13 (2010) 91-93.

[39] G. Beamson, A.J. Papworth, C. Philipps, A.M. Smith, R. Whyman, Selective hydrogenation of amides using bimetallic Ru/Re and Rh/Re catalysts, J. Catal., 278 (2011) 228-238.

[40] B.K. Ly, B. Tapin, M. Aouine, P. Delichère, F. Epron, C. Pinel, C. Especel, M. Besson, Insights into the oxidation state and location of rhenium in Re-Pd/TiO_2 catalysts for aqueous-phase selective hydrogenation of succinic acid to 1,4-butanediol as a function of palladium and rhenium deposition methods, ChemCatChem, 7 (2015) 2161-2178.

[41] L. Ma, D. He, Influence of catalyst pretreatment on catalytic properties and performances of Ru-Re/SiO_2 in glycerol hydrogenolysis to propanediols, Catal. Today, 149 (2010) 148-156.

[42] Y. Takeda, M. Tamura, Y. Nakagawa, K. Okumura, K. Tomishige, Characterization of Re-Pd/SiO_2 catalysts for hydrogenation of stearic acid, ACS Catal., 5 (2015) 7034-7047.

[43] M. Chia, Y.J. Pagan-Torres, D. Hibbitts, Q. Tan, H.N. Pham, A.K. Datye, M. Neurock, R.J. Davis, J.A. Dumesic, Selective hydrogenolysis of polyols and cyclic

ethers over bifunctional surface sites on rhodium-rhenium catalysts, J. Am. Chem. Soc., 133 (2011) 12675-12689.

[44] E.E. Lowenthal, S. Schwarz, H.C. Foley, Surface Chemistry of Rh-Mo/γ-Al_2O_3: An Analysis of Surface Acidity, J. Catal., 156 (1995) 96-105.

[45] Y. Nakagawa, K. Mori, K. Chen, Y. Amada, M. Tamura, K. Tomishige, Hydrogenolysis of C-O bond over Re-modified Ir catalyst in alkane solvent, Appl. Catal., A, 468 (2013) 418-425.

[46] K. Tomishige, M. Tamura, Y. Nakagawa, Role of Re species and acid Ccocatalyst on Ir-ReO_x/SiO_2 in the C-O hydrogenolysis of biomass-derived substrates, The Chemical Record, 14 (2014) 1041-1054.

[47] T. Buntara, S. Noel, P.H. Phua, I. Melián-Cabrera, J.G. de Vries, H.J. Heeres, From 5-hydroxymethylfurfural (HMF) to polymer precursors: catalyst screening studies on the conversion of 1,2,6-hexanetriol to 1,6-hexanediol, Top. Catal., 55 (2012) 612-619.

[48] K. Chen, K. Mori, H. Watanabe, Y. Nakagawa, K. Tomishige, C-O bond hydrogenolysis of cyclic ethers with OH groups over rhenium-modified supported iridium catalysts, J. Catal., 294 (2012) 171-183.

[49] A. Iino, A. Cho, A. Takagaki, R. Kikuchi, S.T. Oyama, Kinetic studies of hydrodeoxygenation of 2-methyltetrahydrofuran on a Ni_2P/SiO_2 catalyst at medium pressure, J. Catal., 311 (2014) 17-27.

Chapter 6

General Conclusions

Cellulose has become a wide interest for worldwide scientists and industries. Pyrolysis, featured with fast reaction rate, is considered as one of the most promising ways for the conversion of cellulose into anhydrosugars, mainly LGA. The two-step conversion of cellulose to LGO was performed with updraft fixed bed pyrolyzer and catalytic reformer with several types of packed bed catalysts. All the catalysts examined in this study (P/AC, S/AC, IL/Al_2O_3, IL/SiO_2, and IL/AC) presented the activity toward LGO formation in catalytic rapid pyrolysis of cellulose, but the catalysts available for the two-step process were limited to the supported IL phase catalysts. Active sites of P/AC and S/AC were deactivated by coke deposition at the initial stage of the reforming and could produce little LGO in the reforming. Due to the richness in active sites (IL itself), the supported IL phase catalysts did not allow LGA, which was supplied from the pyrolyzer at the yield of 38.4 %-C, to survive the reforming during the operation of 0.5 h. The continuous production of LGO with a relatively high yield of 16.6 %-C was demonstrated. However, the supported IL phase catalysts also suffered from the coke deposition. The coke precursor included LGA, resulting in the low selectivity of LGO from LGA at 43.3 %-C. Furthermore, another problem of IL decomposition was quantitatively identified. For avoiding the IL decomposition, the employment of AC and SiO_2 as the support material rather than Al_2O_3, having acidity, was effective, and lower reforming temperature was recommended, although the coke deposition was promoted

when it was too low (e.g., 200 °C).

An acid-catalyzed reaction of LGA to LGO in liquid phase was carried out for the first time. In pure organic solvent, LGA mainly dehydrated two water molecules to form LGO. The best performance of LGO production from LGA was using DMSO over Amberlyst 70, attaining to 39.3% on a carbon basis yield. More importantly, a higher LGO yield of 53% can be observed from cellulose pyrolysis bio-oil due to the presence of not only LGA, but also other anhydrosugar oligomers. The factor dominating the reaction selectivity was the polymerization to degradation products. Nevertheless, in the presence of water, degradation products were significantly suppressed, and LGA predominately converted to glucose, attaining almost 100% yield and selectivity. In aqueous phase, when using cellobiose as substrate, the maximum glucose yield of 87% with cellobiose conversion of 94% was obtained. When using LGA-riched bio-oil as substrate, the maximum glucose yield of 108% with a 13% higher than LGA conversion was observed. In a second stage, the $AlCl_3$-Amberyst 70 catalyzed NaCl-H_2O/acetone biphasic system was elaborated for HMF production from the anhydrosugars, leading to total HMF yield of 61-63% by the use of glucose, LGA and cellobiose as a substrate, respectively. However, HMF yield drastically decreased to 33% from LGA-riched bio-oil because the complexity of bio-oil aggravated the polymerization reactions, suggesting further purification of anhydrodugars from bio-oil is unavoidable for the sake of high HMF yield.

A simple and clean reaction of LGO in water with solid acid catalyst produced HMF

and LA with a substantial yield. The solid acid catalysts, employed in this study, all promoted the LGO conversion, but the selectivity to HMF and LA was significantly affected by the pore structure and acid type. ZSM-5, having pore sizes close to the molecular sizes of LGO and HMF, showed the best rate of LGO conversion (per mass of catalyst) and selectivity among zeolites, and Amberlyst 70, having dense Brønsted acid sites, showed best selectivity. The highest total yields of HMF and LA were 57.6 and 72.2 % on a molar basis, respectively. The kinetic analysis of experimental results revealed that DPs, causing the decrease in HMF and LA yields, were formed directly from LGO (and/or DH) rather than HMF and FF at an early stage of the reaction. Because of the increased formation of DP1 and FF, a high temperature was not necessarily preferred for achieving higher HMF and LA yields, and the best temperatures were identified as 161 °C and 191 °C for ZSM-5 and Amberlyst 70, respectively, under the present experimental conditions. Despite the amount of DPs formed, they had a negligible effect on the performance of the recycled Amberlyst 70 and were readily removed by calcination from ZSM-5.

One-pot selective hydrodeoxygenation of cellulose-derived GVL to 2-MTHF was reported over silica-supported RhRe and RhMo bimetallic catalysts under mild conditions. In heptane solvent, the highest selectivity of *ca.* 86% to 2-MTHF was observed at relatively low temperature (120 °C). On the other hand, when the reaction was conducted in aqueous phase, the precursor (1,4-pentandiol) of 2-MTHF was initially formed rather than 2-MTHF itself, mainly because of the weaker acidic

property of Re species in aqueous phase than in alkane solvent. Introduction of solid acid co-catalysts in aqueous phase could significantly promote the intramolecular etherification of 1,4-PDO to form 2-MTHF. Among the tested sulfo functional group solid acid catalysts and zeolites, ZSM-5 performed best, attaining the highest 2-MTHF selectivity of *ca.*76% from GVL. Moreover, increasing the reaction temperature to 160 °C would substantially over-hydrogenolyze 2-MTHF to pentane with a yield of 94%. In addition, both the $RhMo/SiO_2$ and $RhRe/SiO_2$ bimetallic catalysts could be sequentially reused with little loss in activity by facile calcination.

Achievements

International journal

1. **Huang X**, Kudo S, Sperry J, Hayashi J. Clean Synthesis of 5-Hydroxymethylfurfural and Levulinic Acid by Aqueous Phase Conversion of Levoglucosenone over Solid Acid Catalysts. *ACS Sustain. Chem. Eng.*, 2019, 7 (6), 5892–5899.
2. **Huang X**, Kudo S, Hayashi J. Two-step conversion of cellulose to levoglucosenone using updraft fixed bed pyrolyzer and catalytic reformer. *Fuel Process. Technol.*, 2019, 191, 29-35.
3. **Huang X**, Kudo S, Hayashi J, et al. Hydrogenolysis of γ-valerolactone over silica-supported Rh-based bimetallic catalysts, under preparation.
4. **Huang X**, Kudo S, Hayashi J, et al. Selective conversion of levoglucosan to levoglucosenone over Ambelyst 70, under preparation.

Conferences

1. **Huang X**, Mitsuyama D, Kudo S, Hayashi J. Fast Synthesis of Hydroxymethylfurfural from Levoglucosenone by mixing with Sulphuric Acid and Heating in A Microtube Reactor, *The 18th Asian Pacific Confederation of Chemical Engineering Congress*, paper submitted.
2. **Huang X**, Kudo S, Hayashi J. Production of Levoglucosenone by Catalytic Reforming of Volatiles from Fast Pyrolysis of Cellulose in an Updraft Fixed Bed Reactor. *The 14th Japan-China Symposium on Coal and C1 Chemistry*, Sep. 25-28, 2018, Hokkaido, Japan. Oral presentation.
3. **Huang X**, Kudo S, Hayashi J. Clean Synthesis of 5-Hydroxylmethylfurfural from cellulose-derived levoglucosenone. *The 13th Japan-China-Korea Joint Symposium on Carbon Saves the Earth*, Aug. 12-15, 2018, Ulanqab, China. Poster presentation.
4. 工藤 真二，光山 大貴，**ファン シン**，林 潤一郎.「希硫酸を用いたレボグルコセノンの低温異性化」化学工学会第 83 回年会，大阪，2018 年 3 月 13～15 日.
5. **Huang X**, Kudo S, Hayashi J. Clean Synthesis of 5-Hydroxylmethylfurfural and Levulinic Acid by Aqueous Phase Conversion of Levoglucosenone over Solid Acid Catalysts. *Green Chemistry New Zealand 2017*, Dec. 8-9, 2017, Auckland, New Zealand. Poster presentation.
6. 工藤 真二，**ファン シン**，林 潤一郎.「レボグルコセノンを原料とする HMF クリーン合成」化学工学会第 49 回秋季大会, 名古屋, 2017 年 9 月 20～25 日.

Acknowledgements

Time flies like an arrow, time flies like a shuttle. With the accomplishment of the dissertation, indicating my student career is coming to an end. Recalling on the past, I am filled with gratitude to those who have cared and helped me.

Firstly, I would like to express my sincere gratitude to my advisor Prof. Jun-ichiro Hayashi, for his precious help, very kind help and care in my study and life. At the same time, sincere thanks to my co-advisor A/Prof. Shinji Kudo, for the continuous support of my Ph.D study and related research, for his invaluable supervision, patience, motivation, and immense knowledge. His guidance helped me in all the time of research and writing of this thesis.

Besides my two advisors, I would like to thank Prof. Hisahiro Einaga, as one of my committee members for his insightful comments and encouragement, but also for the hard question which incented me to widen my research from various perspectives. In addition, I would also acknowledge the China Scholarship Council for financial support.

I would also like to thank Ass/Prof. Shusaku Asano, for his stimulating discussions and kind help. I really appreciate my fellow labmates in Hayashi-Kudo laboratory, including Xiangpeng Gao, Li Chen, Shichao Qi, Lu Zhang, Asik, Halim, Ayu, Tianlong Liu, Jingxain Wang, Pacthada, Fu Wei, Aditya, Yan Li, Chengmin Zuo and the Japanese students, they gave me so much useful help and many happy memories in the last three years. Specially, many thanks to master students Mitsuyama-san and Fujiki-san who kindly supported me a lot experiment, technical staffs Shima-san, Hachiyama-san and

Mori-san who made me easy access to research facilities.

Last but not the least, I would like to thank my family for supporting me spiritually throughout studying overseas.